Study of the structural behavior of hybrid elements of Carbon Fiber Reinforced Polymer and Concrete

Thesis by:

Amir Mahboob

Directed by:

Lluís Gil Espert

Ernest Bernat Maso

Barcelona, November 2021

Polytechnic University of Catalunya, BarcelonaTech
Strength of Materials and Structural Engineering Department

Ph.D. Thesis

Abstract

Creating sustainable and public infrastructure is a fairly recent subject the engineering community has been debating. Introducing new building materials or introducing new structural designs is a strategy for constructing buildings that have long-term reliability and low maintenance requirements. Fiber-reinforced polymers (FRP) are one of the innovative approaches in the field of civil engineering that offer promising results in this regard.

In order to maximize the usage of FRP forms, researchers suggested the development of hybrid structural structures by mixing composite materials with standard materials, such as concrete, to enhance the stability, ductility and buckling resistance of single FRP members. Nevertheless, these composite solutions need more preliminary research to prove its feasibility due to the complexity and large range of hybrid components. However, as there is a current shortage of compulsory codes for the design of composite structures and consequently FRP-concrete members, accurate predictive models need to be created. Addressing the above-mentioned issues is essential in increasing the introduction of advanced composite materials in common types of public works and constructions.

Thus, the present work aims at testing the structural efficiency of hybrid slabs made of CFRP sheets under a concrete layer in bending and shear configurations by carrying an experimental and analytical analysis. Using Carbon Fiber Reinforced Polymer (CFRP) bonded with resin is usual to strengthen concrete slabs or other elements. This thesis introduces a novel technological definition of thin CFRP-concrete unidirectional hybrid slabs. In bending part, experimental quasi-static three-points bending tests and modal analysis tests were carry out to analyze the influence of the connection systems on the dynamic response. Moreover, the corresponding analytical methodology to calculate their response are presented. Four different connection strategies between CFRP sheet and concrete were tested. These included flexible mesh embedding and particle-based frictional enhancement. The maximum bending moment, the evolution of the neutral axis, the comparison between external moment (calculated from applied load) and internal moment (calculated from strain distribution), the CFRP-concrete interface shear stress, and the evolution of the vertical displacement at the loading point are the main results obtained from the tests.

In the shear part, this work investigates the shear behavior of hybrid slabs that used different types of particles and/or a flexible high strength fabric to connect both materials: concrete and CFRP sheet. Pure-shear experiments have been carried out to characterize the interface shear response of these hybrid elements. These increase the experimental database on CFPR-concrete shear connection systems. Experimental results showed that the improvement resulting from fabric embedding is far more significant than other tested connection elements at increasing the shear connection strength between the parts of the composite slabs.

Results are divided with technological and scientific contributions. The feasibility of using CFRP sheets in hybrid unidirectional slabs instead of steel sheets is the main technological contribution, which also offers the following advantages: lighter weight and resistance to corrosion. Qualitative and quantitative analysis of the CFRP-concrete connection alternatives point out that combining adherence and frictional based strategies is the most promising method.

An analytical method for the modelling of concrete slabs with CFRP was developed. In function of full cross-section interaction some equations for bending ultimate limit states were suggested. The possibility of using simpler formulas for quantifying interlayer slip effects was analyzed in assessing deflections, flexural stiffness, bending efficiency and normal and shear stress distributions. The proposed analytical method was able to capture the structural behavior and performance of the specimens.

Keywords: CFRP. Concrete. Hybrid slabs. Experimental. Bending test. Shear test. Modal analysis. Shear connection

Resumen

La creación de infraestructura pública y sostenible es un tema de plena actualidad que la comunidad de ingenieros ha estado debatiendo desde hace años. La introducción de nuevos materiales de construcción o la introducción de nuevos diseños estructurales es una estrategia eficiente para construir edificios que tengan fiabilidad a largo plazo y requisitos de bajo mantenimiento. Los polímeros reforzados con fibra (FRP) son uno de los materiales innovadores en el campo de la ingeniería civil que ofrecen resultados prometedores en este sentido.

Para maximizar el uso de formas de FRP se están desarrollando estructuras híbridas mezclando materiales compuestos con materiales estándar, como el hormigón, para mejorar la estabilidad, ductilidad y resistencia al pandeo de miembros individuales de FRP. Sin embargo, estas soluciones compuestas necesitan más investigación preliminar para demostrar su viabilidad debido a la complejidad y la amplia gama de componentes híbridos. Además, como existe una escasez actual de códigos obligatorios para el diseño de estructuras compuestas y, en consecuencia, elementos de hormigón FRP, es necesario crear modelos predictivos precisos para que puedan estandarizarse. Abordar los problemas mencionados anteriormente es esencial para aumentar la introducción de materiales compuestos avanzados en tipos comunes de obras y construcciones públicas.

Así, el presente trabajo tiene como objetivo probar la eficiencia estructural de losas híbridas de láminas de CFRP con una capa de hormigón, en configuraciones de flexión y cortante, mediante la realización de un análisis experimental y analítico. El uso de polímeros reforzados con fibra de carbono (CFRP) unido con resina es habitual para reforzar losas y otros elementos de hormigón. Esta tesis introduce una definición tecnológica novedosa de losas híbridas unidireccionales de hormigón-CFRP de lámina delgada. En la parte de flexión se realizaron ensayos experimentales de flexión cuasi estáticos, de tres puntos, y ensayos de análisis modal para analizar la influencia de los sistemas de conexión en la respuesta dinámica. Asimismo, se presenta la metodología analítica correspondiente para calcular su respuesta. Se probaron cuatro estrategias de conexión diferentes entre la lámina de CFRP y el hormigón. Estos incluyeron el embeber una malla flexible en el hormigón y la mejora de la fricción basada en partículas. El momento flector máximo, la evolución del eje neutro, la comparación entre el momento externo (calculado a partir de la carga aplicada) y el momento interno (calculado a partir de la distribución de deformaciones), el esfuerzo cortante de la interfaz CFRP-hormigón y la evolución del desplazamiento vertical en el punto de carga, son los principales resultados obtenidos de las pruebas.

En el estudio del cortante, este trabajo investiga el comportamiento rasante de losas híbridas donde los materiales de CFRP y hormigón se conectaron mediante diferentes tipos de agregados y textiles flexibles de alta resistencia. Se han llevado a cabo experimentos de corte puro para caracterizar la respuesta de la interfaz de estos elementos híbridos. Estos ensayos aumentan la base de datos experimental sobre sistemas de conexión de corte de hormigón-CFPR. Los resultados experimentales mostraron que la tela embebida produce una mejora en el aumento de la resistencia estructural de manera mucho más significativa que con otros sistemas de conexión probados.

Los resultados de la tesis se dividen en contribuciones de tipo tecnológico y científico. La viabilidad de utilizar chapas de CFRP en losas unidireccionales híbridas, en lugar de chapas de acero, es el principal aporte tecnológico, que además ofrece las siguientes ventajas: menor peso y mayor resistencia a la corrosión. Los análisis cualitativo y cuantitativo de las alternativas de conexión CFRP-hormigón señalan que la combinación de estrategias basadas en adherencia y fricción es el método más prometedor. Asimismo, se desarrolló un método analítico para el modelado de losas de hormigón con CFRP. En función de los principios de la conexión completa se sugieren ecuaciones conceptuales para calcular los estados límite últimos. La posibilidad de utilizar fórmulas más simples para cuantificar los efectos de deslizamiento entre capas fue analizada en la evaluación de deflexiones, rigidez de flexión, eficiencia de flexión y distribuciones de esfuerzos normales y cortantes. El método analítico propuesto fue capaz de capturar el comportamiento estructural y el rendimiento mecánico de las muestras.

Palabras clave: CFRP. Hormigón. Losas híbridas. Experimental. Test de flexión. Test de corte. Análisis modal. Rasante.

Resum

La creació d'infraestructura pública i sostenible és un tema de plena actualitat que la comunitat de l'enginyeria ha estat debatent des de fa anys. La introducció de nous materials de construcció o la introducció de nous dissenys estructurals és una estratègia eficient per a construir edificis que tinguin fiabilitat a llarg termini i requisits de baix manteniment. Els polímers reforçats amb fibra (FRP) són un dels materials innovadors en el camp de l'enginyeria civil que ofereixen resultats prometedors en aquest sentit.

Per maximitzar l'ús de formes de FRP s'estan desenvolupant estructures híbrides barrejant materials compostos amb materials tradicional, com el formigó, per millorar l'estabilitat, ductilitat i resistència al vinclament de membres individuals de FRP. No obstant això, aquestes solucions compostes necessiten més investigació preliminar per demostrar la seva viabilitat a causa de la complexitat i l'àmplia gamma de components híbrids. A més, com hi ha una escassetat actual de codis obligatoris per al disseny d'estructures compostes i, en conseqüència, elements de formigó FRP, cal crear models predictius necessaris perquè es puguin estandarditzar. Abordar els problemes esmentats anteriorment és essencial per augmentar la introducció de materials compostos avançats en tipus comuns d'obres i construccions públiques.

Així, el present treball té com a objectiu provar l'eficiència estructural de lloses híbrides de làmines de CFRP amb una capa de formigó, en configuracions de flexió i tallant, mitjançant la realització d'un anàlisi experimental i analític. L'ús de polímers reforçats amb fibra de carboni (CFRP) unit amb resina és habitual per reforçar lloses i altres elements de formigó. Aquesta tesi introdueix una definició tecnològica innovadora de lloses híbrides unidireccionals de formigó-CFRP de làmina prima. A la part de flexió es van realitzar assajos experimentals de flexió quasiestàtics, de tres punts, i assajos d'anàlisi modal per analitzar la influència dels sistemes de connexió en la resposta dinàmica. Així mateix, es presenta la metodologia analítica corresponent per calcular la seva resposta. Es van provar quatre estratègies de connexió diferents entre la làmina de CFRP i el formigó. Aquestes van incloure l'embegut de malla flexible en el formigó i la millora de la fricció basada en partícules. El moment flector màxim, l'evolució de l'eix neutre, la comparació entre el moment extern (calculat a partir de la càrrega aplicada) i el moment intern (calculat a partir de la distribució de deformacions), l'esforç tallant de la interfície CFRP-formigó i l'evolució del desplaçament vertical en el punt de càrrega, són els principals resultats obtinguts de les proves.

En l'estudi del tallant, aquest treball investiga el comportament rasant de lloses híbrides on els materials de CFRP i formigó es van connectar mitjançant diferents tipus d'agregats i tèxtils flexibles d'alta resistència. S'han dut a terme experiments de tall pur per caracteritzar la resposta de la interfície d'aquests elements híbrids. Aquests assajos augmenten la base de dades experimental sobre sistemes de connexió de tall de formigó-CFPR. Els resultats experimentals

van mostrar que la tela embeguda produeix una millora en l'augment de la resistència estructural de manera molt més significativa que amb altres sistemes de connexió provats.

Els resultats de la tesi es divideixen en contribucions de tipus tecnològic i científic. La viabilitat d'utilitzar xapes de CFRP en lloses unidireccionals híbrides, en lloc de xapes d'acer, és la principal aportació tecnològica que, a més, ofereix els següents avantatges: menor pes i major resistència a la corrosió. Els anàlisis qualitatiu i quantitatiu de les alternatives de connexió CFRP-formigó assenyalen que la combinació d'estratègies basades en adherència i fricció és el mètode més prometedor. Així mateix, es va desenvolupar un mètode analític per a la modelització de lloses de formigó amb CFRP. En funció dels principis de la interfície completa, es suggereixen equacions per calcular els estats límit últims. La possibilitat d'utilitzar fórmules més simples per quantificar els efectes de lliscament entre capes va ser analitzada en l'avaluació de deflexions, rigidesa de flexió, eficiència de flexió i distribucions d'esforços normals i tallants. El mètode analític proposat va ser capaç de capturar el comportament estructural i el rendiment mecànic de les mostres.

Paraules clau: CFRP. Formigó. Lloses híbrides. Experimental. Test de flexió. Test de tall. Anàlisi modal. Rasant.

Acknowledgements

First of all, I would like to convey my deepest gratitude to Prof. Lluís Gil and Prof. Ernest Bernat Maso, my thesis supervisor, for allowing me the chance to function and research under their leadership, for all the encouragement, confidence and help that has been provided over these years. Their guidance, passion and imaginative thought have become a personal source of motivation to me and have supported me as a researcher.

I am very grateful to the Polytechnic University of Catalonia and the Laboratory for Technical Innovation in Structures and Materials (LITEM) for the grant of a research group which has enabled me to take part in the PhD program.

Moreover, from the bottom of my heart I would like to thank my new and former departmental and study community colleagues – Virginia, Borja, Miquel and Amirreza Eskenati for their indispensable support in the implementation of this work, and for the lovely moments we shared.

A special mention is also addressed to the rest of the department staff, for accepting me with open arms in their collective. Additional recognition goes to Prof. Hamidreza Abbasian Jahromi from the K. N. University of Technology for his cordial assistance and the productive discussions we had.

Finally, I would like to express my deepest gratitude to my family, for their unconditional support and encouragement to succeed.

Table of contents

Contents

Table of tables

Annex B

Table of figures

Annex A

Annex B

Table of equations

Outline

The doctoral thesis is divided into six chapters and two annexes, the contents of which are briefly summarized below;

Chapter 1. Introduction

The current chapter contextualizes the subject of the present research and explains quickly the factors that lead to the issue under research. First, the key aim of the study and its main goals are defined, followed by the research methods employed and in view of the document structure. The second chapter consists of an initial description of the civil engineering fiber-reinforced polymer materials, and the production, specifications, and applications of FRP components. The chapter continues with the current state of awareness concerning hybrid FRP-concrete slabs, which addresses the structural framework, functional implementations and emerging contact technologies. The reported primary experimental experiments and analytical formulas are closely analyzed and correlated in direct communication in order to illustrate some of the research needs at this period.

Chapter 2. State of the art

The second chapter provides an overview of fiber-reinforced polymer materials for civil engineering, as well as the fabrication and properties of FRP components. The chapter continues with a discussion of the current state of knowledge for hybrid FRP-concrete beams, including the structural concept, practical applications, and existing connection technologies. In direct correspondence, the published key experimental investigations, analytical formulations, and numerical finite element simulations are thoroughly examined and compared in order to highlight some of the current research needs.

Chapter 3. Experimental campaign

The properties of the constituent materials to be used in the construction of hybrid slab specimens are described and reported on at the beginning part of the third segment. Then, the proposed slab models are identified along with their manufacturing cycle. The section is followed by the introduction of a destructive method by bending and shear tests for obtaining the elastic properties of CFRP-concrete slabs, and its validation results. Next off, the laboratory setups, testing procedure, and experimental results are discussed in the main part of the chapter. The effects of the experimental program are evaluated in terms of the modes of flexural behavior and failure, and composite conduct is established and in a comparative way versus reference specimens. Also, modal analysis tests have been done on all specimens in the lab and result is presented.

Chapter 4. Analytical procedure

Chapter four relates to the suggested theoretical method for the analysis of CFRP-concrete hybrid slabs. It requires formulations of ultimate limit state to predict maximum loads, shear stresses and energies among other parameters. The comparison of the analytical method with previous experimental data and with the findings of the laboratory experiments is seen in the last part of portion.

Chapter 5. Conclusions and outlook

The last chapter outlines the investigation 's key conclusions and suggests potential lines of study for future studies.

Annex A. Bending experimental results

In the first appendix of the document, all experimental plots extracted from bending and shear tests have been presented.

Annex B. Modal analysis tests

The second appendix includes all modal analysis' mode which were shown specimens'

1
Introduction

This section includes some preludes and clarifies several definitions and classification about the concept of this research.

1.1. Composite materials

Composites have been created by mixing several constituents to take the advantages of which such as strength and reduced weight. There are various materials to be used as components to create composites. They can be either traditional ones such as wood fibers and mud matrixes or modern materials including synthetic fibers and polymers. In the last century fiber reinforced polymers have been used in the military application and aerospace and naval industry, then it gradually was extended for civil engineering purposes. Figure 1 shows different types of fibers. The development of advanced composite materials that have taken place in recent decades, together with the lower cost of production, have opened the door to its use in a variety of industries, including construction. In this sense, the use of materials CFRP (Carbon Fiber Reinforced Polymer) for the reinforcement of existing structures is a subject that has remained in the front line of research in recent years. In other words, CFRP is one of the popular composites which are widely used in both buildings structures and in the aerospace industry.

CFRP composites are both tough and lightweight (density of 1500 $kg/_{m^3}$) materials used in the abundant devices utilized in daily life. In general, CFRP composites exploit some special resins such as epoxy, polyester, or vinyl ester.

At the beginning of this century, the development of the plastic industry makes the use of Polymers spread out and gradually it is noticed by the civil engineers.

Reinforced concrete (RC) (also called reinforced cement concrete or RCC) is one of the composite materials in which concrete's relatively low tensile strength and ductility are counteracted by the inclusion of reinforcement having higher tensile strength or ductility (Figure 2). The reinforcement is usually though not necessarily, steel reinforcing bars (rebar) and it's usually embedded in the concrete before the concrete sets. Reinforcing schemes are generally designed to resist tensile stresses in particular regions of the concrete that might cause unacceptable cracking and/or structural failure. Modern reinforced concrete can contain varied reinforcing materials made of steel, polymers or alternate composite material in conjunction with rebar or not. Reinforced concrete may also be permanently stressed (concrete in compression, reinforcement in tension), so as to improve the behavior of the final structure

under working loads. The most common methods of doing this, are known as pre-tensioning and post-tensioning.

For a strong, ductile and durable construction, the reinforcement needs to have the following properties at least:

- High relative strength
- High toleration of tensile strain
- Good bond to the concrete, irrespective of pH, moisture, and similar factors
- Thermal compatibility, not causing unacceptable stresses (such as expansion or contraction) in response to changing temperatures.
- Durability in the concrete environment, irrespective of corrosion or sustained stress for example.
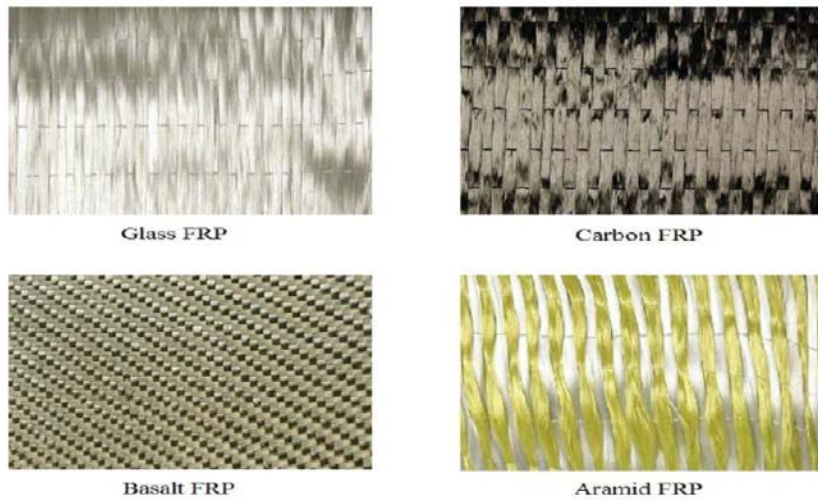
Figure 1. Four types of fibres (Siegel and Siegel 2018).
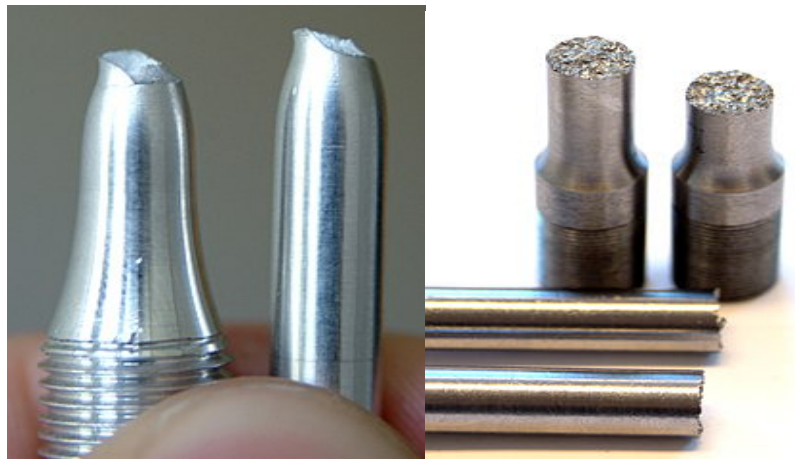
Figure 2. Tensile test of a nodular cast iron demonstrates low ductility (Hassan, Jones, and Mahmud 2012).

It is worthwhile to state that, the process of CFRP manufacturing is friendly to the environment; besides, these composites save energy as its energy consumption is much less in comparison with the other composites (Neagoe 2016).

Using the CFRP has been widely increased in the last decades and it is highly recommended to replace steel with CFRP in the concrete structures. This material has a wide variety of benefits over the steels, including high strength-to-weight ratio and high corrosion resistance; consequently, these plus points lead to increasingly used by the civil engineers.

1.2. Resin

Resin behaves as a matrix that binds the fibers together preparing load transfer among resin, composite and the external loads and supports. The applied force to concrete dissipates through the matrix to the fiber. Therefore, the substrate can carry an equilibrium load and transfer load while the fibers can withstand the tensile forces under the support of the matrix. Resins are categorized by thermoset resin and thermoplastic resin.

Thermoset resin means that the resin can't be reversed or reformed after it is cured. The impregnation into fiber reinforcing fibers is done at room temperature while it is in state of liquid before it is being cured and changes into solid form.

1.3. Composite concrete

Concrete is a mixture of different materials composed of aggregate bonded together with a cement paste that hardens over time-based (28 days). Concrete is simply the best building material for many applications. The issue is how to make concrete stand up to environmental and structural loads for long-term performance. A true composite bound the material of concrete together in a matrix of fine cement, with metal rebar usually incorporated for strength. The performance of the composite construction is quite perfect since concrete is good in compression and steel or composite is well in tension. By joining the two materials together, these strengths can be exploited to result in a highly efficient and lightweight design. A composite material is a mixture of constituent substance with remarkably different properties compensating each other weakness.

Composite concrete slabs are commonly used around the world to exploit its several advantages such as high strength-to-weight ratio.

Carbon Fiber Reinforced Polymer (CFRP) composites is enabled material for improved concrete performance. Composite rebar and reinforcing grids continue to find use, in a number of applications. More recently, products have been developed and applications are beginning to increase for fiber-reinforced concrete, a material that uses steel or polymer fibers as reinforcement in pavements, floor slabs and precast parts.

1.4. Hybrid systems

Among the various kinds of composites, pultruded FRP is one of the most used materials. FRP provide a wide range of properties; nevertheless, its downsides cannot be neglected. These drawbacks include:

Low stiffness in compare to the concrete, making either instability or large deformations; consequently, constraints of the structure should be increased which increase the limitation of the structures.

Lack of specific codes to authorize using of these composites and making help to overcome several issues is another problem. Leading to use of these composites as a tough task.

Therefore, hybrid slab benefits such as low-cost and shape resemblance advantages of FRP. On the other hand, FRP inherent properties make brittle behavior, moderate flexural stiffness and instability failure modes; consequently, it has been searched for another way to omit its downsides. One of the well proposed alternatives is a hybrid type of element which provided a wide range of both structural and economical properties.

Little by little the technological evolution has allowed thinking of hybrid structures that incorporate the composite materials already from the design phase. Several researches have been carried out in this line, most of which are oriented to type slab or column solutions. In the first, it is wanted to exploit the FRP traction resistance by placing it away from the flexion axis through pultruded FRP profiles or drawer structures in the case of bridges that are combined with massive concrete elements in the compressed side. In the case of the columns, the FRP has been used as a confinement of the concrete, which allows the generation of a three axial stress state in the nucleus, significantly increasing the carrying capacity of this type of structural element.

Hybrid FRP-concrete is an element consisting concrete section for compression. The tension part is booted by FRP which is either mechanically connected or adhesively bonded to concrete. The hybrid element system has been employed in civil engineering applications specifically in marine infrastructure projects.

Most of the hybrid members prepare not only higher structural efficiency but also lower cost. FRP-concrete let the engineers take plus points of the added composite and optimizes usage of both materials.

There are several criteria about the hybrid members should be concerned to get high results. These criteria include:

- Cost-effectiveness and high quality of the composite
- Placing FRPs in areas subjected to tension
- Fire resistance

By applying these criteria, following advantages of the hybrid systems will be obtained:

- Increase the strength-to-weight ratio
- Make longer of the service life
- Increase Resistance to aggressive factors

In this technological context, the main objective is set for the thesis project: to develop and characterize hybrid surface structural elements that combine the FRP in the form of a

collaborative plate, which can be used even as formwork, with a compression head of concrete. This approach seeks to limit or eliminate the need for reinforcement with steel and the corrosion problems currently associated with reinforced concrete structures.

1.5. Applications of CFRP profiles in civil engineering

Strength of the building always regarded as a special factor for designers. As time goes on the effect of the increasing service loads and degradation of existing concrete structures, leads to strengthening or retrofitting.

Structural damage caused by natural disasters or accidents, design and implementation mistakes, also changing regulations or altering the structures' application, as well as corrosion in steel and chemical degradation of concrete, can be cited for reasons of reinforced weakness; consequently, the wide variety of the problems related to the use of the steel plates such as it is not applicable to the slab strengthening of the plain concrete components and the limit for field, bring about other composite materials are proposed to make either strength or retrofit structures.

1.6. Aim and objectives

The main objective of the thesis is to characterize the behavior of hybrid superficial structures composed by thin FRP sheets and concrete. In particular, the first partial goal will be the development of different connection solutions between FRP and concrete and their experimental study, whereas modelling the mechanical response with analytical analysis would be the second main goal.

In order to achieve these aims, the following objectives were defined with their related activities:

1) To find, to order, to review and to present the existing information that supports the current research interest and necessity. Related activities are:

- Review previous hybrid element solutions with CFRP investigations in this field.
- Evaluate the guides and manuals published recently.

2) To design, to execute and to analyze the results of an experimental campaign to characterize the mechanical properties of the component materials for the intended structural solution. Related activities are:

- Perform characterization tests on the FRP material.

- Develop a nondestructive technique which can be used to determine the elastic properties of hybrid members and composite profiles.

- Design several hybrid specimens and fabricated each with different configurations.

- Test each of the specimens flexural and shear characteristics until failure and the analysis of their behavior focused on both flexural and shear capacities.

3) To design, to execute and to analyze the results of an experimental campaign to characterize the mechanical response of superficial structures composed by thin FRP sheets and concrete defined by different connection solutions. In particular, it is intended to study the concrete-FRP interaction. Related activities are:

- Conduct several flexural and shear tests to evaluate the ultimate limit state.

- Validate the analytical procedure with experimental data.

4) To adapt existing analytical formulations to model the mechanical response of superficial structures composed by thin FRP sheets and concrete. Related activities are:

- Propose an analytical procedure for the design of FRP-concrete hybrid slabs under short-term loading.

- Investigate and offer design equations for ultimate limit states

1.7. Research methodology

In order to study the different connection systems and to assess the novel proposal of using a flexible fiber fabric as FRP-concrete connector, three types of tests were defined. First of all, experimental modal analysis was aimed to assess the performance of the studied connections in a non-destructive method with the final goal of providing a qualitative comparison. Second, destructive bending tests were also conducted to provide quantitative data to compare the different studied connection systems. Third: destructive shear tests were conducted to check the direct shear response of hybrid specimens. Direct results of these tests like force-displacement curves, CFRP-concrete relative sliding and strain distribution are aimed to describe the mechanical response and the failure mechanism from a global point of view. In addition, some calculated variables are used to provide clear evidences of the failure mechanism (position of the neutral axis), practical information of the equivalent shear transferring capability (FRP-concrete equivalent shear stress) or to assess the ductility of the studied connections (external energy).

The tasks for developing the research methodology are:

Four main tasks are defined to meet the development of the thesis: Documentation, Characterization of component materials, Experimental campaign on hybrid elements and analytical development. All these tasks are briefly described in the following paragraph

1.7.1. Documentation

Despite being aware that the process of documentation and search of bibliographic sources will be extended to carry out a greater part of effort and scientific articles with the objectives of:

1- To contextualize the topic of research seeking to respond to existing needs in the field of construction.
2- Detect information gaps or specific research topics where less work has been done in accordance with existing scientific publications.
3- Define in detail the scientific objectives in accordance with the bibliographical evidence consulted.
4- Summarize order and present the information obtained from the consultation of bibliographic sources for the preparation of the initial version of the chapter on the State of Art of the thesis.

1.7.2. Characterization of component materials

1- Locate study and use existing information in the literature for the definition of the type of fibers and resins to be used in the production of the FRP compound.
2- Define in detail, apply it and document the production process of CFRP laminates with suitable shape to be used in hybrid structures.
3- Choose, produce and characterize experimentally the type of concrete to be used for the manufacture of hybrid elements.
4- Characterize the mechanical performance of the CFRP and concrete.
5- Define innovative reinforced concrete hybrid systems to fully exploit its advantages such as stiffness, ductility and dissipation capacity.

1.7.3. Experimental campaign on hybrid elements

1- Design different CFRP-concrete sheet connection solutions.
2- Define, execute and document the execution system of hybrid elements of CFRP sheet and concrete for each type of connection.
3- Design the destructive mechanical tests defined the global geometry of the specimens, the conditions of support, the method of load and the sensors to incorporate in order to characterize the structural response and obtain the variables necessary to adapt the calculation tools.
4- Determine the main resistant properties and the structural response at the interface level of the hybrid elements from the execution of destructive tests and the analysis of the experimental results obtained.
5- Evaluate elastic mechanical properties of their major essential materials using a nondestructive method based on the free vibration response.

1.7.4. Analytical development

1- Due to the lack of codes and manuals for designing and checking composite concrete with CFRP, it has been started to develop analytical procedures.
2- Study the existing analytical models for the calculation of mixed structures with steel and concrete to detect the variables to be determined experimentally through the trials to adjust a new model.
3- Propose analytical solutions to characterize the behavior of hybrid elements of Carbon Fiber Reinforced Polymer and Concrete.
4- Propose an analytical model for hybrid omega shape slab based on Euler Bernoulli formulas.

2

State of the art

2.1. Introduction

Nowadays CFRP composite materials are used in concrete with either continuous or discontinuous fibers mostly with resin to strengthen the concrete slabs. The use of this material brings about a better strength and stiffness; nevertheless, some of its drawbacks such as heterogeneity and anisotropy of the concrete are undeniable.

Moving from slab configuration to slab elements, several significant researches on strengthening RC slabs can be found. (Soltanalipour et al. 2020) investigated the shear behavior of composite slabs subjected to 4-points bending tests. Two load arrangements were used, concluding that FRP-concrete contact forces depended on the loading configuration. Large differences in concrete crack distribution were pointed as the main cause of this contact stress variation. (Alampalli 2006) studied on composite slabs reinforced with FRP. They performed experimental tests and proposed an analytical method. Their results demonstrate that composite slabs with additional reinforcing FRP bars had higher ductility and load capacity than the specimens with less reinforcement. (Bank 2013) stated that CFRP sheet provided a considerable effect on the shear capacity and ductility enhancement of concrete slabs subjected to shear efforts. (Parvin et al. 2010) defended that CFRP strengthening improved the performance of all studied slabs with openings except the ones with circular openings. (Moradi, Naderpour, and Kheyroddin 2020) observed, from experimental tests, that FRP strengthening increased the resistance and ductility of all specimens. (Dan et al. 2010) tested RC slabs strengthened with externally bonded FRP. Results showed an improvement in maximum load capacity and a significant rise in mid-span deflection in comparison with the control slab. (Anon 1996) investigated the strength and ductility of existing RC slabs and bridge decks before and after FRP strengthening. Experimental findings illustrated retrofitted RC slabs could significantly increase their overall flexural capacity and ductility. (Firmo, Correia, and França 2012) performed experimental and numerical investigations about the behavior of CFRP-strengthened slabs against fire. Although strength decrease, CFRP laminates showed a considerable performance under high temperature. (Khalifa and Nanni 2002) suggested that externally bonded CFRP could be an effective alternative for repairing damaged concrete slabs. Finally, (Mohammed et al. 2020) studied the behavior of concrete slabs and slabs strengthened by FRP externally in finite element method. The numerical results modeled the interfacial behavior between FRP sheets and concrete.

Apart from FRP strengthening solutions, some researchers have worked on studying the possibility of including FRP profiles in hybrid concrete structures. (Correia, Branco, and Ferreira 2007) studied the combination of a GFRP pultruded profile with concrete. FRP was attached with epoxy adhesive to the concrete element. The result of four-points bending tests presented that shear failure happened in the concrete slab. (Yao, Teng, and Chen 2005) found the best way to maintain maximum joint operation between FRP and the concrete by casting fresh concrete onto a water-based adhesive. (Gai et al. 2011) investigated FRP formworks for concrete floor slabs. Progressive longitudinal failure may cause the experimental failure of specimens with incomplete shear connections.

Shear strengthening is far less investigated and superficial FRP-concrete connection studies are mostly limited to the bonded case. Hence, there is little research on hybrid FRP-concrete slabs and even less on mechanical connection between these two parts when FRP is used as a reinforcement for new structures.

Another reason of the popularity of the Carbon Fiber Reinforced Polymer (CFRP) to strengthen both slabs and walls, is that the openings has been greatly used which provided an opportunity to apply CFRP plates to the slab or wall before the opening is made.

At the early stage, CFRP civil engineering applications had been restricted by some rehabilitation which provided limited experiences. Although, recently the new form of CFRP usage have been proposed for civil engineering projects; thus, it is predicted that the hybrid members will be used widely in civil infrastructure projects in the future.

Regarding considerable cost of rebuilding structures, in recent years, the problem of reinforcing and repairing weak and damaged structures has been raised in a wide range of FRP applications (Nystrom et al. 2003). The strengthening of reinforced concrete slabs using FRP has been accepted commonly used method in most parts of the world. Figure 3 shows strengthened structure with FRP.

Figure 3. Strengthened structure with FRP (Nystrom et al. 2003).

The main reason of using FRP would be achieving high capacity, without changing the dimensions and shape of the structural element.

The efficiency and versatility of this new construction material are a result of outstanding mechanical, physical and chemical properties. Besides the lightweight and high strength

characteristics, composite manufacturers (Raza et al. 2020) emphasize the fact that structures built with pultruded FRP (PFRP) profiles are more durable, require virtually no maintenance and can be constructed in a simple, rapid manner, without the use of extensive scaffolding.

In spite of their great potential, CFRP has some disadvantages like (Jumaat, Rahman, and Rahman 2011):

1-Cost: The cost of FRPs is the main disadvantage in almost all cases. Glass FRP reinforcing bars and aramid fiber or carbon fiber for pre-stressing tendons.

2- Shear: Shear isn't properly understood, even in structures with steel reinforcement. It is already noted that FRPs aren't ductile, and yet we persist in using formulae for FRP reinforcement that look like the plastic theories for steel with "adjustment" factors added that try to limit the strains in the FRP to those that would have been present in elastic steel structures.

3- The resistance of fibers to corrosion has been mentioned as a benefit, but they are not perfect. The Fibers don't "rust" but the resins in FRPs are also liable to various mechanisms for degradation.

4- Fire Resistance of FRP: When exposed to fire, FRP materials may suffer charring, melting, delamination, cracking and deformation. Figure 4 shows that the FRPs, lose strength with rising temperatures, and Carbon-Fiber losing less than other FRPs (Turkowski et al. 2017).
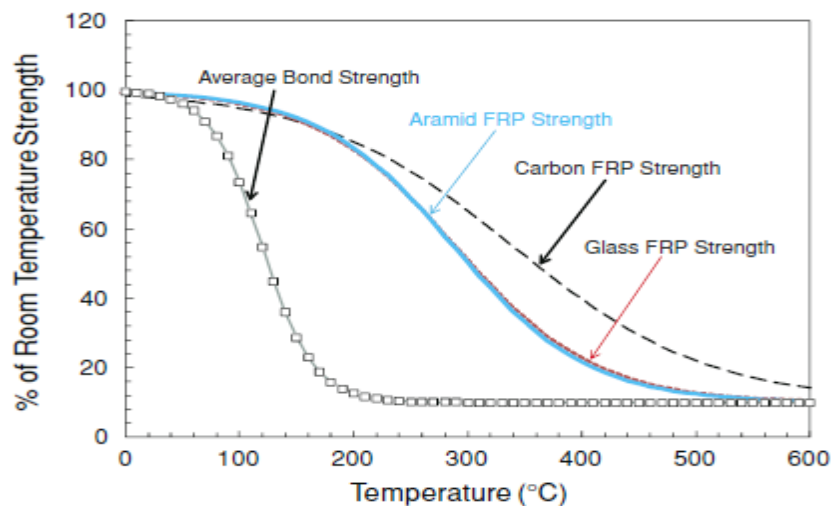
Figure 4. Change in FRP strength and bond strength with temperature increase.

To better illustrate the diversity of FRP composites applications in civil engineering, Figure 5 presents the utilization possibilities in a tree diagram (Neagoe 2016).
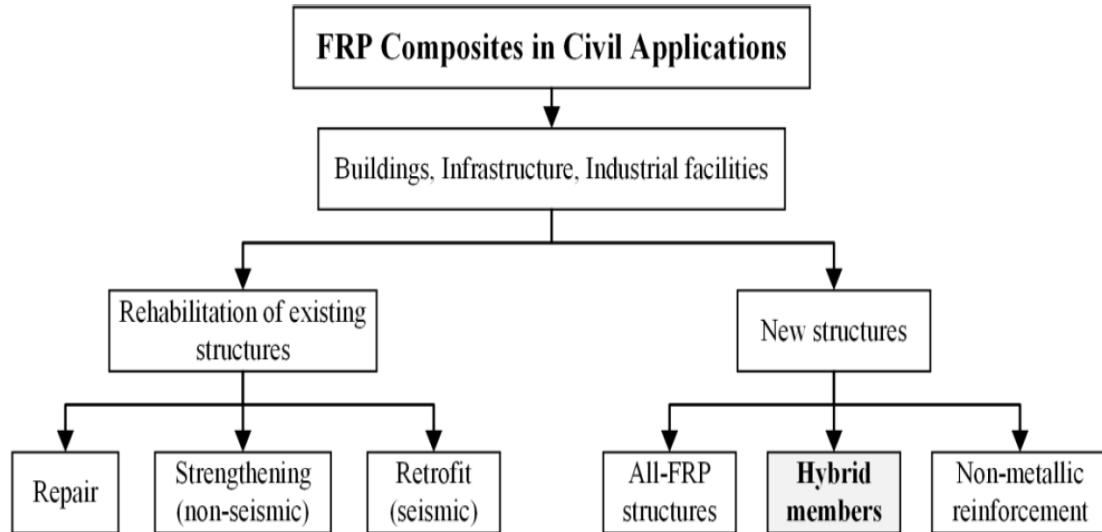
Figure 5. FRP Composites and their application in Civil Engineering (Neagoe 2016).

Nowadays the CFRP composites have been widely observed meeting the need of the load carrying structures with different purposes such as fuselage of commercial and military aircraft or the pressure vessel for a rocket propulsion system (Bernat-Masó and Gil 2019). Therefore, it has been an important research topic among engineers. CFRP composite has been used as a tendon of post tension slab. It can apply a beneficial compressive prestress and enhance the pre-fracture and post-fracture performance of the slab behavior (Speranzini and Agnetti 2015),(Correia, Branco, and Ferreira 2009). It is suggested that steel plates could be replaced by Carbon Fiber Reinforced Polymer (CFRP) plates (Jnaid 2020).

In the recent years, CFRP has been widely used in several kinds of different structures, such as road bridges, pedestrian, frames, building floors and roofs, cooling towers, offshore platforms, trusses, and so on. There are great numbers of the structures using CFRP composite, which are either rehabilitation project or temporary structures.

2.2. Literature review

This study focuses on the structural behavior of hybrid elements of Carbon Fiber Reinforced Polymer and concrete; consequently, it needs to present a laconic history of CFRP and its application on concrete structures and a brief introduction about steel sheets-concrete composites as reference solution that anticipates the proposed structural elements this research is focused on.

In what follows, historical research about the advantages and development of the composite material are introduced.

2.2.1. FRP as materials:

In recent decades, FRP material has been regarded as an appropriate option of material for construction which arise a great deal of investigation about its properties.

An important survey (Karim and Hoo Fatt 2006) describes several analytical models to simulate the rate-dependent response of various types of polymer matrix composites. An elastic-viscoelastic developed model for an orthotropic material without tension/compression symmetry and used an extension of that model to describe an experimental methodology to generate material constants (Karim and Hoo Fatt 2006).

Madhukar (Drzal and Madhukar 1993) experimentally investigated the effect of the fiber adhesion on compressive response. They reported that the compressive modulus has been slightly affected by the fiber surface treatment; moreover, they presented the failure is delamination as a result of the lack of the poor fiber bonding.

Another study about the compression test carried on by Moran (Moran, Liu, and Shih 1995). As can be seen in Figure 6, the load curve induces several deformation stages. First its behavior is linear, then its linearity it decreases and finally, the plastic deformation appears. They also reported a band broadening phenomenon is appeared called cold drawing due to the propagation of the localized bends in the fibers (Moran et al. 1995).
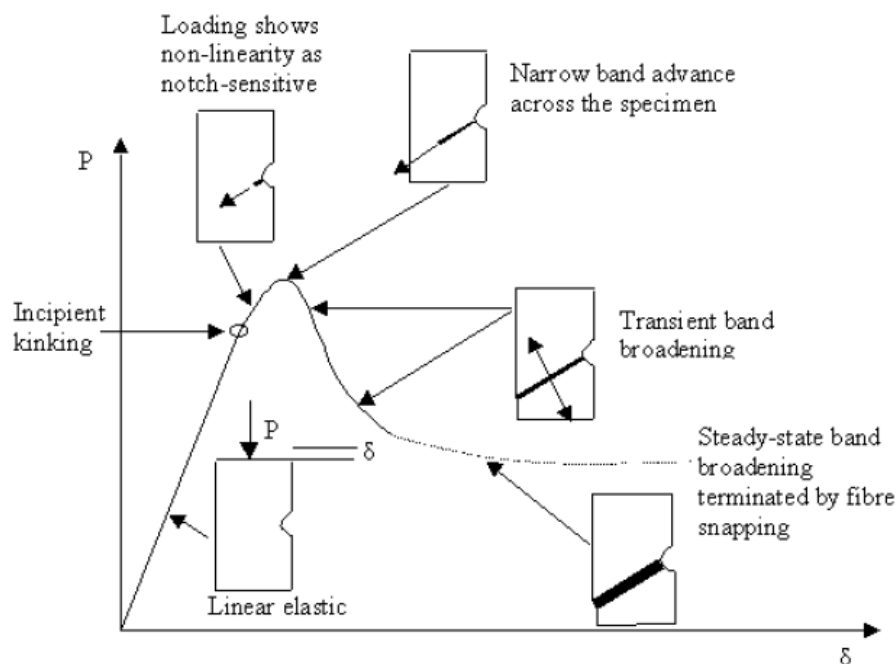
Figure 6. Load curve and the associated deformation stages (Moran et al. 1995).

Karayaka (Karayaka and Sehitoglu 1996) detected a significant impact of temperature on the compressive strength of carbon-fibre composites by pure coincidence in their experiments. They reported that the temperatures below 100°C uniform development of longitudinal matrix cracks are the real reason of the failure; on the other hand, at temperatures above 100°C, localized matrix failure brings about deformation (Karayaka and Sehitoglu 1996).

2.2.2. FRP used as strengthening of previously cured concrete structures: research

FRP strengthened concrete can be either prepared by the in situ wrapping of FRP sheets or strands in a wet layup process. It frequently reported that FRP composite is very viable for circular columns; although it has less effect for square or rectangular columns. Bonding precured FRP laminates is the alternative option (Saiidi, Gordaninejad, and Wehbe 1994).

(Shi et al. 2020) Conducted 6 tests to compare the structural behavior of the slabs with bonded CFRP. They concluded that the CFRP system brings about increasing both load-carrying capacity and stiffness of slabs. They also investigated the failure mechanism validated the results against an analytical model based on a modified yield line theory (Shi et al. 2020).

(Chakrabortty et al. 2011) Developed a novel hybrid solution for a slab consisting of a GFRP pultruded profile, a CFRP laminate, and a concrete block all wrapped up using filament winding. The results revealed that the composite layers enhanced both stiffness and load capacity of the slab; furthermore, it costs is lower in contrast to the normal concrete and have more ductility (Chakrabortty et al. 2011).

(Bedon and Louter 2016) Simulated the bending performance of post-tensioned structural glass slabs with adhesively bonded CFRP tendons. The numerical model is validated by the four-point bending experimental test. The outcomes indicated that the proposed FE model could be further developed to fully assess and optimize the examined design concept (Bedon and Louter 2016).

2.2.3. FRP used as strengthening previously cured concrete structures: applications

Another study to investigate the slab behavior is carried on by (Mosallam and Mosalam 2003). They investigated the concrete slabs repaired and retrofitted with fiber reinforced polymer. The outcome revealed that using the composite increases the structural capacity of the slab. The CFRP strengthened slab appears far better performances as Its load carrying capacity increases five times in comparison to the as built slabs (Mosallam and Mosalam 2003).

(Wu, Li, and Sakuma 2006) Proposed using epoxy resins to bond the concrete to the outside shell. The flexural stiffness of the system is increased by the use of CFRP sheets. In addition, flexural has been controlled by the use of CFRP sheets (Wu et al. 2006).

2.2.4. FRP-concrete hybrid structures: research

(Saiidi et al. 1994) Conducted some experiments to investigate the flexural behavior of the custom-made I-shaped profiles connected to concrete slabs with an epoxy layer. They proved that analytical calculation to estimate bond strength is inaccurate and at the end of this research it is recommended to use the pultruded shapes due to better fiber orientation, more effective shear mechanisms and lower expense (Saiidi et al. 1994).

(Canning, Hollaway, and Thorne 1999) Carried on some experiments to investigate web buckling phenomenon. To prevent this phenomenon, GFRP layers and a polymer foam core

were used in the hybrid structural members. They concluded that the wet adhesive bonding method between the fresh concrete and the FRP could be regarded as an effective technique to avoid web buckling phenomenon (Canning et al. 1999).

(Nassani 2020) Drew an analogy between the experimental result of load-midspan deflection curve of a single hybrid GFRP-concrete slab and the numerical results from a linear elastic three-dimensional FE model, and analytical solutions, this comparison revealed that the result of the flexural response is accurate and the significance of angular deformations for higher loads was shown (Nassani 2020).

(Deskovic, Triantafillou, and Meier 1995) Carried out some experiments at the Swiss EPFL to investigate the short-term and long-term behavior of a novel hybrid concrete slab with layers of FRP (Figure 7), (Figure 8). The results showed that the hybrid slab can achieve perfect structural responses.
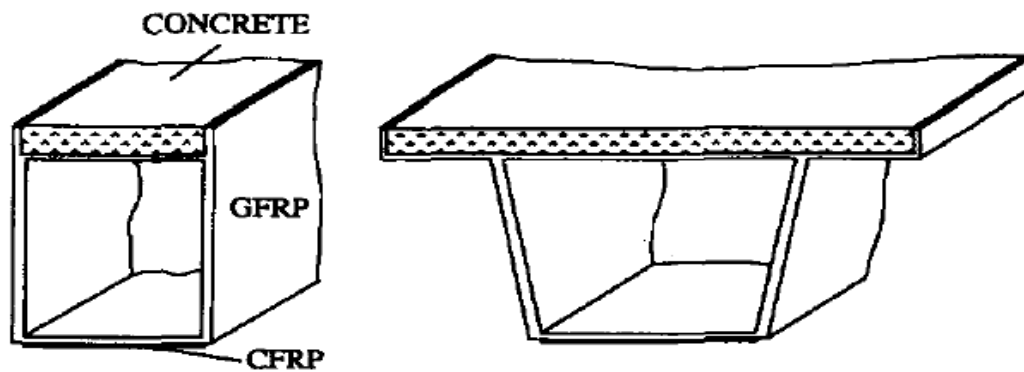
Figure 7. Slab section made of FRP and concrete materials by combination (Deskovic et al. 1995).
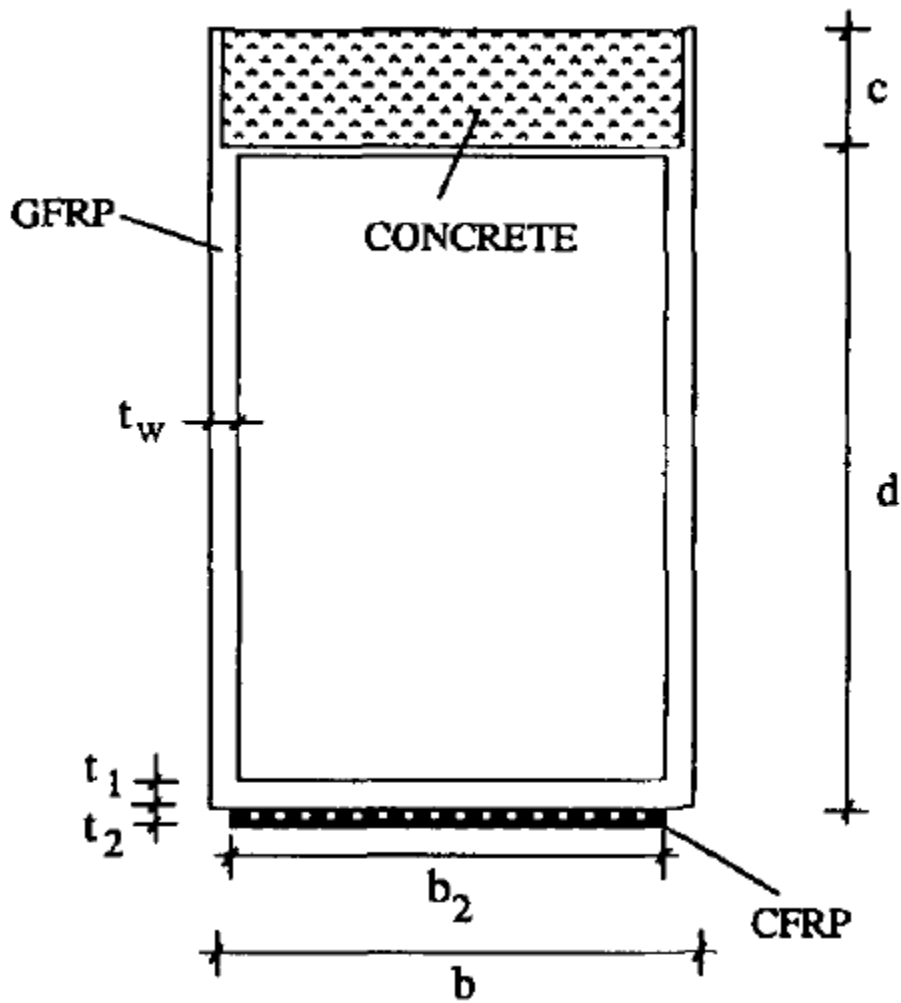
Figure 8. Cross section variable of Hybrid FRP concrete slab (Deskovic et al. 1995).

Connected GFRP profiles with concrete slabs were investigated by (Fam and Skutezky 2006). They studied the failure of the hybrid slab due to the loss of strength and web buckling phenomenon. They also presented a critical shear span-to-depth ratio to control the web buckling phenomenon (Fam and Skutezky 2006).

2.2.5. FRP-concrete hybrid structures: applications

The first utilization of CFRP tubes is as girders for the bridge superstructure. (Karbhari and Zhao 2000) conducted some laboratory test to investigate the serviceability and ultimate limit state of the hybrid girders, anchorages, and girder-deck (Karbhari and Zhao 2000).
(Vasquez and Karbhari 2003) Investigated the behavior of CFRP strengthened slabs. The main aim of their study was to evaluate the performance of the CFRP on the slabs; furthermore, they studied the failure mechanism and the post debonding response. The result revealed that the crack of the CFRP strengthened slab has the more desirable pattern in comparison to the slab which is not used CFRP (Vasquez and Karbhari 2003).

2.3. Characteristics

FRP materials, relating to structural behavior, have a continuous elastic stress-strain relationship before collapse, higher axial tension compared to steel profiles, weaker transverse resistance, and comparatively minor elasticity modulus. The composite pultruded material 's benefits over conventional materials include: low self-weight, lower fatigue and environmental tolerance, long-term resilience, strong strength-to-weight ratio, optimized properties and structure, thermal stability, electromagnetic flexibility, low maintenance, and fast transport and assembly (Nanni, De Luca, and Jawaheri Zadeh 2014).

As in other composites, the properties of FRP components are essentially based on the characteristics of their constituent materials, the direction and structure of the fiber reinforcement, and also on the interaction of the fiber matrix. Therefore, external variables such as charging conditions and environmental factors also affect the response.

Carbon fiber is made from precursors of polyacrylonitrile (PAN), pitch, or rayon material. The primary shape used in civil engineering applications is carbon fiber centered on PAN. PAN carbon fiber is extremely durable and has fairly small modulus. Pitch reinforced carbon fiber has higher modulus but lower power, rendering it ideal for applications in the aerospace industry. Precursors for radius and isotropic pitch are used to manufacture low-modulus carbon fiber. The carbon fiber can be graded as high modulus and low modulus depending on its mechanical properties. Carbon fiber has a strong strength in fatigue, good tolerance to alkali or acid attack, weak thermal expansion coefficient (CTE), fairly low impact resistance, and high electrical conductivity; When in close interaction with metals it may cause galvanic corrosion. It is also not readily wet by resins; thus, sizing is important until it is deposited in the resin. Carbon fiber is typically about 10 times more flexible than carbon fiber, which is almost three times greater in intensity which modulus than quartz (Nanni et al. 2014).

2.4. Hybrid slab solutions

2.4.1. Concept and structural applications

Despite their tremendous promise, fiber-reinforced polymer components pose many disadvantages as contrasted with their steel counterparts: a comparatively low stiffness (especially for glass FRP), which can lead to design limitations due to instability or broad deformations, an intrinsic fragile nature and a partially evolved attachment technology. However, the absence of definitive codes and the current high initial costs of such specialized materials preclude a broad usage of composite profiles in civil engineering applications. To address some of these problems, researchers have suggested incorporating new hybrid components that incorporate the benefits of FRP with those of traditional materials to achieve superior structural members.

Many of the up-to-date constructed hybrid members is developed by mixing fiber-reinforced polymer forms with concrete, leading to the lower expense and greater structural strength of the resulting functional approach. Concrete is often favored, because it can provide

containment, improve flexural integrity, resilience and rigidity. In fact, the extra weight from the concrete component can be helpful in the sense that the device would provide improved damping, as light systems are usually predisposed to inacceptable vibrations. Since composite products may be customized to satisfy anticipated requirements, the integrated FRP-concrete approach helps engineers to take advantage of each component 's preeminent properties and to maximize the usage of both products.

Following a detailed review of the current and potential uses of advanced polymer composites in civil infrastructure, it was proposed that hybrid FRP-concrete members reflect the future in this area (Hollaway 2003), as they possess excellent in-service properties and mechanical characteristics. In fact, these innovative concepts can be seen in a broad range of contexts, and detailed studies have been carried out in North America, Europe and Asia (Wu et al. 2014), based on their positive findings.

In a recent analysis of the present and potential usage of FRP composites in construction (Hollaway 2010), the review carried out proposed that the following three conditions be followed in order to effectively incorporate the hybrid systems in modern structures:

- Resource savings in terms of the most desirable balance of expense and good quality and output total costs.

- The reinforced content will preferably be used in tensioned environments.

- The defense to fire need not be important.

As for FRP-concrete columns, the overwhelming majority of the prototypes suggested depend on pultruded FRP parts attached to concrete slabs. The composite profile's key function is to hold the stress and shear in the member, whilst the concrete surface helps to withstand strain and balance flexural behavior. Due of their reduced manufacturing costs, most of the prototypes prefer glass FRP (GFRP), while the top slabs are usually constructed from normal strength reinforced concrete. As outlined below, the FRP components and the concrete layers may be linked by a bonded joint, mechanical joint, or combination joint.

The major advantages of the FRP-concrete slabs over conventional reinforced concrete slabs are:
- Higher strength-to-weight ratio

- Extended service life and reduced maintenance

- Resistance to aggressive external factors

- Lower transportation and installation costs

- Reduced formwork

Compared to single FRP component, the hybrid slabs possess the following benefits:

- Enhanced strength and stiffness

- Better resistance to instability phenomena and impact loading

- ▪ Improved vibrational characteristics
- ▪ Elevated structural redundancy and ductility

Some of the notable disadvantages of hybrid FRP-concrete slabs at the present time are related to:

- ▪ Interface/connection problems

- ▪ Little available data and experience

- ▪ High initial costs and environmental concerns (*i.e.*, recycling of FRPs)

2.4.2. Experimental research studies

Some hybrid slab architectures have been developed and experimentally tested over the past decades. The most significant cases have been chosen for analysis and contrast from the published inquiries. The FRP-concrete slabs were arranged according to the form of the material to help represent the leading styles that are possible at the moment.

2.4.2.1. Examples of hybrid slabs with concrete-filled FRP

Throughout the early 1980s, after the popular usage of FRP sheets to reinforce concrete columns, one of the first possibilities for integrating FRP with concrete throughout constructing modern structural elements came about. The key concept was to fill the FRP forms with concrete in full or in part to achieve hybrid components of superior mechanical characteristics and efficiency. An early research carried out by (Fardis and Khalili 1982) studied the flexural efficiency of a slab built from a concrete-filled box of rectangular glass fiber reinforced plastic (GFRP). The purpose of the GFRP shape was to provide partial containment in the compressive zone and to carry tensile and shear forces, while concrete filling contributed to the member's compressive strength, ductility and rigidity, preventing the FRP shape from buckling locally. Since concrete was constrained by the sides of the box at both ends, the connection was not essential in the bending response.

At the end of the 1990s, the Carbon Shell Program was implemented as an alternate construction system for short and medium span bridges. The concept uses prefabricated carbon fiber-reinforced polymer (CFRP) tubes as girders filled with lightweight concrete and then joined to the bridge superstructure by a conventional pre-fabricated, cast-in - place or advanced composite deck system. (Karbhari and Zhao 2000) have recorded preliminary findings from evaluating the hybrid girders, anchorages, and girder-deck assemblies for both serviceability and ultimate limit conditions, demonstrating the promise of the proposed structural solution. The groundbreaking system was employed in constructing the Kings Stormwater Channel Bridge in 2001.

(Fam and Skutezky 2006) Studied the flexural reaction of partly filled circular and rectangular GFRP tubes to minimize the weight of the concrete packed forms. Twenty circular slabs under four-point loading were tested at bending. Some nine separate GFRP tube types were used, and one was constructed completely from steel. The concept often varied by the presence or location of an inner tube or by concrete positioning. Results revealed that the flexural behavior

relies strongly on the tube's rigidity and diameter-to-thickness ratio, and to a far lesser degree on the concrete power.

Concrete containment added insignificantly to the flexural strength; nevertheless, the member's ductility was increased. In addition, it has been demonstrated that if there is no relation between the two separate materials, slip will occur which will reduce the hybrid element's structural efficiency. For the rectangular GFRP-concrete slabs shown in Figure 9, the findings suggested that whole the concrete-filled pultruded tubes displayed higher rigidity than the concrete-filled filament-wound tubes of the same length, due to lack of fibers in the direction of the hoop, they failed prematurely through horizontal shear.
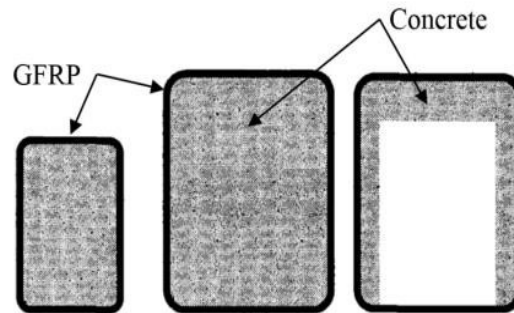
Figure 9. Hybrid slab designs investigated by (Honickman and Fam 2009).

In recent years, numerous scholars have suggested better versions of the concrete-filled hybrid solutions. To demonstrate this, (Wu et al. 2006) Proposed utilizing epoxy resins to bind the concrete core to the exterior shell to avoid major slippage. CFRP sheets were then known to improve the system's flexural rigidity, and GFRP sheets with strong tear strains were wrapped in the slab's hoop direction to bear the shear load and provide containment. Finally, it required a minimum reinforcing ratio of steel rebars to monitor the origin and spread of flexural cracks.

(Teng et al. 2007) Addressed the logic and benefits of hybrid FRP-concrete-steel double-skin tubular components in a paper where the authors proposed possible uses in buildings that are subjected to rough conditions, such as bridges, costal buildings and numerous tower structures. As main features in maintaining the efficiency of the hybrid members are highlighted the shear link between the inner tube and the concrete heart, and the joint between the tubular component and concrete decks.

Eventually, (Chakrabortty et al. 2011) Produced and examined a novel hybrid tubular solution consisting of a pultruded GFRP mold, a CFRP base laminate, and a concrete core, both bundled up using filament winding. The experimental findings revealed that the external composite coating stopped the concrete component from debonding from the pultruded box and improved the slab's rigidity and load efficiency. Furthermore, it was found that the composite slabs of standard concrete or steel fiber strengthen concrete had greater ductility than the high-strength concrete slabs, but at the cost of marginally lower rigidity and flexural capacity

2.4.2.2. Examples of hybrid slabs with trapezoidal FRP sections

Eventually, a specific type of hybrid FRP-concrete slabs was developed specifically for the design of vehicular bridge superstructures for short span vehicles. A form of composite slabs typically has a trapezoidal FRP design that makes part of the girder structure, connected to the top with a reinforced concrete slab that serves the deck system's function (Neagoe 2016).

 (Mieres et al. 2006) and (Gutiérrez et al. 2008) Clarified in depth the features, and the short-term actions, of the integrated Cantábrico highway overpass inaugurated in Spain in 2004. The girders of the bridge were made from low elastic modulus carbon fibers and high strength, which were pre-impregnated with epoxy resin. Additionally, there was a polyurethane core in the trapezoidal closed section of the slabs to resist web buckling. Alkali-resistant GFRP pultruded I profiles that acted as shear connectors were bonded uniformly, in a cross-sectional orientation, on top of the CFRP plate. The deck was realized with usual intensity from cast-in - place reinforced concrete. The findings of the quasi-static testing carried out on autonomous, dynamically indeterminate hybrid slabs showed that the bridge configuration effectively fulfilled the specified serviceability and protection requirements, and that the distribution of shear and bending moment profiles along the member's length varied from the hyperstatic to the isostatic cases under the loading.

It was found that the prevailing failure mechanisms at the reaction points and joint parts were shear regulated, which may have triggered more than one failure mode, including delamination of the reinforced concrete slab from the central load-bearing plate, joint isolation, which diaphragm buckling support.

(Siwowski, Rajchel, and Kulpa 2019) Focused on the construction and field assessment of a hybrid FRP-concrete superstructure framework used in a prototype vehicle bridge constructed. The structure featured a series of a dozen GFRP trapezoidal structures with an open side at the top to accommodate concrete castings. At the upper part of the profiles, horizontal braces were mounted to avoid deformation of the cables. The concrete floor was then poured down to the center of the profiles, embedding the metal braces and ensuring an appropriate joint motion inside the hybrid members was created. The findings revealed no major loss of stiffness and composite activity after two years of testing, indicating the efficacy and advantages of this innovative building method.

More recently, (Honickman and Fam 2009), (Fam and Honickman 2010), (Kim and Fam 2011) performed several experiments on hybrid girders in which commercially usable GFRP sheet-pile trapezoidal pultruded types were mixed with reinforced concrete, as seen in Figure 10. For recent bridge superstructure designs the designers tried to show the ability of the novel composite concrete for serving as the main load-bearing element.
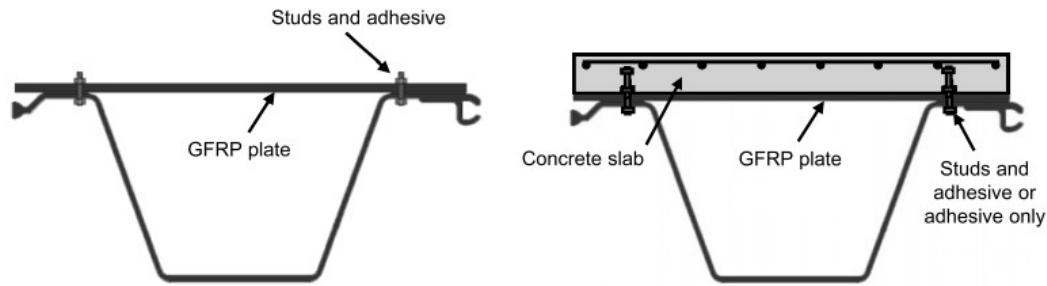
Figure 10. Hybrid FRP-concrete girders analysed (Fam and Honickman 2010).

Different cross-sections were studied, where the composite structures were packed with concrete in whole or in part, and both adhesive bond and shear stud systems were tested. Nevertheless, debonding was the key mode of hybrid slab failure and more work on this subject is needed (Neagoe 2016).

2.4.3. Analytical design formulations

2.4.3.1. Design codes and guides

As per author knowledge, there are currently no European or American standards of authority for constructing systems with pultruded FRP profiles or hybrid FRP-concrete components. Nonetheless, in the last decades, many guides and manuals have been published which collect suggested rules of good practice for FRP structural shapes typically made from thermoset resins reinforced with long glass fibers. Therefore, the American Society of Civil Engineers (ASCE) released the Structural Plastics Development Manual in 1984 (Gray et al. 1984), preceded subsequently by the Fiber Reinforced Polymer (FRP) Structures (Gray et al. 1984) to Pre-Standard for Load & Resistance Factor Mode (Lesko and Cousins 2013). In 1996, for the structural design of polymeric composites, the European Structural Polymeric Composites Community released the EUROCOMP Design Code and Handbook (Herrmann and Bucksch 2014), which was meant to act as the framework for a possible Eurocode. The Guide to the Development and Construction of Structures made of FRP Pultruded Elements (Grimaldi 2007) was released in 2008 by the National Research Council of Italy. Commonly, the guides and manuals specify a philosophy of design, partial safety variables or factors of resistance, as well as guidelines and equations for members design and their corresponding connections in framed structures. Analytical relationships are given for the design of compact, tensioned, flected, shear, torsioned or mixed loaded components. In addition, calculations for global and local volatility, vibration thresholds, and features of long-term activity are often sometimes used (Neagoe 2016).

A variety of companies from the pultrusion industry have created their own concept guides beyond the previous outlets (Fiberline Composites 2003), (de Buhan, Bleyer, and Hassen 2017). Many of them also precede the above manuals by many years. The equations and load tables required for design, rules and relationships for bonded and/or bolted connections, details of the manufacturing and construction techniques, and environmental considerations. Nonetheless, most of the above topics refer to the FRP profiles provided by the companies and are not widely considered relevant.

The design criteria for flexural and FRP modules and their related interfaces were also addressed by (Bank 1987), which contrasted requirements for the following specification bases: permissible stress architecture, specification of the load and resistance element, architecture of limit states, and design dependent on efficiency. The author suggested that while analytical equations have been extensively established and tested over the years for traditional structural components, there is less agreement on the expressions proposed for modeling relations, which are also still empirically oriented. Most recently, on this subject, the ASCE released Design Guide for FRP Composite Connections (Mosallam 2011), which includes the standards for bolted, adhesively bound, and mixed composite joints. On a final stage, following more experimental testing, the protection coefficients used in the design of FRP profile structures are likely to be modified or updated shortly.

As previously mentioned, there are no established guidelines for the construction of hybrid FRP-concrete slabs and, thus, the criteria for conventional composite slabs have been reviewed, with particular attention to the shear relation structure and preliminary findings on reliability interaction. Adhesion (that is, mere bonding);

- frictional interlock provided by peculiar shapes of the interface profile;
- mechanical interlock provided by specific treatments and deformations of the steel interface (*i.e.*, indentations and embossments).
- dowel action provided by anchor devices and systems.

2.4.3.2. Steel-concrete composite slabs as precursor

For steel-concrete composite slabs, component contact can occur at the interface between the concrete slab and the steel profile due to the characteristics of the attachment structure. After multiple push-out experiments it was found that several variables are affected by the established load-slip relationships (Md Yatim and E. Shanmugam 2016), such as:
- joint configuration;
- number, capacity and stiffness of shear connectors;
- concrete slab strength and cracking phenomena;
- size, arrangement and strength of slab reinforcement in the proximity of the connectors;
- thickness, mean longitudinal stress and degree of compaction of the concrete surrounding the connectors;
- uplift forces on the connectors; and
- chemical bond and friction.

Construction codes usually prescribe design rules that attempt to restrict interface shear slip, as this phenomenon strongly influences the overall structural response of composite components, especially in sensitive regions where high internal forces occur. Alternatively, it has been suggested that completely composite slabs are not necessarily the most cost-effective option and that complete shear links are challenging to obtain in certain cases (Yamaguchi et al. 2005). Higher connector numbers can thus be used in construction. In addition, Eurocode 4

notes that if all cross-sections are in Class 1 or Class 2, partial shear principle can be used for slabs in structures, but only in regions of deteriorating bending moment and only for equal spans greater than 20/25 m (Herrmann and Bucksch 2014).

It also includes the calculation of tension at the serviceability limit level to take into consideration the enhanced volatility arising from significantly insufficient communication due to the slip of the shear connection. Nonetheless, where absolute shear communication is provided and a minimal shear relation is formed in houses, the effects of insufficient interaction may be ignored: (i) the specification of the shear link is in compliance with the regulations; (ii) either no fewer shear connectors are required than half the amount for the maximum shear link, or the forces arising from the elastic actions operating on the shear connectors in the serviceability limit state do not surpass the design shear capability of the connector; And (iii) in the case of a ribbed slab with ribs transversal to the base, the ribs shall not reach 80 mm in height. The deformations of a composite slab can be calculated in these conditions, assuming a stable shear relation. The Code notes that account should always be made of the impact on the deflection of concrete cracking in hogging moment areas (Neagoe 2016).

Since deflections will control geometry, in particular when slabs are built unpropped, an early draft version of Eurocode 4 (Herrmann and Bucksch 2014) gave an analytical relationship to measure deflections of clearly assisted or continuous slabs with partial shear attachment based on the construction system used, $0.4 \leq \eta < 0.5$:

$$\delta = \delta_c + c(\delta_a - \delta_c)(1-\eta) \qquad (2.1)$$

Where the degree of shear contact is measured, c = 0.3 for unpropped construction and 0.5 for propped construction, δ_c is the deflection of full association with the composite slab, and δ_a is the deflection of the steel slab working alone. The equation was borrowed from (BSI 1985), which, in addition, adapted the procedure from a description (Md Yatim and E. Shanmugam 2016) of work studies carried out on this. The subjective aspect of the interaction, which results from the impossibility of forecasting deflections correctly in a specific way, was the source of its exclusion from the final version of the Eurocode.

In the Commentary part I3 of the current Specification for Structural Steel Buildings developed by the American Institute of Steel Construction (American Institute of Steel Construction 2010), It is claimed that when a composite slab is influenced by deflection, the design will restrict the slab 's actions to the elastic spectrum under serviceability load combinations, or accept the amplification effects of inelastic action over deflection otherwise. For measure the corresponding elastic moment of inertia of a partly composite slab, the following formula is provided here:

$$I_{equiv} = I_s + \sqrt{\eta}(I_{tr} - I_s) \qquad (2.2)$$

where I_s designates the moment of inertia for the structural steel section, and I_{tr} the moment of inertia for the fully composite uncracked transformed section.

Because it is always impossible to measure exact flexural stiffness values which involve inelastic effects, the norm states that an effective value of the moment of inertia should be used as 75% of the corresponding elastic moment of inertia for short-term deflections instead. To prevent undue slippage and substantial decrease in stiffness, the minimum degree of shear contact for the implementation of this method is set at 0.25.

The Australian standard for steel-concrete composite structures that deals with the design of simply supported slabs (Standards Australia 2003):

$$Ieff = Itr + 0.6(1-\eta)\,(Is-Itr) \qquad (2.3)$$

At the cross-sections exposed to severe bending to short- or long-term loads. The effective rigidity is then used in a simplistic manner to estimate the strength of the associated deflection components, using a linear elastic structure.

Certain architecture codes preferred to create relationships to evaluate the efficient rigidity of composite slabs in operation of the shear link systems' versatility. The relative rigidity of a merely assisted two-part ($i = 1, 2$) composite members is thus conveyed through:

$$El_{\text{eff}} = \sum_{i=1}^{2} (E_i I_i + \gamma_i E_i A_i a_i^2) \qquad (2.4)$$

Where E_i, I_i, A_i, and a_i designate the elastic modulus of part i, the corresponding moment of inertia, the cross-sectional area, and respectively, the distance from the part's centroid to the slab's principal neutral axis.

The γ_i parameter is computed from:

$$\gamma_i = \left[1 + \frac{\pi^2 E_i A_i s_c}{K_c L^2}\right]^{-1} \qquad (2.5)$$

where s_c constitutes the spacing of the mechanical fasteners along the interface, K_c the slip modulus, and L the slab's span. Eurocode 5 (Arya 2009) notes that for continuous slabs or other supporting conditions, the span value should be adjusted according to the provisions. Furthermore, the suggested approach is suitable only for linear elastic analysis of composite slabs of fixed or uniformly variable connector length, with the exception of situations where the vertical acting loads produce a sinusoidal or parabolically bent moment distribution.

A second precedent was found in the Chinese Steel Structure Design Code (Chinese National Standard Management Group 2012), which indicates a particular method of measuring the deflection of steel-concrete composite slabs and is often focused on the elastic rigidity of the shear link system. The code states that interlayer slip effects, irrespective of the shear capacity of the connectors used, will be recognized when using a decreased flexural rigidity. In addition, it specifies that partial composite construction of continuous slabs with a rectangular cross-section and spans of about 20 meters is only allowable. That the increased bending stiffness just needs to be implemented in places with moments of sagging. The term given for the reduced flexural stiffness is thus:

$$B = \frac{EI_{eq}}{1 + \zeta} \qquad (2.6)$$

Where EI_{eq} represents the equivalent flexural stiffness of the composite slab under complete interaction assumptions, and a ζ reduction coefficient of stiffness adapted here in a clearer form as:

$$\zeta = \frac{EI_{eq}}{EI_0}\left[\frac{7.2}{(\alpha L)^2} - \frac{54}{(0.9\alpha L)^4}\right] ; \; \zeta \leq 0 \rightarrow \zeta = 0 \qquad (2.7)$$

Where EI_0 is the flexural stiffness of the composite slab considering no shear interaction, and αL the composite action parameter.

2.4.3.2. Analytical research studies

Because of the absence of guidelines and codes to build and test FRP-concrete hybrid structures, researchers have begun to develop their own analytical procedures. To illustrate this, (Deskovic et al. 1995) Proposed a series of mathematical relations aimed at characterizing the nonlinear flexural behavior of hybrid rectangular FPR-concrete slabs. Equations were provided and tested against experimental results for estimating the failure chain, the displacements, the fragile web shear fracture and the web shear bucking load. In a research on composite T-slabs using reduced-scale rectangular FRP tubes and concrete slabs (Chakrabortty et al. 2011). (Fam and Skutezky 2006) also studied the web shear bucking phenomenon in investigating the efficiency of external filament-wound hybrid FRP-concrete slabs, with focus on the moment-deflection reaction. (Santos Neto and La Rovere 2010),(Gonilha, Correia, and Branco 2014) Defined mathematically, in addition to the descriptions of theoretical tests, serviceability and failure aspects of hybrid GFRP-concrete footbridge girders.

The results of interlayer slip and versatility of shear contact were ignored in all the above investigations. In comparison, (Correia et al. 2009) Proposed analytical equations for calculating the bending response of single-span and multi-span hybrid GFRP-concrete slabs which took into account the slip strain forming at the interface and the additional deflection due to partial shear interaction. The slip strain was derived from a Knowles-specified formulation (Correia et al. 2010) that tests the property for a merely assisted slab submitted to a point fee. At the same period, as proposed by (Wang 1998), the deflection contribution was derived from the equation of the Euler-Bernoulli composite rod, which is clearly assisted and uniformly equipped. More recently, (Nguyen, Zatar, and Mutsuyoshi 2015) suggested an effective moment of inertia to achieve the lower flexural rigidity of specific high-performance hybrid slabs with mechanical shear connectors:

$$Ieff = IF + \eta 2(Itr - IF) \qquad (2.8)$$

where I_F designates the moment of inertia of the FRP girder, I_{tr} the moment of inertia of the fully composite FRP-concrete transformed section, and the degree of shear connection. The equation was derived from the general from presented by (Grant, Fisher, and Slutter 1977), with $m = 2$:

$$Ieff = IF + \eta m(Itr - IF) \qquad (2.9)$$

For steel-concrete girders with or without a formed steel deck, (Grant et al. 1977) suggested m = 0.5, as found later in the AISC 360-10 (American Institute of Steel Construction 2010) specifications for composite slabs with steel headed studs or steel channel anchors. For the partial interaction analysis of composite slabs with profiled sheeting and non-welded shear connectors, (Crisinel 1990) indicated a unity value for m.

In particular for composite slabs made of traditional materials such as steel, concrete and timber, several researchers have researched the question of partial shear contact. The first theoretical links were independently given for layered systemic members by (Guo et al. 2018). The static research carried out by Newmark et al. was focused on the Euler-Bernoulli composite slab theory and was a foundation for subsequent investigations, where the key hypothesis defined that the link structure is described by an elastic uniform material with constant rigidity where the interlayer shear stress is proportional to the interface slip formed. So, (Girhammar 2009) analyzed the static and fluid activity of slab-column components with interlayer slip and deduced exact and condensed closed-form solutions for the displacement functions and different internal acts of composite slabs in the first and second order.

A generalized theoretical model, tested against experimental results and design code criteria, was developed to examine the shear slip effects in steel-concrete composite slabs exposed to positive and negative bending moments (Nie and Cai 2003). The research showed that a common function of flexural stiffness reduction may be used irrespective of the charging and supporting circumstances.

(Faella, Martinelli, and Nigro 2002) Established a displacement-based finite element model for steel-concrete composite slabs with flexible shear contact and a simpler analytical technique that accounts for concrete slab cracking and the subsequent strain stiffing effect, nonlinear link action, and reduction of contact stiffness in hogging bending moment regions. The simpler method is based on the stiffness and yielding slip of the connector, and has been developed from the formula suggested by (McCutcheon 1986). However, the approach has a more analytical nature and may thus involve more adjustment. For high strength steel composite slabs (El-Sayed and Algash 2021) recommended that a revamped elastic structure be introduced for the concrete slab to measure the results of inadequate contact.

With respect to timber-concrete composite slabs with ductile connections (Frangi and Fontana 2003), an elasto-plastic model was developed, focused on the ability of the shear connectors to escape the difficulties in evaluating the shear transfer mechanism 's rigidity. The model was effectively correlated with experimental results, and tested further (Persaud and Symons 2006). The theoretical models were constructed on the Euler-Bernoulli composite slab theory in previous documents, however, a more precise technique based on the Timoshenko slab theory could be required in some cases. In particular, (Schnabl et al. 2007) and (Xu and Wu 2007) also considered the effect of transverse shear deformation on displacements in each layer of a composite slab and concluded that shear deformation is more relevant to determine for two-layer slabs with high contact rigidity, strong flexural-to-shear moduli ratio, and short duration.

(Martinelli, Nguyen, and Hjiaj 2012) Performed a comparative analysis of theoretical frameworks for composite steel-concrete slabs with limited contact using a dimensionless formulation. Based on the Timoshenko slab principle, shear-rigid and shear-flexible models were discussed, and the analysis suggested potential threshold values above which such effects were marginal, such that a simplified method might be used (Neagoe 2016).

To conclude, some of the formulations suggested to describe the flexural actions of traditional composite slabs can be applied in a clear fashion and optimized for the configuration of pultruded FRP-concrete hybrid slabs, in order to take into account, the shear contact effects correlated with the existence of the mechanical contacts in those components.

2.4.4. Numerical simulations

2.4.4.1. Introducing the Abaqus software

Abaqus is one of the most powerful software in the case of simulation based on FEM method that perform different types of analyzes very well. And due to the user-friendly environment compared to other similar software, in recent years has attracted many users.

Abaqus software is capable of analyzing metal structures, reinforced concrete structures, analyzing fluid reservoirs by considering the interaction of water and structures, concrete and earth dams as well as temperature-dependent creep analyses, heat transfer both linear and nonlinear static, as well as linear and nonlinear dynamics as well as fluid dynamics.

ABAQUS software has a graphical environment and allows the user to produce models quickly and easily, as well as to import the model geometry from another modeling software. The specifications of materials and physical characteristics can be assigned to the model, which along with Abaqus load and boundary conditions include very powerful choices in order to mesh the desired geometry and also confirm the results of the analytical model that can be seen in each stage of the analysis. Finally, after completing the model processing phase, the results can be seen graphically in the Visualization module (Sakr et al. 2021).

2.4.4.2. Suitable models for materials and characterization

Concrete is a very complex material because of its nature and even at low stress levels it behaves completely nonlinearly. The main reasons for the nonlinear concrete response, in addition to the nonlinearity of the material itself, can be summarized in the environmental effects, cracking, biaxal hardness and softening of the strain. Among the therapies presented to explain the behavior of concrete, two therapies of plasticity and the mechanism of failure are most consistent with the actual behavior of concrete, each of which predicts the behavior of reinforced concrete in many cases, but in some areas their accuracy decreases. It seems that the most complete model for simulating concrete behavior is a model that combines plasticity and failure. Such a model is obtained by researchers based on existing models, which in fact combines the isotropic behavior of elastic breakdown with the concept of isotropic plastic behavior in pressure and tension. Abaqus also utilizes such a model to simulate concrete behavior. In concrete damaged plasticity model, CDP is defined as a software for plastic behavioral concrete (in tension and pressure), which can be added to the desired failure mechanics for tension and pressure by entering appropriate parameters. To consider the effects of interaction between concrete and rebar, such as the continuity of concrete slip with rebars and the effect of throam nails, the properties of these effects can be approximately and simplified by introducing tensile hardening in the concrete model. The CDP model is capable of defining tensile hardening and therefore, with relative precision, the effect of

redisdistribution of concrete stresses after cracking can be entered into the calculations. In addition to elastic parameters (modulus of elasticity and Poisson coefficient), numerical values of five plastic parameters and specific parameters representing concrete behavior in elasticity and pressure should be given to the software by CDP model. The first parameter in introducing the plastic properties of concrete is the dilation angle (ψ) , which is the variable angle of the weberbolic function of the current potential used to define the potential of unerring plastic flow. This numerical angle is between 15 and 56 degrees and shows the slope that the plastic potential is high in enclosure stresses, and in fact the ratio of volume to shear strain changes and the bigger the concrete, the more saturable. The best angle between 15 and 30 degrees has been determined according to the tests. The second parameter of plasticity is the definition of CDP in the centered exit software or eccentricity(ε). ε Speeds up the approaching of the plastic potential function to its asymptotic, and the higher the amount, the more curvature in the low potentials. The exit value of the focus is considered as the default in the software 0.1. Another plastic specification to be introduced is the ratio of two-directional pressure succumbing stress to one-directional pressure subduing stress, which in experiments is usually numerically obtained between 1.1 and 1.16. The default value of this parameter is no later in software 1.16, which many of the researches in technical literature have considered as a suitable value for concrete types (Simulia 2019). The fourth parameter in the definition of the plasticity section of the CDP model is the K parameter, which spec determines the shape of the surrender surface and can have a value between 0.5 and 1. Another plastic specification to be introduced is the ratio of two-directional pressure succumbing stress to one-directional pressure succumbing stress, which in experiments is usually numerically obtained between 1.1 and 1.16. The default value of this parameter is no later in software 1.16, which many of the researches in technical literature have considered as a suitable value for concrete types. The last CDP parameter in the plasticity parameters is the viscosity parameter (μ) , which shows the comfort time of the viscoplastic system (Simulia 2019).

2.4.4.3. Post-failure strain stress behavior

In general, identifying the behavior after failure in concrete and expressing post-failure stresses is a function of cracked strain ε_t^{ck} .

$$\varepsilon_t^{ck} = \varepsilon_t - \varepsilon_{ot}^{el} \qquad \varepsilon_{ot}^{el} = \frac{\sigma_t}{E_0}$$

(2.10)

With bearing information, tensile damage curves in Abaqus can be obtained as:

$$d_t - \varepsilon_t^{ck}$$

(2.11)

This program automatically converts the strain values to plastic strain values:

$$\varepsilon_t^{pt} = \varepsilon_t^{ck} - \frac{d_t}{(1-d_t)} \frac{\sigma_t}{E_o}$$

(2.12)

As can be seen in Figure 11, with the amount of stress and pressure or tensile strain of concrete, the parameters of failure and elastic elasticity of concrete can be obtained equivalent plastic strain (Lee 1964).
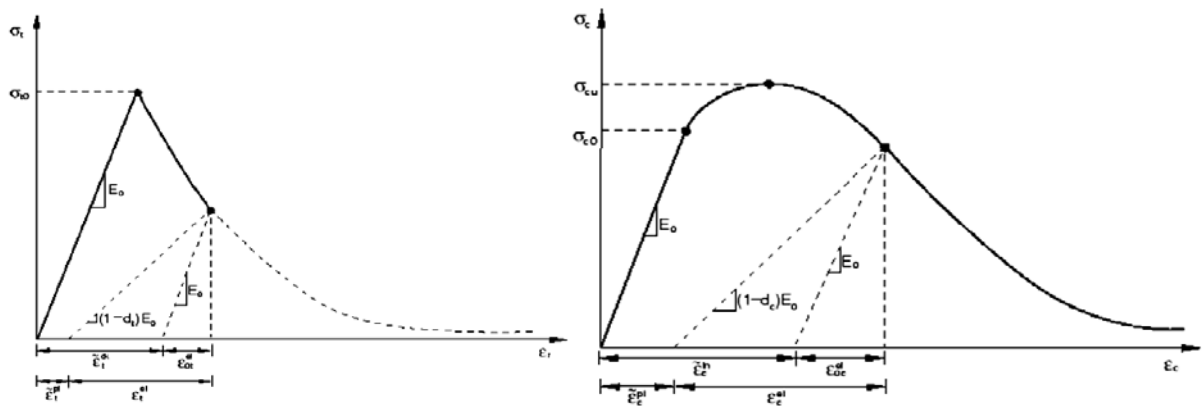
Figure 11. Plastic strain and non-elastic strain in concrete response curve to uniaxial load in tension and compression respectively from left to right (Lee 1964).

2.4.4.4. Concrete tensile behavior

As we know, when the leave occurs in reinforced concrete, it is still able to withstand some traction perpendicular to the left, which is called residual tensile hardness. There are different methods for introducing the tensile behavior of concrete to the software: strain, displacement and refusion energy. A simple linear model is used to model the tensile behavior of concrete as shown in the Figure 12 (Lee 1964).
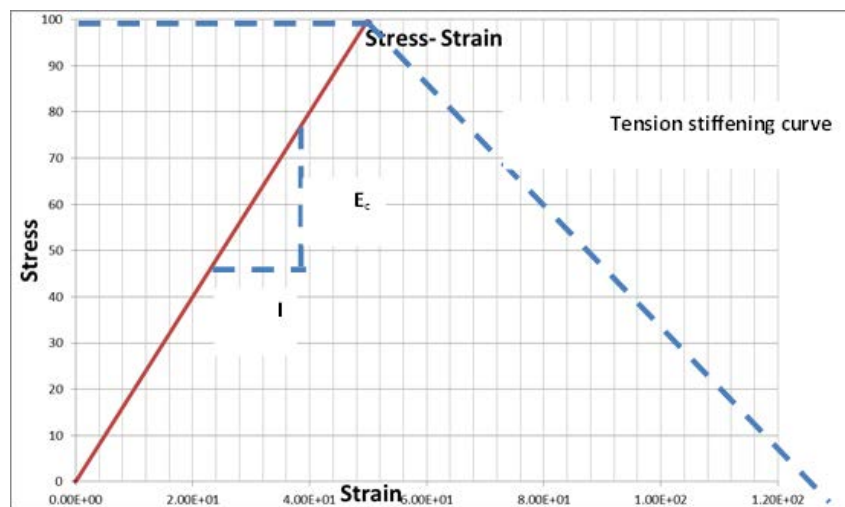

Figure 12. Curve of concrete behaviour in tensile (Lee 1964).

2.4.4.5 FRP sheets

Polymeric fibers arming in long way are hardly nonlinear behavior and consider their behavior linearly. Also, transverse loads have been observed in the deviation plane from nonlinear behavior. But the amount of nonlinearization is not comparable to in-page cutting. Usually, this nonlinear behavior, which is combined with transverse loads, can be ignored. Therefore, FRP materials have elastic and linear behavior until break-up (reaching the final strain) and suffer a curious breakdown in their final resistance. Therefore, the behavior of FRP materials

can be indicated by introducing an elastic linear behavior. Figure 13 shows FRP's stress-strain curve (Biscaia, Chastre, and Silva 2013).
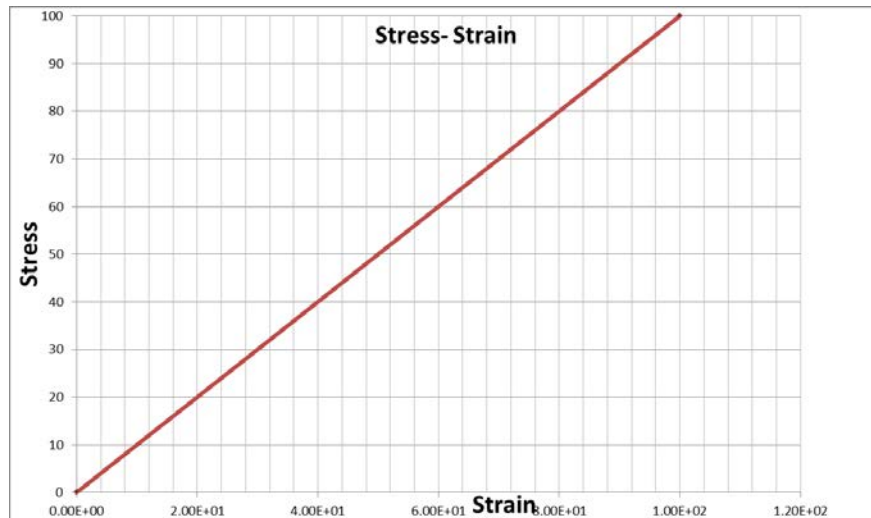

Figure 13. FRP's stress-strain curve (Biscaia et al. 2013).

2.4.4.6. Separation of FRP sheet from concrete based on developed finite element method

Separation of adhesive at the end of FRP sheet occurs when the amount of shear and axle stresses at the end of the sheet exceeds the strength of concrete. According to researches (Li et al. 2019), numerical control of the end detachment of FRP sheets can be investigated as limiting the maximum strain in FRP sheets.

Due to the nature of the failure of FRP sheets, which is usually associated with sudden failure, most of the models presented for simulation, the problem of detaching the FRP sheet from concrete has a high error. The use of the finite element method developed due to the insertion of discontinuity in the field of displacement will slow down the errors. Among them are researchers who have focused on separating the FRP sheet by the developed finite element method (Santhakumar, Chandrasekaran, and Dhanaraj 2004).

In their research, (Santhakumar et al. 2004) concluded that the use of the Heaviside function to model the separation, could not suitable. This is because there is a sudden jump in the Heaviside function. However, by distancing from the leave, the effect of leave on the points is less. For this purpose (Lee 1964) for modeling discontinuity Exponential function is used in cut-out elements.

2.5. Summary and research needs

In order to combat corrosion issues, several studies on progressively replacing steel reinforcement elements with composite ones have been conducted in recent years. Hybrid steel-concrete thin slabs in which the steel acts as formwork are also candidates for update in the coming years. Achieving a reliable connection between fiber-reinforced polymer (FRP) and cast-in-place concrete is key to promoting this technology. This study analyzed different

connection systems and proposes the novel approach of embedding a flexible fiber fabric as a superficially distributed connector between concrete and FRP.

The study presented herein analyses, for the first time, the effect of a flexible fabric mesh as a connector between CFRP sheet and concrete, for producing hybrid structures aimed to support bending efforts. The potential benefits of this study include: (i) opening the possibility of replacing thin steel sheets by FRP sheets avoiding the corrosion problems typical of aggressive environments; (ii) characterizing a connection technology based on distributing the load-transferring mechanism to be more compatible with FRP materials whose mechanical connection is always controversial; and (iii) providing the order of magnitude of the load-bearing capacity of thin slabs produced with this novel connection based on flexible fiber fabric.

3

Experimental campaign

3.1. Introduction

Recent work indicates that there is still a great need to study FRP-concrete hybrid slabs' flexural behavior experimentally, and to find structural solutions with lower costs.

The work presented in this chapter focuses on the study of the experimental structural performance of hybrid slabs constructed from carbon fiber-reinforced polymer (CFRP) sheets mechanically attached to reinforced concrete (RC), suitable for building floors as well as superstructures of footbridges.

The hybrid framework proposed is designed to maximize the key benefits of its composing materials while resolving some of the problems that characterize their individual behavior. Therefore, it is assumed that the CFRP members will primarily bear the tensile force in the composite structure, with the concrete layer serving as a compressive and stabilizing top part. Commercially available resin and fibers to manufacture CFRP was used to lower weight and normal strength concrete was chosen to improve the slab ductility. Due to the hybrid nature of the constructive method, the effect of the mechanical joint between the two constituent parts was also given special consideration.

First part of the experimental campaign (bending) focuses on the mechanical characterization of the structural response of hybrid elements made of a CFRP sheet and a concrete block on it. The connection between these two elements was performed using different alternatives that include a flexible glass fiber grid, gravel particles adhered to the inner face of CFRP or sand particles also adhered to the inner face of CFRP. This research also looks for detecting different failure modes, to analyze the load-displacement relationship and to calculate the shear stress and the neutral axis position from acquired experimental data from bending tests (Anlytical procedures are included in chapter 4).

Second part of the experimental campaign (shear) aims to investigate the interface shear mechanical response of hybrid CFRP sheet – concrete slabs characterized by using mechanical connectors such as bonded particles or a high strength glass fiber mesh. Experimental analysis of these elements is included. The experimental methodology is novel and adapted to the requirements of the definition of the proposed hybrid CFRP-concrete system and the possibility of using a flexible fabric as connector, which is also a novel idea.

3.2. Bending

3.2.1. Materials

3.2.1.1. Concrete

In this project, all specimens were cast using commercial dry concrete (FIASA HS-25) distributed in 25kg bags. It is composed of 300kg/m^3 of Portland cement with continuous 0 to 12mm of lime gravel aggregates and plasticizer. It was mixed with a water/cement ratio of 0.6, reaching a compressive strength below 25MPa.

Six non-destructive concrete impact hammer tests were conducted on each specimen just before destructive bending test in order to determine the concrete compressive strength at the testing time. The average compressive strength is summarized in Table 1 for each specimen.

3.2.1.2. CFRP sheet

CFRP sheets were manufactured from three orthogonal layers of unidirectional Masterbrace FIB 300/50 fibers. Two of these layers were placed with the fibers oriented along the slab longitudinal direction and the intermediate one was placed in the transversal direction. Fibers were impregnated with Resoltech 1204 epoxy resin. A ratio of 50% of fibers/resin was used to assure the complete impregnation of fibers even with manual brushed lay-up (see Figure 16c). These materials are show in Figure 15b. and Figure 15e., respectively. Resulting CFRP sheets were 2mm thickness. Uniaxial tensile tests on samples obtained from CFRP sheets were performed to determine the tensile strength and the elastic modulus along the longitudinal direction. These tests were conducted on the base of the ASTM international standard. The average values of elastic modulus and ultimate tensile strength of this handmade composite material were 45.55 GPa and 1120 MPa, respectively.

3.2.1.3. Mesh

Flexible glass fiber grids (alkali-resistant fiberglass), distributed as MapeGrid (G220) were bonded to the top surfaces of the CFRP sheets to perform one of the tested connection technologies between CFRP and concrete. It was intended to generate a connection system based on the mechanical interlocking of the concrete. Grid tows spacing was 25mm in both directions (see Figure 14a). The mesh was made of primed, glass fiber disposed in a woven pattern. Superficial grid weight was 225 g/m^2 and its tensile strength was 45 kN/m in the ASTM international standard. The same epoxy resin used to produce CFRP sheets was used to bond glass fiber grid to the CFRP sheet.
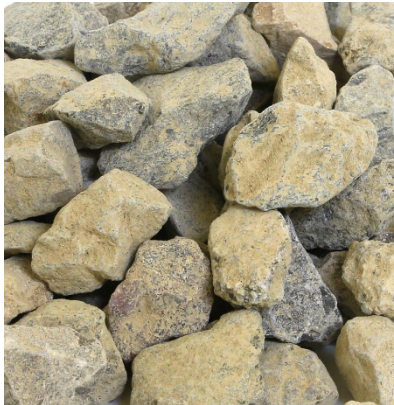
3.2.1.4. Sand and Gravel

Sand and gravel particles were used to provide a frictional connection between the lower parts of the inner side of CFRP sheet and the concrete block in some specimens. These materials are shown in Figure 15. Sand and gravel had a diameter of 0-4 mm and 5-12 mm: These were obtained from a local producer: Sorres i Graves Egara.
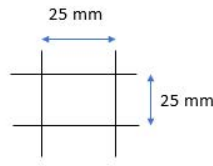
| a) Mesh | b) CFRP sheet |

| c) Gravel | d) Sand | e) Resin |

Figure 14. Materials

3.2.2 Bending tests' specimens

Eight medium scale hybrid slabs considering four connection alternatives (two specimen repetitions per alternative) were cast and tested in bending. Figure 14 represents the external geometry of all specimens. Alternative connection systems combined glass fiber mesh, gravel and sand according with the specifications listed in Table 1. Labelling of specimens was in the form of XYZ-#, where X is "S" for all cases meaning gravel was used, Y is 0 if no sand is included or "S" if sand is considered, Z is 0 if no grid was placed, "M" if mesh was included and it was aligned orthogonal to the edges of specimens or "I" if the mesh was placed with an inclination of 45º of the tows respect the longitudinal direction of the unidirectional slab. Finally, # takes the values 1 or 2 for the first and second repetitions respectively.
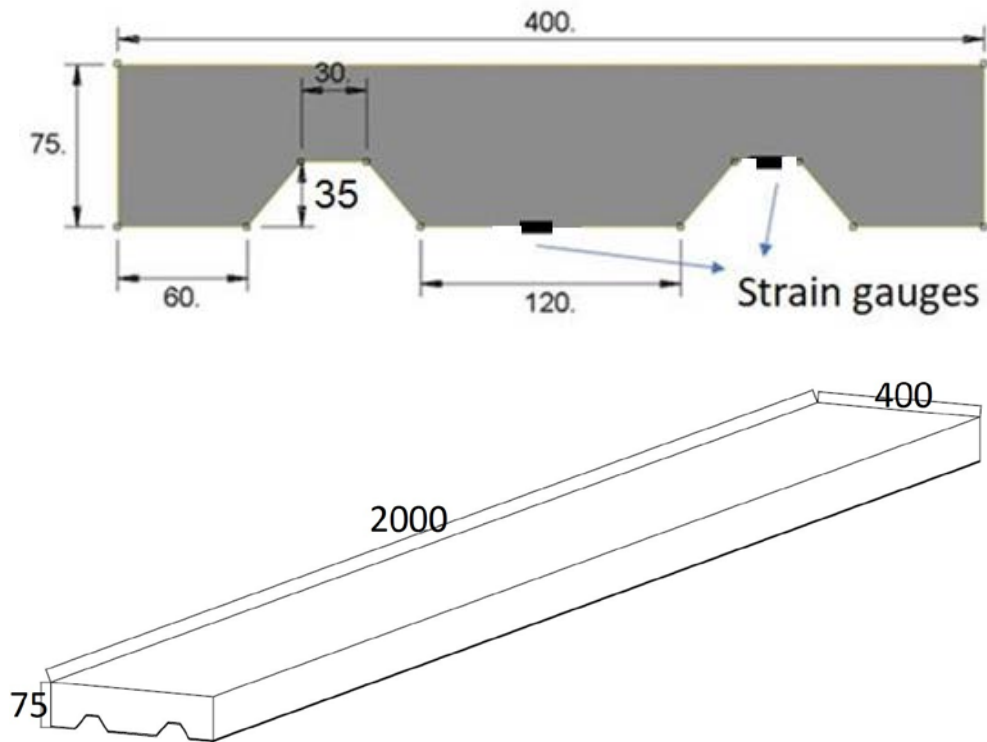
51

Figure 15. Details of the specimens (dimension are in mm)

Table 1. Details of the specimens

Specimen	Gravel	Sand	Mesh	Inclined Mesh (45°)	Concrete compressive strength (MPa)
S00-1	Y	N	N	N	19.0
S00-2	Y	N	N	N	20.8
S0M-1	Y	N	Y	N	20.0
S0M-2	Y	N	Y	N	22.6
SSM-1	Y	Y	Y	N	16.4
SSM-2	Y	Y	Y	N	20.4
SSI-1	Y	Y	N	Y	20.0
SSI-2	Y	Y	N	Y	20.9

3.2.3 Methodology

3.2.3.1. Experimental modal analysis procedure

Experimental modal analysis was used for all slab specimens to determine the vibration modes and the associated frequencies and damping ratios. Tests were conducted by impulse excitation. An impact hammer was used to excite the structure at different points (52 points) controlling the applied force along time whereas a uniaxial accelerometer was used to register the acceleration caused by impacts in a fixed point. Transient time weighting was used to acquire impact data and exponential time weighting to acquire acceleration data excluding the response force by the hammer during impact time and using only free vibration data. Slabs were simply supported during tests. More details about equipment and data post-processing may be found in (Bernat-Maso et al. 2017; Bernat-Masó and Gil 2019).

3.2.3.2 Bending test setup

Tree-points bending tests were performed on simply supported specimens. The free span was 1800mm and the load was indirectly applied through an imposed descending displacement at a rate of 1 mm/min until specimen failure. An oleo-hydraulic actuator of 50kN force range and 150mm displacement range equipped with a load cell and a LDVT was used for this purpose. A steel HEB120 profile was used as loading tool to distribute load along slab width. Vertical displacement at the load application section was also externally measured with two 100mm range potentiometers with 0.2% linearity. Two external LVDTs with 20mm range and 0.2% linearity were used to measure the relative displacement between CFRP sheet and concrete block at both slabs ends. Finally, two strain gages of 350 ohms resistance connected with 4 wires were installed on the external face of CFRP sheet at mid-span position and two different heights as observed in Figure 14. The cracks of the specimens were mapped and test observations were recorded during tests. Figure 16. shows test setup for slabs.
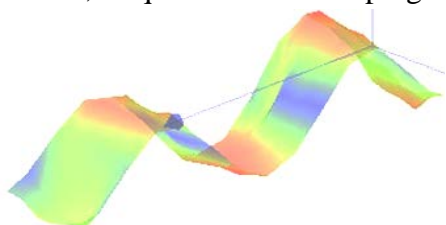

b) CFRP sheet connection before casting

a) Bending test configuration

c) Manufacturing CFRP sheet

d) Modal analysis instrument
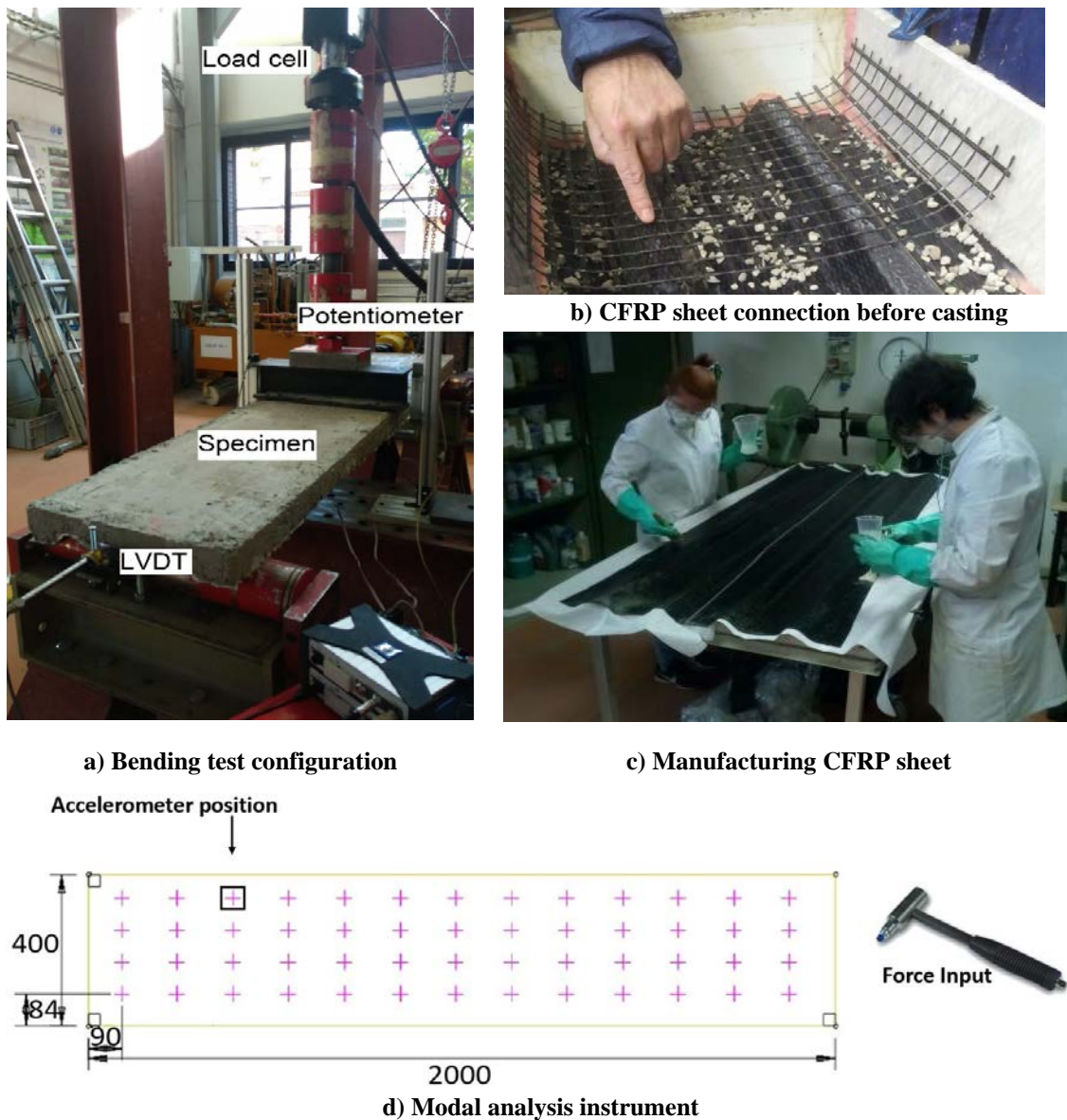
Figure 16. Test Setup

3.2.4 Tests' result

3.2.4.1. Modal analysis

Modal shapes and associated frequencies (ω) and damping ratios (ζ) were experimentally obtained from modal analysis. Table 2 summarizes the results of the vibrational response of all specimens. Only the third bending mode was identified in all tests, so it was used for comparison among them. SSM-1 specimen showed an abnormally low vibration frequency (269 Hz) in comparison with the rest of specimens. Damping ratio of SSM-1 specimen is also higher than the value for all other tests. These facts are in accordance with results of analytical calculation, that showed that internal bending moment at mid-span section, which was calculated from strain measurement, was balanced with external bending moment, which was calculated from the value of the applied load, during all test in all cases except for SSM-1 specimen. It can be observed in Figure 17 and it is explained later on in Analytical chapter.

Table 2. Vibration modes, frequencies and damping ratios for specimens

Third bending mode			
Specimen	ω (Hz)	$\bar{\omega}$ (Hz)	ζ (%)
S00-1	312	307.0	1.22
S00-2	302		1.69
S0M-1	358	367.5	1.71
S0M-2	377		1.18
SSM-1	269[1]	323 .0	4.93
SSM-2	323		1.35
SSI-1	349	332.0	1.28
SSI-2	315		2.52

[1] Discarded from average vibration frequency calculation
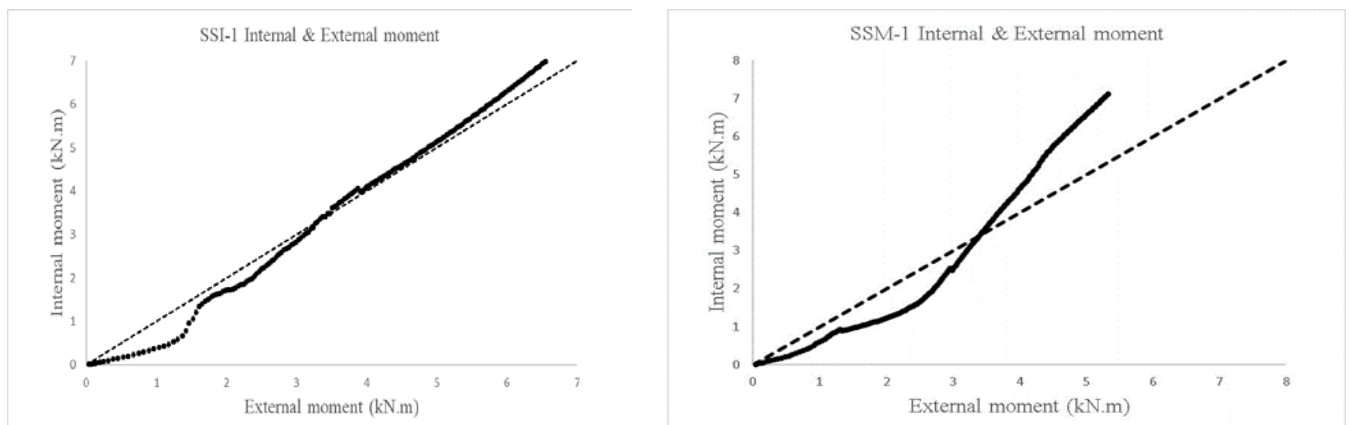
a) Balanced. SSI-1 case representing all tests except SSM-1   b) Not balanced response. SSM-1 case.

Figure 17. Internally calculated and externally calculated bending moments at mid-span.

3.2.4.2 Bending test results

Four types of plots are included to represent the structural behavior of tested slab specimens under tree-points bending test. These are force vs. vertical displacement at mid-span (see Figure 18), neutral axis position vs. vertical displacement at mid-span (see Figure 19), CFRP-concrete contact tangential stress vs. vertical displacement at mid-span (see Figure 20) and cumulative external energy vs. vertical displacement at mid-span (see Figure 21).

3.2.4.2.1. Force vs. vertical displacement

Plots representing force-vertical displacement response for all tested cases are shown in Figure 18. Vertical displacement data was obtained by averaging both external potentiometers data. All plots show similar response characterized by a first linear part up to the first crack opening (around 2kN force) and a second part which is non-linear and captures the concrete cracking process up to the maximum load. After that, some cases showed a post-failure response with load decrease.

Regarding the overall comparison of the maximum load-bearing capacity, it is observed that including the mesh connection (S0M, SSM and SSI vs. S00 specimens) causes an approximate average increase of the maximum load of 60%. It is also observed that placing sand, theoretically intended to increase frictional response, provides the opposite result reaching lower load-bearing capacities if comparing SSM with S0M specimens. Finally, it is observed that S00 group plot showed less displacement compared to other groups. Hence, incorporating the mesh to the connection system allows to reach grater deformations.
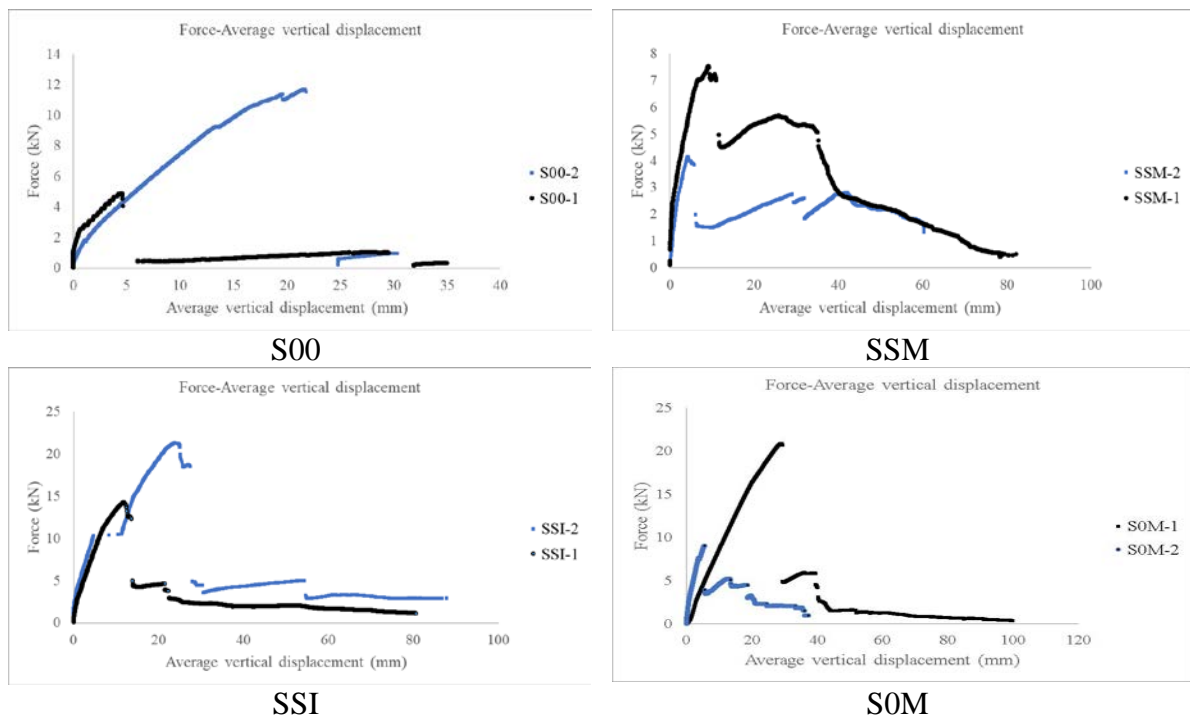

Figure 18. Force-Average vertical displacement plots.

3.2.4.2.2. Neutral axis vs. vertical displacement

Figure 19. includes neutral axis vs. vertical displacement at mid-span plots for all specimens except for the case S0M-1. Position of the neutral axis was calculated from two strain measurement points data imposing the hypothesis of strain compatibility in section. One of the strain gages of S0M-1 specimen failed and it was not possible to calculate the position of the neutral axis directly from experimental data in this case. Like in the previous section, vertical displacement was calculated with the average data of the external potentiometers.

Neutral axis 0-reference was the bottom of the section. When neutral axis position was over 35mm all CFRP sheet was subjected to tensile stresses, whereas when this variable was below 35mm it indicated that the top part of the CFRP sheet was compressed.

All cases showed a suddenly drop of the neutral axis position from over 35mm to under 35mm, which was associated with the qualitative CFRP-concrete disconnection failure observation. In addition, this drop corresponded with the maximum load applied during test. It has to be remarked that when the neutral axis was below 35mm, the fiberglass mesh was compressed, so no longer connection between CFRP and concrete was expected to be provided by this component.

The post-maximum response, after the neutral axis drop, was characterized by an almost constant value of the position of the neutral axis for all cases except SSI-1 that increased again over 30mm in a sudden change to finally decrease again.
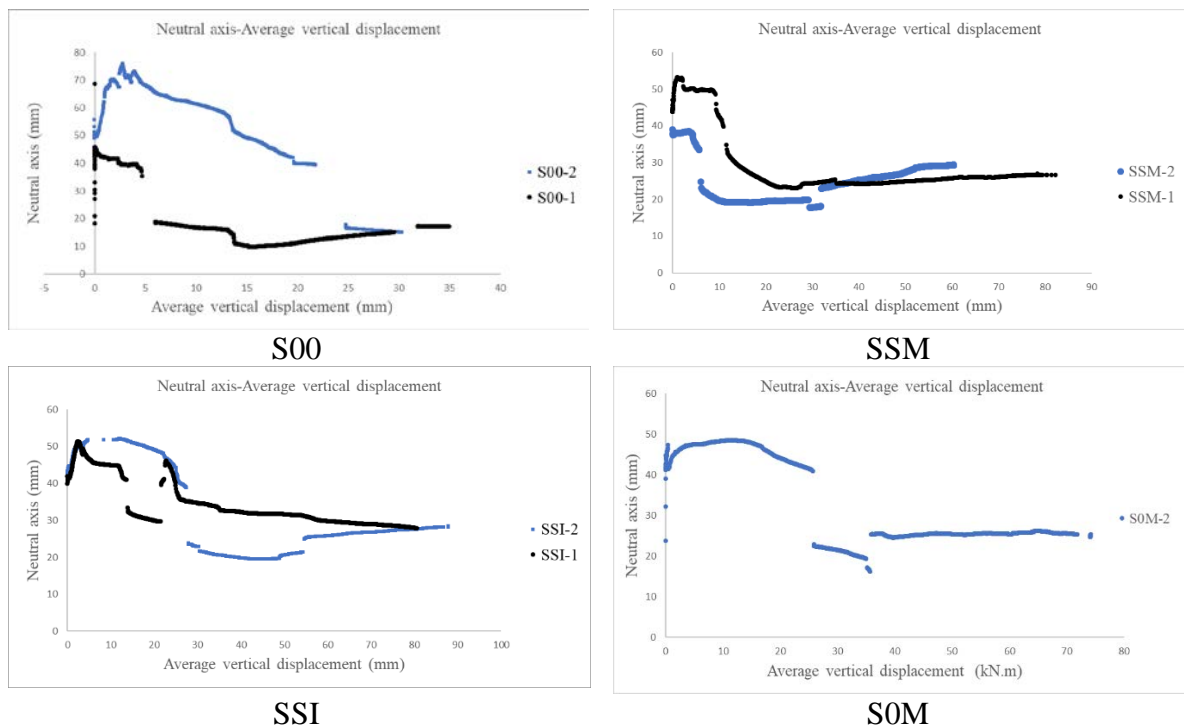

S00

SSM

SSI

S0M

Figure 19. Neutral axis -Average vertical displacement plots.

3.2.4.2.3. CFRP-concrete Shear Stress vs. vertical displacement

Figure 20. shows the CFRP-concrete connection Shear stress vs. vertical displacement plots. Like in the previous sections, vertical displacement was calculated by averaging the data from the external potentiometers. The CFRP-concrete shear stress was calculated by dividing the total compressive or tensile force normal to the mid-span section by the CFRP-concrete idealized contact surface in half of the length of the slab (length x width = 1m x 0.4m = 0,4m2). This total compressive/tensile force was calculated from strain distribution and force equilibrium, so it was not available for specimen S0M-1.

The overall shape of the plots (Figure 20) was really similar to those in Figure 18. It can be seen that after reaching the maximum shear stress, the diagram fell downward almost to 0 value for S00 cases, indicating that no connection mechanism remained after reaching the maximum load-bearing capacity. In contrast, cases SSI and S0M did not drop to zero and maintained a constant-like shear stress. Finally, SSM cases showed a secondary shear stress increment after the maximum load point.
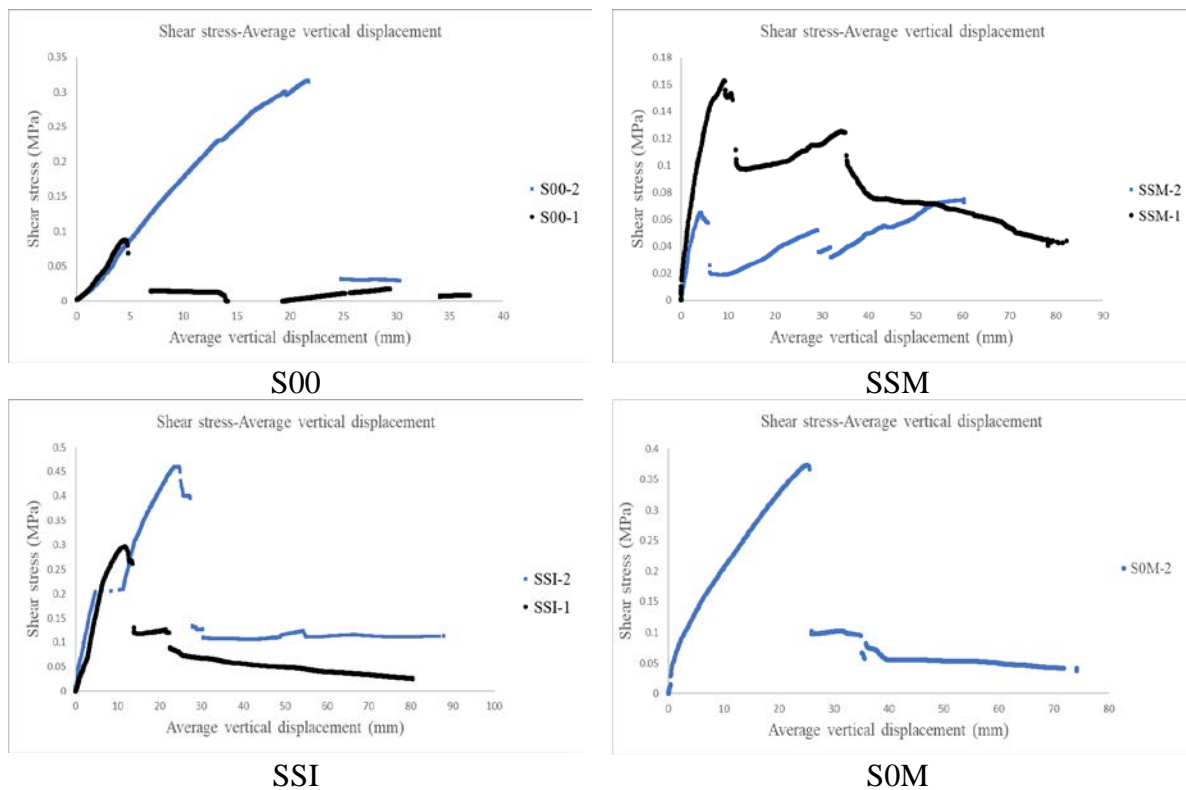
Figure 20. Shear Stress-Average vertical displacement plots.

3.2.4.2.4. External Energy vs. vertical displacement plots

Figure 21. presents the evolution of the cumulated external energy during tests. External energy was calculated from force and vertical displacement at the loaded section (mid-span). These plots are divided in two parts: before (solid line) and after (dashed line) reaching the maximum

load. The qualitative result that arises from these plots is the proportion between the energy cumulated before the peak load and the energy absorbed by the system after it, which is an indirect measurement of the energy dissipation capability of the damaged structure. Hence, this result is related with the safety this type of slabs may offer.
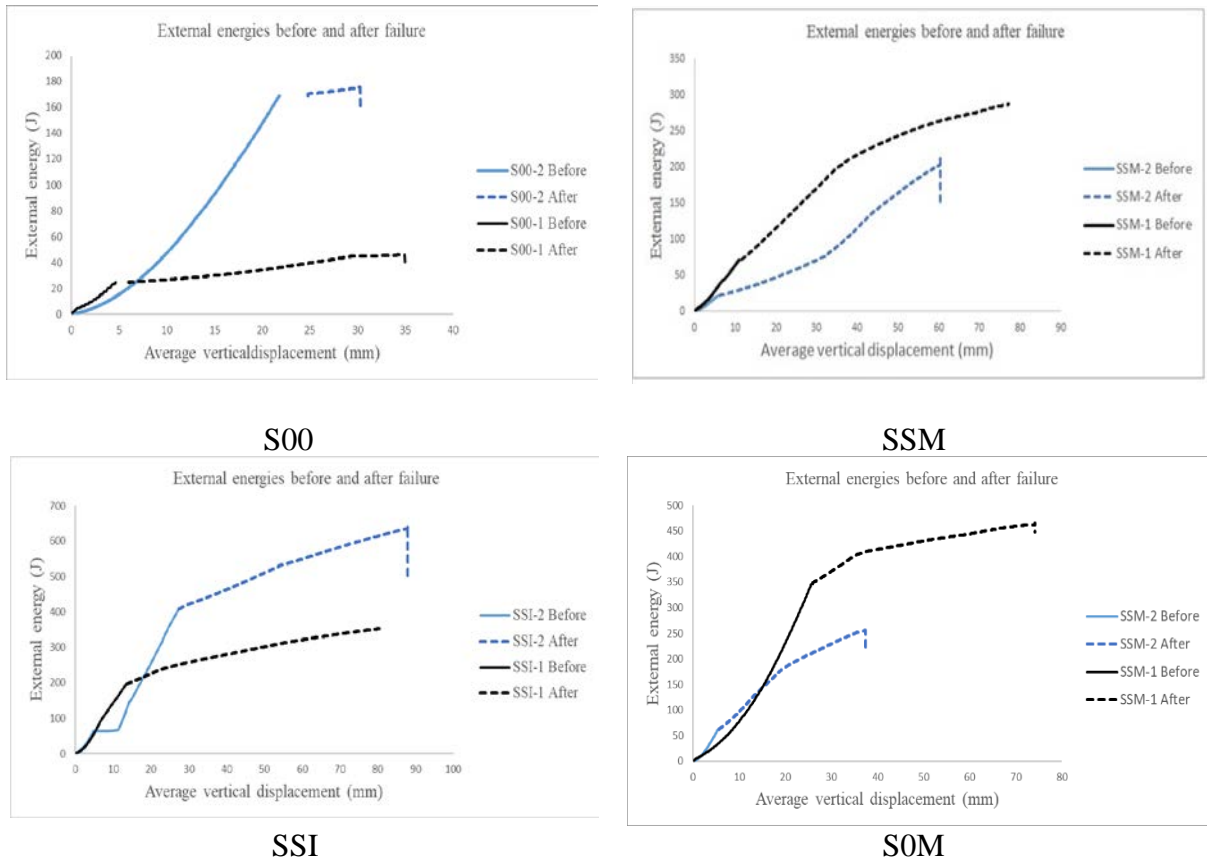

Figure 21. Cumulative external energy before and after reaching the maximum load

3.2.5 Modes of failure

Pictures of different specimens after failure are included in Figure 22. In all cases, failure was due to CFRP sheet debonding from concrete. For the cases with no connection (S00), this debonding process was sudden and completely extended along one half of the slab. For the cases with connection elements (sand, gravel, mesh), the final failure picture was really similar but the debonding process evolved progressively from the mid-span section to the slab end, including the progressive formation of bending cracks observed in the concrete block lateral face for the cases SSM and S0M. In contrast, SSI specimens showed no bending cracks before debonding.

| S00 | SSM |

| S0M | SSI |

Figure 22. Typical failure mode of all specimen types

3.2.6. Bending comparison and discussion

Initially, it has to be pointed out that the obtained results show a significant variability, which makes it not suitable to perform an individual quantitative comparison. Hence, the analysis of the influence of the different connection techniques between CFRP sheet and concrete is mostly qualitative.

First of all, non-destructive experimental modal analysis tests were effective at distinguishing between connection techniques. Incorporating the flexible mesh to connect the CFRP sheet with the concrete block made the major difference causing a significant increase of the analyzed bending vibration frequency (S00 vs. S0M). Similarly, it seems that inclining the mesh led to a stiffer response (SSI vs. SSM) whereas adhering sand particles on the internal CFRP surface (SSM vs. S0M) clearly decrease the stiffness of the hybrid structure, which may be related to a poorer CFRP-concrete connection because of promoting a sliding surface more than increasing frictional resistance.

Modal analysis results showed the abnormal response of SSM-1 specimen too, which was mostly related with a poorer concrete quality (see Table 2), that affected the CFRP sheet-concrete block compatibility according with Figure 17. However, the load-bearing capacity results showed that SSM-1 specimen resisted even greater load than its twin specimen SSM-2. Hence, the presumable negative effect on CFRP-concrete connection may had been located in the instrumented mid-span section affecting results in Figure 17 but not reducing the global structural CFRP-concrete connection thanks to the grid distribution effect.

All these data seem to indicate that modal analysis is more dependent on individual materials' properties than on connection mechanisms for the little excitation loads it works with.

Regarding the applied load, it is clear that incorporating the mesh (S0M, SSM and SSI vs. S00) allowed slabs to withstand a residual strength after reaching the maximum peak and the corresponding load drop. Hence, the mesh really acted as a connector providing concrete-CFRP partial interlocking even after connection failure. Regarding sand particles, it was observed that incorporating them caused a decrease of the load-bearing capacity (SSM vs. S0M) that was also translated into a lower vibration frequency from modal analysis. However, it has to be

remarked that in SSM case the slope of the force-displacement curve after the peak load is positive, so incrementing the supported load again. Moreover, the load drop in SSM cases is less significant than in other cases. Altogether seems to indicate a premature partial failure of the connection, which remained with enough capacity to increase the withstand load again. In comparison, other connection types with mesh (S0M and SSI), whose breaking damage was more extensive when happened, showed a greater load drop and avoided the possibility of increasing the resisted load when increasing the displacement after the maximum. Hence, sand particles weakened the connection that failed at an earlier stage.

Finally, regarding the inclination of the mesh, it seems to have a clearly positive effect on the load-bearing capacity of the slab (SSI vs. SSM). In addition, this case showed a better connection that was translated in less bending cracks developed during tests and a failure mechanism that simultaneously mobilized almost all CFRP-concrete contact surface of one half of the slab. However, this case (SSI) showed the second greater load drop due to connection failure after no mesh (S00) cases. It can also be observed in the cumulative energy plots, that showed that S00 and SSI cases are the ones that failed in a sudden way with little energy cumulated after the maximum load in comparison with S0M and SSM cases that failed in a more stepped way.

The analysis of the neutral axis position results at mid-span section clearly indicated that the slab failure happened in all cases when the neutral axe moved from a position over 35mm to a position below 35mm (0-reference at the bottom, 35mm threshold value indicating the upper position of the CFRP sheet), so the CFRP became compressed with possible local buckling failure (due to the little thickness of the sheet) and the connection mesh became also compressed losing its connection capacity. In fact, CFRP sheet local buckling was observed in S00 specimens due to the total disconnection between CFRP sheet and concrete block that left CFRP with no restrain from previously surrounding concrete.

Like in force diagram, SSM cases showed an increase of the neutral axis position after failure, which may be related with the delayed effect of the connection system that partially failed, so the damage evolved in a slower way during progressive CFRP-concrete debonding. This response is even more clear in the tangential stress plots that showed that SSM specimens were the only ones increasing the shear stress after the load drop, so definitively proving the partial failure caused by sand particles.

3.2.7. Bending experimental conclusions

After performing 8 bending tests on CFRP sheet – concrete hybrid slabs with four different connection alternatives: (i) gravel particles, (ii) gravel particles + mesh, (iii) gravel particles + sand particles + mesh and (iv) gravel particles + sand particles + inclined mesh, the following conclusions were obtained:

- Gravel particles bonded to the inner CFRP sheet surface bring superficial connection with concrete. However, this connection type is clearly fragile.
- Including a flexible structural glass fiber mesh as a connector between CFRP sheet and concrete allows to increase the load bearing capacity, produces residual strength after

connection failure and increases the stiffness of the vibrational response of slab specimens.

- Including sand particles bonded to the inner CFRP sheet surface contributes to create a weakness surface that causes an earlier partial connection failure, reducing the load-bearing capacity but increasing the relative energy absorbed by the system after failure.
- Inclining the mesh contributes to distribute shear forces more uniformly because fibers are oriented in a direction closer to the shear effort to be resisted. This configuration makes all CFRP sheet – concrete contact surface to collaborate so the load-bearing capacity increases but the failure becomes more fragile.
- All CFRP sheet – concrete hybrid slabs failed when the neutral axe moved into the CFRP area causing the top part of the CFRP, and the connection fiberglass mesh when present, to be compressed.
- Distinguishing cumulative energy before and after failure brings a qualitative estimation of the capacity of the slabs to dissipate energy after being damaged.

Finally, results seem to indicate that the optimum solution with the studied variables would have been including gravel particles and an inclined glass-fiber mesh. Hence, testing this specific combination is a must for future researches.

3.3. Shear

3.3.1. Materials

Same materials than bending specimens were used in shear part for manufacturing the specimens.

3.3.2. Shear tests' specimen

A total of ten hybrid specimens specifically designed for the direct shear test of the CFRP-concrete interface were produced and tested. All specimens were made with the same type of CFRP sheets with omega shape (see Figure 24) and the same concrete but different connection systems between them. Specimen geometry consisted of two parts with different lengths as shown in Figure 24 and Figure 26. The longer part worked as reaction side whereas the shorter part was the tested one to evaluate the CFRP-concrete connection. Tested specimens with alternative connections are listed in Table 3.

For specimens naming, the format of XYZ- # was formed, where X is 0 if gravel was not used or "S" if gravel was included, where Y is 0 if sand was excluded or "S" if sand was included, where Z is 0 if there was no grid, "M" if mesh was embedded in longitudinal-orthogonal direction or "I" if it was installed with 45º inclination of the tows respect the longitudinal axe of the specimen. For the first and second repetitions of the same test, # displays the values 1 or 2, respectively.

Figure 23. Formwork and CFRP connection of specimen S0M-1 before pouring concrete
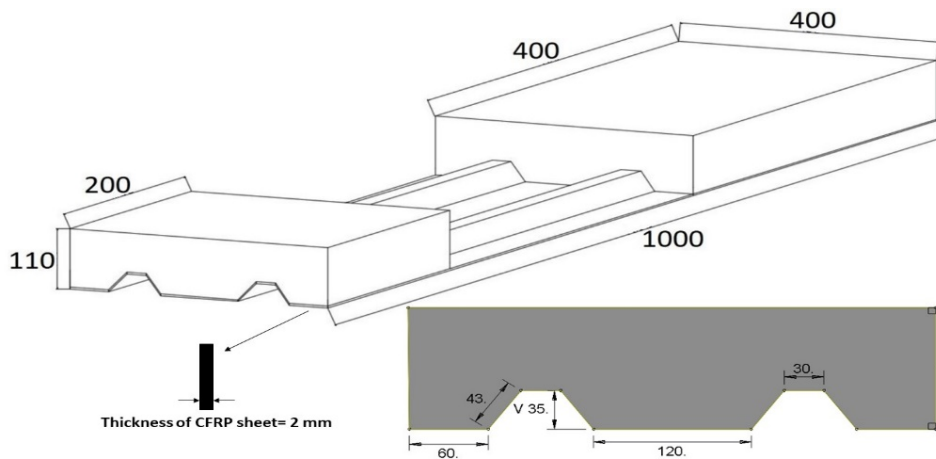

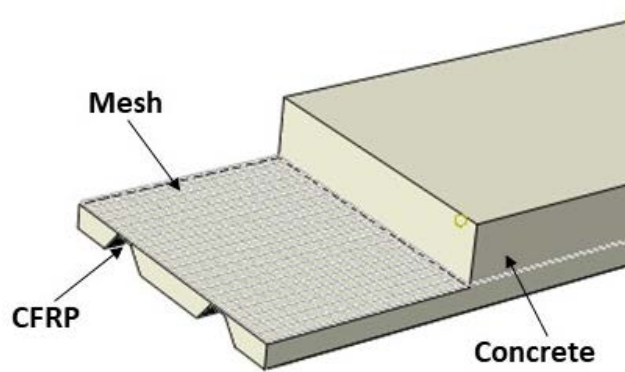Figure 24. Details of the specimens (dimensions are in mm)

Figure 25. Schematic of specimen

Table 3. Details of the specimens

Name	Gravel	Sand	Mesh	Inclined Mesh (45°)	Compressive resistance (MPa)
000-1	N	N	N	N	18.9
000-2	N	N	N	N	19.0
S00-1	Y	N	N	N	19.0
S00-2	Y	N	N	N	20.8
S0M-1	Y	N	Y	N	20.0
S0M-2	Y	N	Y	N	22.6
SSM-1	Y	Y	Y	N	19.6
SSM-2	Y	Y	Y	N	20.2
SSI-1	Y	Y	N	Y	20.0
SSI-2	Y	Y	N	Y	21

*In shear part we have one more model (000), due to reviewing impact of each material in shear test

Figure 26. Shear test setup configuration

3.3.3. Shear testing procedures and measurements

The shear test method was the same for all experimental specimens. A manual hydraulic jack was placed between the two blocks of the specimen, reacting on the longer part and testing the short one. Force was applied through a steel loading tool (U80 steel profile) that increased the contact area between the jack and the tested block to avoid local concrete damage. The applied force increased gradually and it was continuously measured with a 10kN UC9 load cell. Two LVDT sensors with a range of 20 mm and 0.02% linearity were placed to measure the relative displacement between the concrete of the shorter block and the CFRP sheet. One sensor was placed at each side of the jack to control possible in-plane rotations. A data acquisition system recorded all data at 50Hz. Figure 26 shows the test setup.

3.3.4. Shear tests' results

The force-displacement and stress-strain graphs obtained from the experimental shear tests are shown in Figure 27. It can be observed that bonding gravel to the inner face of CFRP sheet contributes to increase the shear strength (000 vs. S00). In addition, specimens without fabric (000 and S00) reached lower shear resistance than the ones with fabric (S0M, SSM and SSI). Moreover, specimens with no fabric embedded (000 and S00) showed a clear decrease of the supported force after reaching the shear strength whereas specimens with fabric (S0M, SSM and SSI) showed high residual strength after reaching the maximum shear capacity. This fact

indicates a greater capacity to dissipate energy. SSI and S0M specimens reached similar load bearing capacity, although S0M specimens are far stiffer than SSI and SSM. Regarding to the failure mode it was observed that 000 and S00 specimens failed by neat sliding of the interface between CFRP sheet and concrete whereas S0M and SSM specimens required breaking fabric fibers that remained completely bonded to the CFRP sheet. Finally, SSI showed a partial debonding of the fabric from the CFRP sheet, which is a slight curvature along longitudinal axe observed at the end of the tests. Figure 28 shows the failure mode.

000

S00

S0M

SSM

SSI
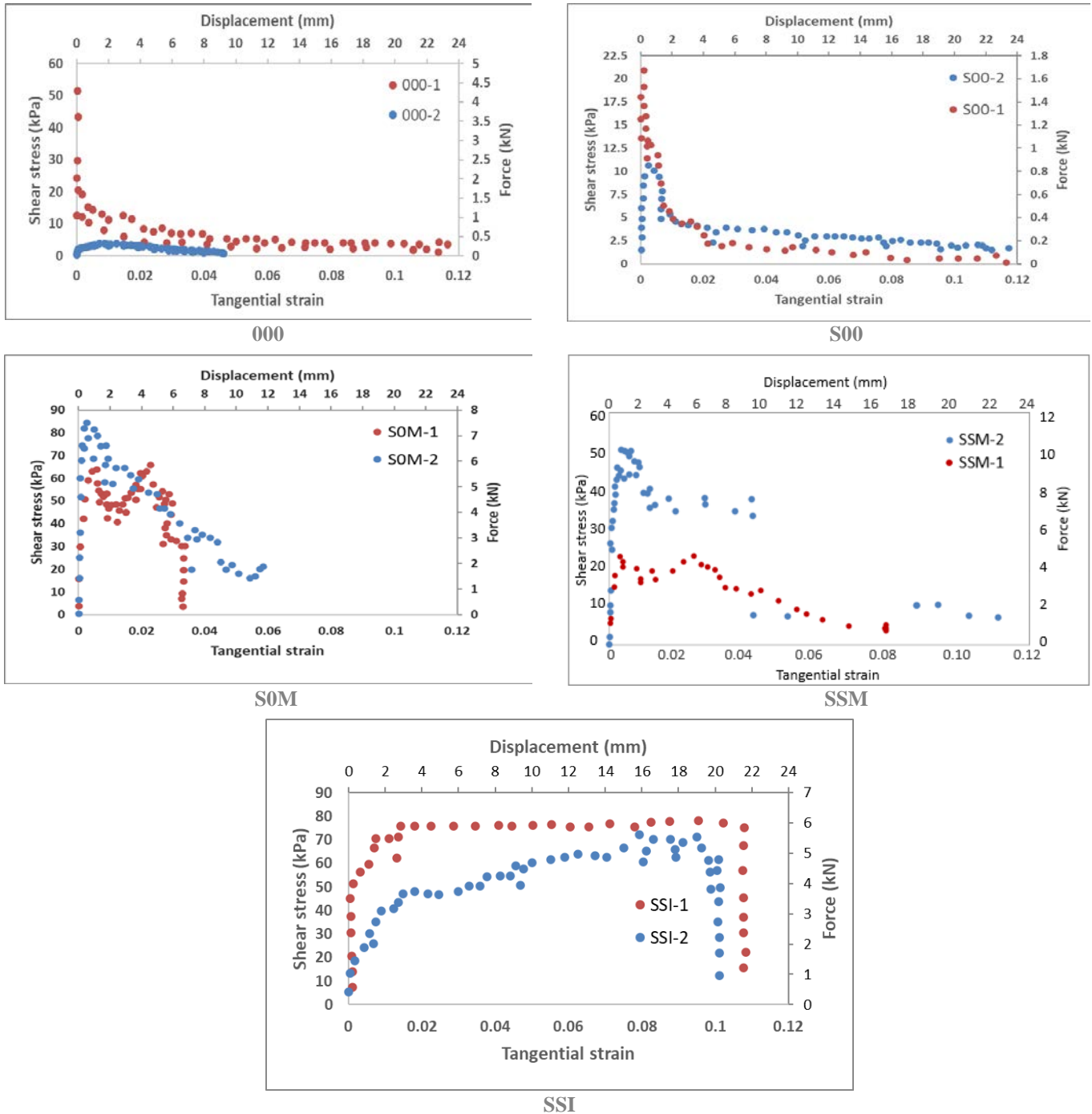
Figure 27. Force vs. relative displacement of concrete respect CFRP and Shear stress vs. average tangential strain of connection area. Experimental results.

Figure 28. Shear test failure mode.

3.2.5. Shear comparison and discussion

All specimens failed in the surface contact of CFRP and concrete. The smallest block resisted up to a maximum value of force and then physically separated from the CFRP sheet. In the case of samples 000 and S00, the failure was sudden and the load dropped instantaneously. Minor friction due to the roughness of the surfaces remained, but only for very low load values. For samples S0M and SSI, the failure was progressive. The load reached a maximum and the connection started to separate, but friction related to the existence of glass fiber meshes maintained the load value. The ultimate failure occurred with a mixed mode, combining the breakage of the fibers and the debonding of the mesh.

The force–displacement plots are shown in Figure 27. Force was measured directly and displacement was calculated as the average of both LVDTs. These plots also include the values of the average shear stress and tangential strain. The calculation of shear stress (in kPa) was performed by dividing the value of force by the surface area of the small block, which was 80,000 mm2. Moreover, the calculation of tangential strain was performed simply by dividing the average displacement measured with LVDTs (in mm) by the length of the small block, which was 200 mm.

From the plots of Figure 27, it is possible to see the differences in the performance before the nonlinear behavior was achieved. The interface with no treatment (000 case) produced very sparse results. The value of stresses ranged from 53.75 kPa to 0.37 kPa (143 times) for a mean level of strain of 0.004. The reason for this high variability relies on the unpredictable bond capacity of both materials because the samples were handmade manufactured. Basically, there is a frictional mechanism between concrete and CFRP that depends mostly on the roughness. For the S00 case, differences were smaller and the span of stresses was from 20.87 kPa to 10.63 kPa (2 times) with a mean strain of 0.002. Moreover, the inclined mesh (SSI case) presented values of stress from 51.25 kPa to 18.5 kPa (2.8 times) with a mean strain of 0.0013. Finally, the straight mesh (S0M case) spanned from 60 kPa to 29.86 kPa (2 times) with a strain of 0.004. From the analysis of stress variation, it is clear that the untreated surface showed an irregular response; therefore, this technique is not recommended for practitioners. It may produce non-

conformities in the execution that are more severe than those that occur with hand manufacturing. The surface treatment improved the homogeneity of the results. The mean average stresses presented two groups: case S00 (aggregate connections) with a level of 15.75 kPa and cases S0M and SSI (mesh connections) with a level of 44.93 kPa and 34.88 kPa, respectively. This result indicates that the loads that could withstand the connection with the meshes were larger than in other cases. Therefore, the mechanical performance of the flexible material is more competitive than the traditional roughening with aggregates.

Another significant difference could be found in the shape of the plots presented in Figure 27. For the cases 000 and S00, the level of strain within quasi-elastic behavior was very small, less than 0.002. After this, the system failed, and it was unable to bear any relevant load. The performance is clearly fragile with a sudden failure. For straight mesh (SSM), the quasi-elastic behavior occurred under very small strains of only 0.004, the same order of the other cases; however, failure did not occur. A slow hardening took place until a peak average stress of 74.07 kPa was reached, and then a softening of the system took place until a failure with a strain close to 0.046 (11 times) occurred. The failure was progressive, not sudden; it involved a mechanism that allowed the dissipation of more energy (larger area under the curve). The inclined mesh (SSI case) displayed similar behavior in the beginning, including a nonlinear hardening until a peak stress of 61.94 kPa was reached, with a strain level of 0.01, and, from this point, the system was capable of maintaining the same level of stress for an impressive failure strain of 0.11 (11 times). This indicates a pseudo-plastic behavior that dissipates a great deal of energy compared to the other systems, because the area under the plot is much larger. It is clear that there is a tightening effect of the mesh over the concrete that produces a friction mechanism.

For both samples with mesh connections, the material had a positive effect. During the loading process, after the peak load, several complex damages took place: cracking of concrete, debonding of the tows and the concrete, mechanical locking of concrete in the mesh gaps, and the breakage of threads. Nevertheless, for the SSM, damage continued to grow, and the system was unable to withstand the applied load, losing stiffness and producing a softening effect. On the contrary, the SSI was capable of maintaining the same load level. The reason for this pseudo-plasticity lies in the mesh position.

The inclined mesh has several advantages compared to the straight mesh. Firstly, the contribution of fibers to the strength comes from a tightening effect. The strength of fibers is very high compared to the levels of load, so its contribution to the load-bearing is negligible. Hence, the placement in a non-optimal direction (in terms of only the stress response) is not a limitation. Secondly, straight fibers are distributed discontinuously; there are strands only every 25 mm and hence there are important gaps with no fibers. Moreover, the flexibility of the perpendicular fibers cannot produce an effective locking mechanism in the gaps. On the contrary, the inclined mesh covers the whole width with its strands and does not leave any empty spaces without fibers. Moreover, the inclined threads can produce a more effective locking mechanism in the gaps. Hence, the inclined mesh provides a uniform response that helps to maintain a high level of friction.

3.2.6. Shear experimental conclusions

In this part, experimental study of CFRP-concrete hybrid elements subjected to in-plane interface shear tests were carried out. The mechanical response of different CFRP-concrete connection strategies (no connection, gravel, gravel + fabric and gravel + sand + inclined fabric) was analyzed and discussed. The following concluding remarks can be made:

- As expected, specimens without connectors (000) showed the weakest shear resistance. This fact may provide additional safety when calculating hybrid elements neglecting this contribution.
- Gravel components bonded to the inner CFRP sheet surface brought significant superficial connection to the concrete, causing a shear resistance increase but maintaining the brittle failure mode. Gravel particles also contribute to increase initial shear stiffness.
- Embedding a flexible structural glass fiber fabric as a connector between the CFRP sheet and the concrete increased the shear load bearing capacity and clearly enhance the post-peak shear strength, changing the failure mode to a progressive one.
- Bonding sand particles to the inner surface of the CFRP sheet seems to be counterproductive because of the formation of a weak surface that also reduces the shear stiffness of specimens. However, this statement requires further research.

The inclination of the fabric led to distribute the shear forces more evenly, because all tows are connected to concrete and CFRP sheet, stressing the full connection area in a more uniform way and allowing a maintained shear strength practically at the peak load. It means this connection showed a plastic-like response even combining only fragile materials.

Finally, the reported results suggest that the optimal solution may be combining gravel aggregates with inclined fabric without fine (sand) aggregates.

4

Analytical procedure

4.1. Introduction

Several research on the strengthening of concrete structures of the FRP have culminated in the first guidelines for the construction of concrete structures. Strengthened with FRP applied externally. Examples of such guidelines are in American (Soudki and Alkhrdaji 2005), European (FIB Bulletin 14 2001) and (ACI 440.2R-08 2008) in American. While externally bonded FRP reinforcement for concrete structures is a rapidly evolving technique (Zhang and Huang 2021), there is currently no comparable degree of reliability for the guidelines for reinforcing concrete structures with FRP. Some relevant case studies, such as the effective strengthening of a concrete bridge on the London Underground (Sen, Liby, and Mullins 2001), show the benefits of composite reinforcement. Due to the limited experimental evidence available in the literature, these hypotheses were not tested with a sufficient number of experimental findings. One of the first research on the flexural behavior of polymer composites reinforced with carbon-fiber reinforced concrete slabs is that of (El-Sayed and Algash 2021). Current design guide lines suggest a method to predict the flexural behavior of reinforced FRP components, typically within the elastic range of the materials, based on classic equilibrium and strain compatibility.

The analytical technique was validated successfully against the results obtained during the test campaign and reported in chapter 3 against useful experimental evidence for hybrid slabs. The effectiveness of using provisional communication outcome approaches has also been evaluated in this way. Validation process involves an analysis of serviceability and failure, combined with flexural action predictions. Formulas used for drawing experimental plots plus a definition of each parameter were described in the last part of the analytical portion.

4.2. Methodology

Analytical post-processing of the experimental test has been carried out with the aim of assessing the interaction phenomena or proving the total interaction of the tested connections. The calculations hypothesis is based on Euler-Bernouilli assumptions of plane section and force and moment equilibrium in the calculation section.

Linear-elastic response of FRP in tension and compression, linear elastic response of mesh in tension and parabolic-constant response of concrete in compression were assumed. No compressive contribution of mesh was considered.

In addition, total compatibility assumptions (strain continuity) were imposed in the first calculation approach to assess the possibility of total interaction between concrete and FRP. Complementary, hypothesis of constant curvature but strain gap in concrete-FRP interface was assumed to represent partial interaction case for its evaluation.

Finally, the calculation of the ultimate bending moment based on the first hypothesis of total compatibility, form material and geometry definitions are proposed.

4.2.1. Analytical post-process assuming total compatibility

Initially, Figure 29 shows a schematic representation of stress and strain distributions.

For every measurement point along testing time up to failure point, the following procedures were implemented:

The neutral axis position (x) was calculated from the strain measurement at the bottom ($\varepsilon_{b,FRP}$) and top ($\varepsilon_{t,FRP}$) of the FRP sheet:

$$x = \frac{\varepsilon_{b,FRP} \cdot H_{FRP}}{\varepsilon_{b,FRP} - \varepsilon_{t,FRP}} \qquad \text{(Eq 1)}$$

Where HFRP is the height of the FRP sheet (35mm for experimental cases).

Also, from the strain at the bottom of the FRP sheet ($\varepsilon_{b,FRP}$), the tensile young's modulus of FRP ($E_{t,FRP}$) and the area of the bottom plates ($A_{b,FRP}$), the corresponding tensile force was calculated ($F_{b,FRP}$):

$$F_{b,FRP} = A_{b,FRP} \cdot E_{t,FRP} \cdot \varepsilon_{b,FRP} \qquad \text{(Eq 2)}$$

Where $A_{b,FRP} = 480\text{mm}^2$ for tested cases and $E_{t,FRP} = 45.5\text{GPa}$ from experimental data.

Similarly, the force resulting from the normal stresses on the top plates of the FRP sheet ($F_{t,FRP}$) was calculated distinguishing if it was in tension (using $E_{t,FRP}$) or compression (using $E_{c,FRP}$):

$$F_{t,FRP} = \begin{cases} A_{t,FRP} \cdot E_{t,FRP} \cdot \varepsilon_{t,FRP} & if\ \varepsilon_{t,FRP} > 0 \\ A_{t,FRP} \cdot E_{c,FRP} \cdot \varepsilon_{t,FRP} & if\ \varepsilon_{t,FRP} < 0 \end{cases} \qquad \text{(Eq 3)}$$

Where $A_{t,FRP} = 120\text{mm}^2$ for tested cases and $E_{c,FRP} = 3.09\text{GPa}$ from resin producer data, in compression.
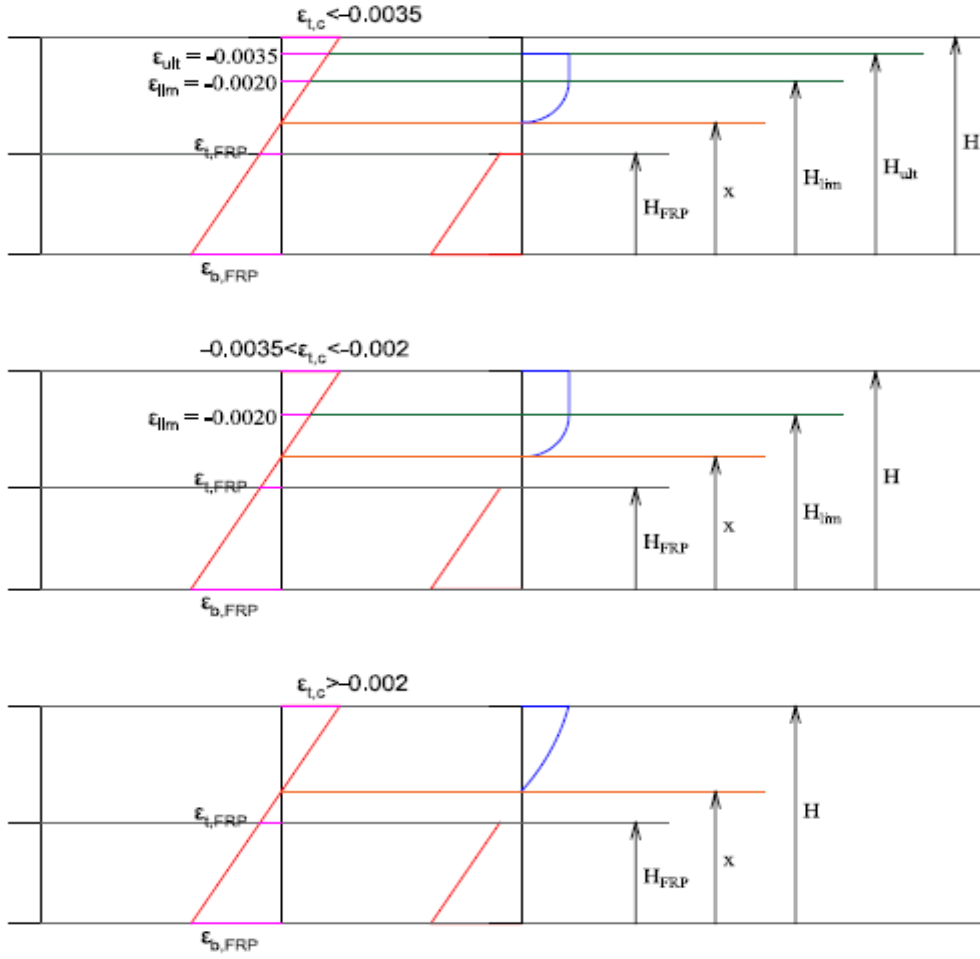
Figure 29. Strain and stress distribution for complete interaction hypothesis depending on top concrete strain case.

The force resulting from the normal stresses in inclined plates of FRP sheet section ($F_{i,FRP}$) was also calculated from the strains at bottom and top of the FRP sheet, the position of the neutral axis, the compressive and tensile young's modulus of FRP and the area of these inclined plates ($A_{i,FRP}$):

$$F_{i,FRP} = \begin{cases} A_{i,FRP} \cdot \dfrac{\varepsilon_{b,FRP} + \varepsilon_{t,FRP}}{2} \cdot E_{t,FRP} & if\ \varepsilon_{t,FRP} > 0 \\ A_{i,FRP} \cdot \left(\dfrac{x}{H_{FRP}} \cdot \dfrac{\varepsilon_{b,FRP}}{2} \cdot E_{t,FRP} + \left(1 - \dfrac{x}{H_{FRP}} \right) \right) \cdot \dfrac{\varepsilon_{t,FRP}}{2} \cdot E_{c,FRP} & if\ \varepsilon_{t,FRP} < 0 \end{cases} \quad \text{(Eq 4)}$$

Where $A_{i,FRP} = 344\text{mm}^2$ for tested cases.

The point of application of the resulting force of the inclined plates of FRP ($x_{i,FRP}$) was calculated as function of the strains measured at the top ($\varepsilon_{t,FRP}$) and bottom ($\varepsilon_{b,FRP}$) plates assuming a trapezoidal stress distribution:

$$x_{i,FRP} = \frac{\varepsilon_{t,FRP} \cdot \frac{H_{FRP}^2}{2} + \left(\varepsilon_{b,FRP} - \varepsilon_{t,FRP}\right) \cdot \frac{H_{FRP}^2}{6}}{\frac{\varepsilon_{b,FRP} + \varepsilon_{t,FRP}}{2} \cdot H_{FRP}} \qquad \text{(Eq 5)}$$

Total tensile force in FRP (F_{FRP}) was calculated by adding forces in bottom, top and inclined FRP plates:

$$F_{FRP} = F_{b,FRP} + F_{i,FRP} + F_{t,FRP} \qquad \text{(Eq 6)}$$

From the tensile strain at the top of the FRP sheet ($\varepsilon_{t,FRP}$), the tensile strength of the mesh (F_m^{ult}), the ultimate tensile strain of the mesh (ε_m^{ult}) and the width of the mesh, which is the same than the width of the specimen (b), the corresponding tensile force in the mesh was calculated ($F_{t,m}$). It is assumed that the mesh cannot withstand compressive forces and it behaves lineal elastic in tension up to failure:

$$F_{t,m} = \frac{F_m^{ult}}{\varepsilon_m^{ult}} \cdot \varepsilon_{t,FRP} \cdot b \qquad \text{(Eq 7)}$$

Where, F_m^{ult}=45kN, ε_m^{ult}=0.018 according with mesh manufacturer and b = 400mm for tested specimens. Assuming total strain compatibility, the strain at the top edge of the concrete ($\varepsilon_{t,c}$) was calculated from the bottom strain in FRP and neutral axis position:

$$\varepsilon_{t,c} = \varepsilon_{t,FRP} - \frac{\varepsilon_{b,FRP}}{x} \cdot (H - H_{FRP}) \qquad \text{(Eq 8)}$$

Where H was the total height of the specimen (75mm for tested cases).
The position (H_{lim}) of the compressive concrete strain corresponding to the limit between parabolic and constant response ($\varepsilon_{c,lim} = -0.002$) was calculated from strain compatibility as:

$$H_{lim} = H_{FRP} - \frac{x}{\varepsilon_{b,FRP}} \cdot \left(\varepsilon_{c,lim} - \varepsilon_{t,FRP}\right) \qquad \text{(Eq 9)}$$

Similarly, the position (H_{ult}) of the compressive concrete strain corresponding to the crushing failure ($\varepsilon_{c,ult} = -0.0035$) was calculated from strain compatibility as:

$$H_{ult} = H_{FRP} - \frac{x}{\varepsilon_{b,FRP}} \cdot \left(\varepsilon_{c,ult} - \varepsilon_{t,FRP}\right) \qquad \text{(Eq 10)}$$

From this point and on three situations were considered depending on the strain value calculated for the top concrete edge ($\varepsilon_{t,c}$):

4.2.2. Assuming concrete crushing ($\varepsilon_{t,c} \leq -0.0035$)

Concrete compressive force was calculated assuming two additional contributions: the parabolic stress area and the constant stress area. Rectangular concrete cross section with b width was assumed for all cases. The contribution of the parabolic area ($F_{p,c}$) was calculated

using the values of the concrete compressive strength (f_c) and the height where parabolic stress distribution was assumed, limited by neutral axis position (x) and H_{lim}:

$$F_{p,c} = \frac{2}{3} \cdot b \cdot f_c \cdot \left(H_{lim} - \left(H - abs(\varepsilon_{t,c}) \cdot \frac{x}{\varepsilon_{b,FRP}} \right) \right)$$ (Eq 11)

The contribution of the constant stress area ($F_{c,c}$) was calculated from the distance defined between H_{lim} and H_{ult}:

$$F_{c,c} = b \cdot f_c \cdot (H_{ult} - H_{lim})$$ (Eq 12)

The point of application of the compressive forces in concrete was calculated according with the position of the centre of gravity of the area enclosed by a parabola and the centre of the rectangle respectively:

$$x_{p,c} = \left(H - abs(\varepsilon_{t,c}) \cdot \frac{x}{\varepsilon_{b,FRP}} \right) + \frac{3}{5} \cdot \left(H_{lim} - \left(H - abs(\varepsilon_{t,c}) \cdot \frac{x}{\varepsilon_{b,FRP}} \right) \right)$$ (Eq 13)

(Eq 14)

$$x_{c,c} = H_{lim} + \frac{H_{ult} - H_{lim}}{2}$$

The internal bending moment resulting from stress distribution on the three component materials (FRP, mesh and concrete) was calculated by addition of the bending moment generated by the stresses on each one of them. Hence, internal bending moment (Mint) was calculated as:

$$M_{int} = M_{FRP} + M_m + M_c$$ (Eq 15)
$$M_{FRP} = M_{b,FRP} + M_{i,FRP} + M_{t,FRP}$$ (Eq 16)
$$M_{b,FRP} = F_{b,FRP} \cdot x$$ (Eq 17)
$$M_{i,FRP} = F_{i,FRP} \cdot \left(x - x_{i,FRP} \right)$$ (Eq 18)
$$M_{t,FRP} = F_{t,FRP} \cdot (x - H_{FRP})$$ (Eq 19)
$$M_m = F_{t,m} \cdot (x - H_{FRP})$$ (Eq 20)
$$M_c = M_{p,c} + M_{c,c}$$ (Eq 21)
$$M_{p,c} = F_{p,c} \cdot \left(x_{p,c} - x \right)$$ (Eq 22)
$$M_{c,c} = F_{c,c} \cdot \left(x_{c,c} - x \right)$$ (Eq 23)

Where the contribution of the FRP is divided by the contribution of each part: bottom, top and inclined. See Equations 16-19. The contribution of the mesh was calculated with and the contribution of the concrete results from adding the contribution of the parabolic (Equation 22) and rectangular (Equation 23) stress distribution areas.

This internal moment calculated from strain measurement was compared with the external bending moment calculated from the applied force (F) and the distance between supports (L) in a three-points bending test configuration:

$$M_{ext} = FL/4 \qquad \text{(Eq 24)}$$

4.2.3. Assuming concrete plasticization ($-0.002 \geq \varepsilon_{t,c} \geq -0.0035$)

The procedure was the same than for case in subsection 4.2.2 but assuming that the contribution of the constant stress area in concrete was calculated from the distance defined between H_{lim} and the total height of the specimen H:

$$F_{c,c} = b \cdot f_c \cdot (H - H_{lim}) \qquad \text{(Eq 25)}$$
$$x_{c,c} = H_{lim} + \frac{H - H_{lim}}{2} \qquad \text{(Eq 26)}$$

4.2.4. Assuming concrete in the parabolic stage ($\varepsilon_{t,c} \geq -0.002$)

The procedure for this third case was analogous to the previous ones but defining the parabolic stress distribution area on concrete between the neutral axis (x) and the total height of the specimen (H):

$$F_{p,c} = \frac{2}{3} \cdot b \cdot f_c \cdot \left(H - \left(H - abs(\varepsilon_{t,c}) \cdot \frac{x}{\varepsilon_{b,FRP}} \right) \right) \qquad \text{(Eq 27)}$$

$$x_{p,c} = \left(H - abs(\varepsilon_{t,c}) \cdot \frac{x}{\varepsilon_{b,FRP}} \right) + \frac{3}{5} \cdot \left(H - \left(H - abs(\varepsilon_{t,c}) \cdot \frac{x}{\varepsilon_{b,FRP}} \right) \right) \qquad \text{(Eq 28)}$$

In this case there was no rectangular stress area in the concrete.

4.3. Analytical post-process assuming partial compatibility

First of all, a schematic representation of stress and strain distributions is included in Figure 30. The procedure of this second general hypothesis was analogous to the total compatibility one but considering that there was a strain gap between top FRP plate and concrete at the same position. Strain in mesh was assumed to be the same than strain in the top plates of FRP, like in section 4.2. Hence, strain distribution in FRP and concrete corresponded to the same curvature (same slope was considered) but two different neutral axes were defined.
The strain in the concrete at the top FRP position ($\varepsilon_{c,F}$) was calculated as part of the strain in top FRP ($\varepsilon_{t,FRP}$):

$$\varepsilon_{c,F} = \varepsilon_{t,FRP} \cdot (1 - k) \qquad \text{(Eq 29)}$$

Where k is the interaction coefficient that has the lower value of k=0 (total interaction).
The neutral axis position for the concrete (x_c) was calculated considering the same curvature than for FRP sheet but different strain value at the level of the top plate of FRP sheet ($\varepsilon_{c,F}$):

$$x_c = H - \frac{abs(\varepsilon_{t,c}) \cdot x_F}{\varepsilon_{t,FRP}} \qquad \text{(Eq 30)}$$

$$\varepsilon_{t,c} = \varepsilon_{t,FRP} \cdot (1 - k) - \frac{\varepsilon_{b,FRP}}{x} \cdot (H - H_{FRP}) \qquad \text{(Eq 31)}$$
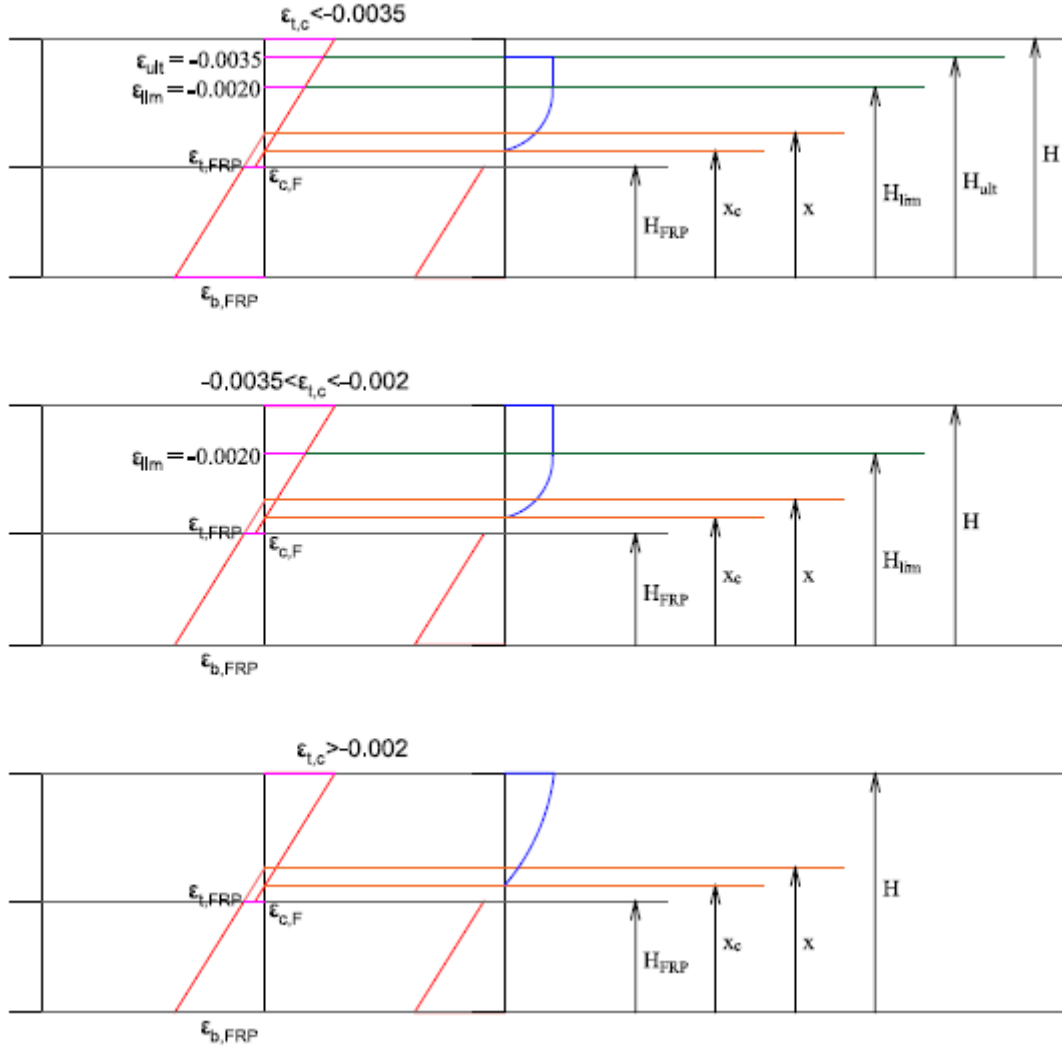
Figure 30. Strain and stress distribution for partial interaction hypothesis depending on top concrete strain case.

While $\varepsilon_{t,c}$ is the strain at the top edge of the cross-section. Depending of the value of $\varepsilon_{t,c}$ the three calculation cases (see subsections 4.2.1, 4.2.2 and 4.2.3) were implemented the same way with the only difference that internal bending moment contribution of the concrete stresses were referred to the corresponding neutral axe (x_c). Hence, changing the value of x by x_c in equations 11, 13, 22, 23, 27 and 28. The linear compression and crushing limits for concrete are also modified accordingly:

$$H_{lim} = H_{FRP} - \frac{x}{\varepsilon_{b,FRP}} \cdot \left(\varepsilon_{c,lim} - \varepsilon_{c,F}\right) \qquad \text{(Eq 32)}$$

$$H_{ult} = H_{FRP} - \frac{x}{\varepsilon_{b,FRP}} \cdot \left(\varepsilon_{c,ult} - \varepsilon_{c,F}\right) \qquad \text{(Eq 33)}$$

4.4. Calculation of theoretical load-bearing capacity assuming total compatibility

The basis of the calculation procedure of this third application of analytical model are the same than the ones described in section 1 with the following differences:
- Internal normal force equilibrium was imposed.
- One strain value is fixed according with the supposed failure mode. Hence, if the tensile failure of FRP was imposed, the fixed variable was $\varepsilon_{b,FRP} = 0.025$ obtained from tensile strength and tensile young's modulus experimentally determined. If the tensile failure of connection mesh was imposed, the fixed variable was $\varepsilon_{t,FRP} = 0.018$ indicated by mesh provider. Finally, if the compressive crushing of concrete was imposed, the fixed variable was $\varepsilon_{t,c} = -0.0035$.

These two data replace the previous strain measurements in the top and bottom plates of FRP. Iterative calculation procedure was implemented, imposing different values of the neutral axe position (x) to find the one that met the force equilibrium condition. For this position of the neutral axe, all variables can be calculated, internal bending moment is calculated and theoretical applied force that causes the considered failure mode was calculated by assuming that internal and external (three-points bending configuration) bending moments had the same value. For all calculated cases the failure mode which fulfils all other strain limits (no other materials have previously failed) was concrete crushing.

4.5. Results

Results of the analytical calculations are presented in this section. First of all, the post-process of the experimental data assuming total compatibility are exposed in figures below:
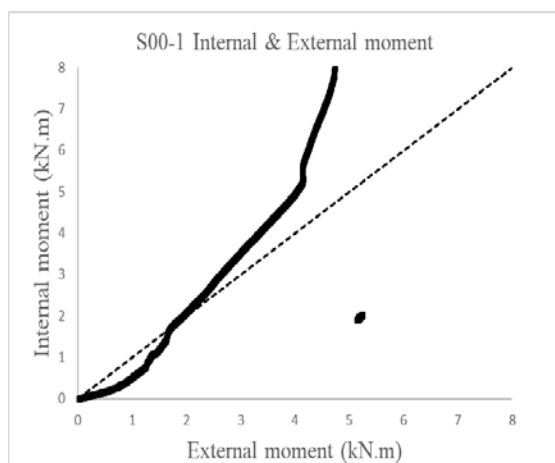
Figure 31. S00-1 response.
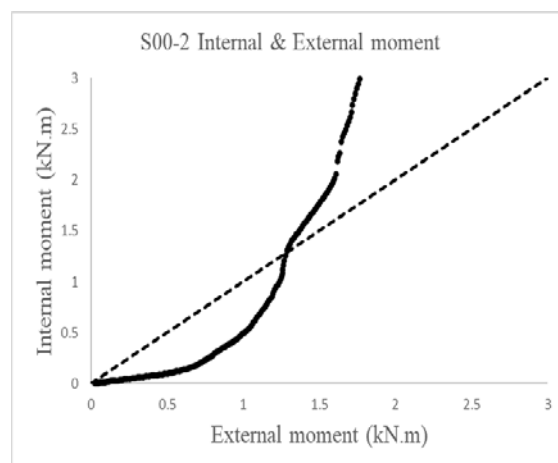
Figure 32. S00-2 response.
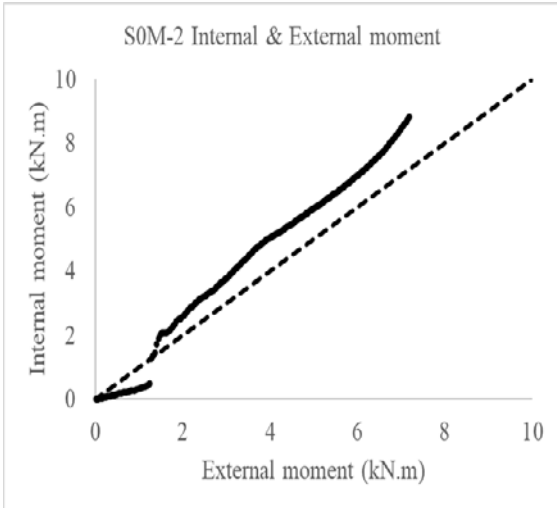
Figure 33. S0M-2 response.
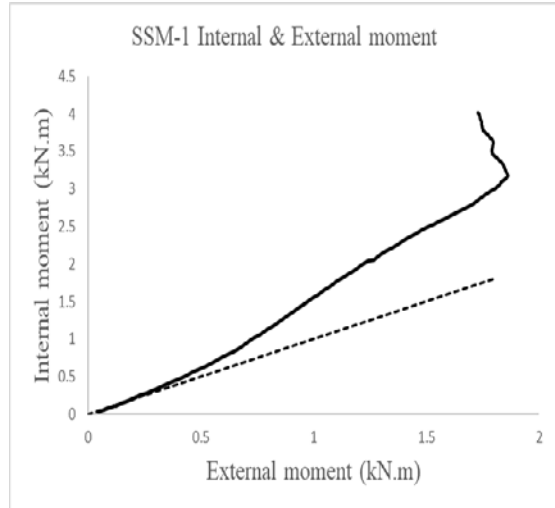
Figure 34. SSM-1 response.
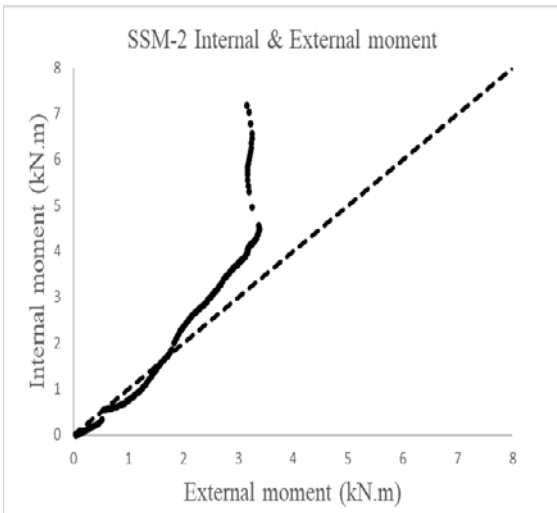
Figure 35. SSM-2 response.
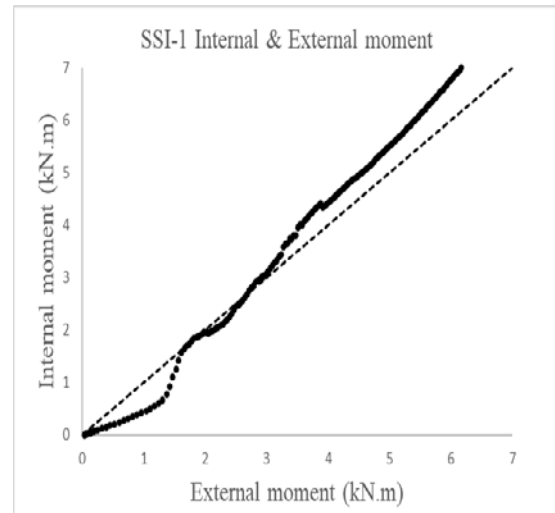
Figure 36. SSI-1response.
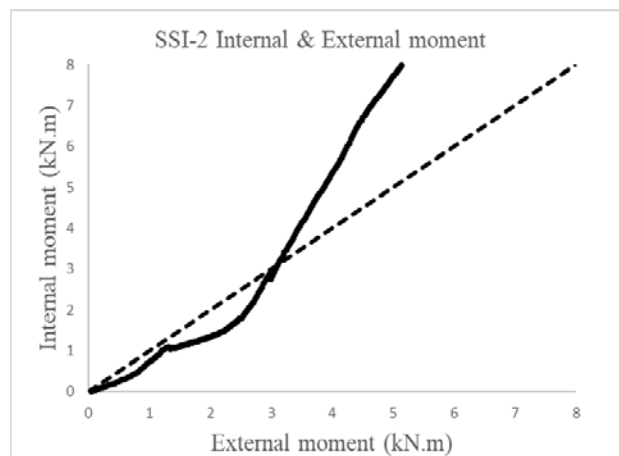
Figure 37. SSI-2 response.

As it can be seen, the fitting between internal and external bending moment can be improved. It was tested to adjust the concrete compressive strength to reduce the error in the cross-section force equilibrium. Manual compaction and poor concrete penetration may justify this

76

hypothesis of considering lower values of concrete compressive strength (Figure 38 shows voids in concrete). Results by fitting concrete compressive strength are plot in the following graphs:

Figure 38. Voids in concrete
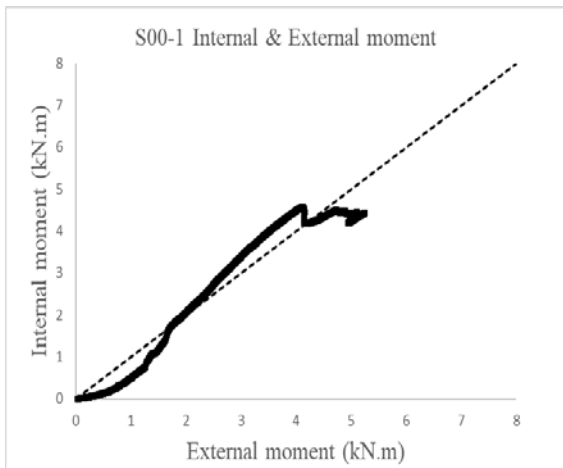
Figure 39. S00-1 response.
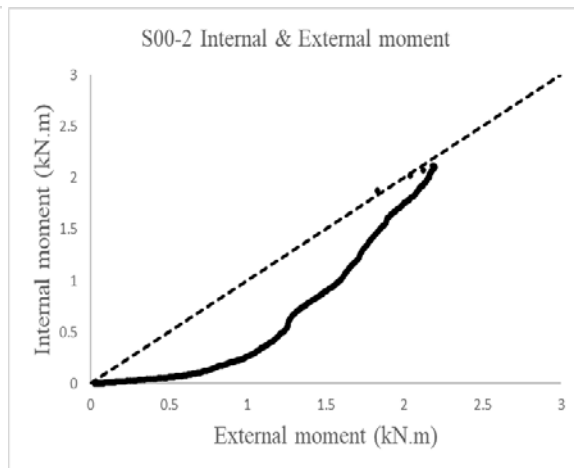
Figure 40. S00-2 response.
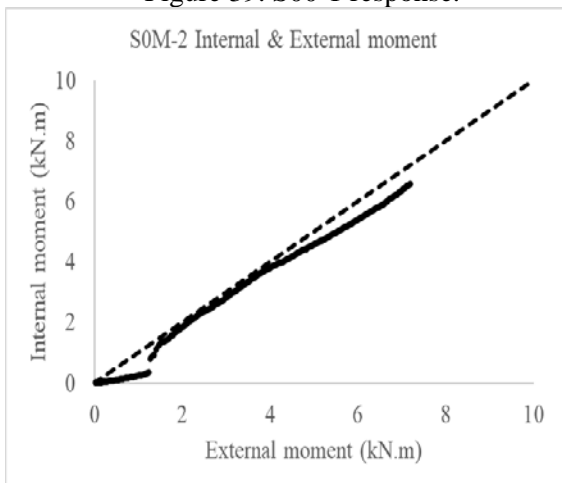
Figure 41. S0M-2 response.
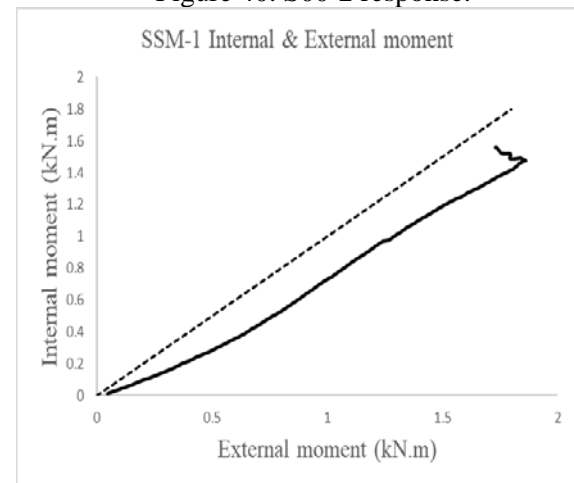
Figure 42. SSM-1 response.
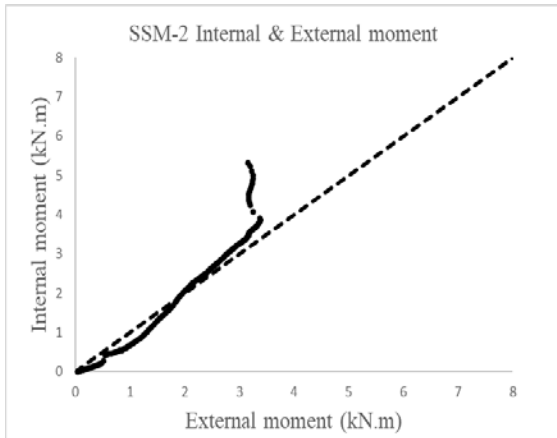
Figure 43. SSM-2 response.
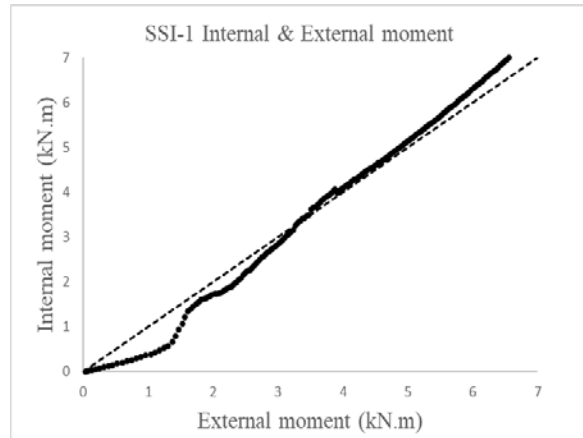
Figure 44. SSI-1 response.
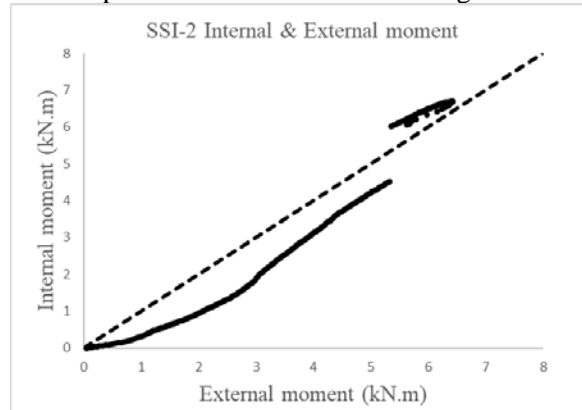
Figure 45. SSI-2 response.

After compressive strength fitting (see values of f_c in Table 4), specimens S00_2, SSM_1 and SSI_2 still sowed significant difference in the trend of internal vs. external bending moment check. The rest of specimens' calculation reduced the error, supporting the idea that superficial concrete strength measured by impact hummer may not be representative. In some of the cases the adjusted concrete compressive strength is surprisingly low, even 0, supporting the idea that concrete did not really contribute to the load-bearing capacity of those cases because of its poor quality. For S00_2, SSM_1 and SSI_2 cases it was proposed to recalculate the section equilibrium assuming partial interaction (as described before) and maintaining the adjusted value of the concrete compressive strength, aiming to adjust the value of the partial interaction coefficient (*k*). Results of optimum *k* value were 3.45, 3.07 and 0 respectively for the listed specimens. Hence, that total compatibility ruled for the case of SSI_2 specimen. Internal vs. external bending moment comparison is presented for the other two cases in the following plots:
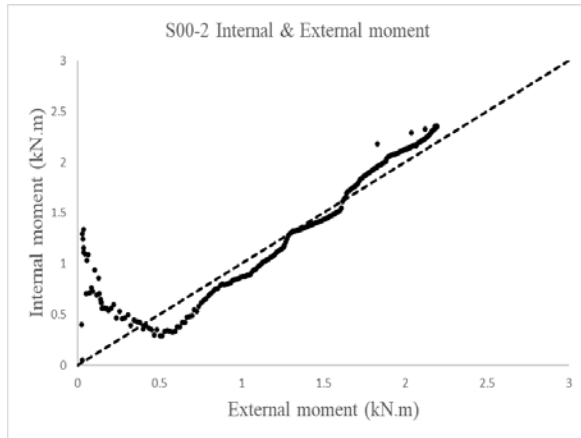
Figure 46. S00-2 response.
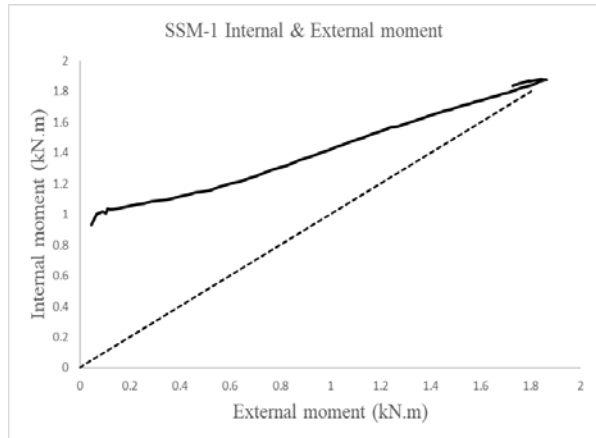
Figure 47. SSM-1 response.

It was observed that the fitting significantly improved for S00_2 case. Hence for the specimens with no specific connection elements it was correct to consider partial interaction between concrete and FRP sheet. In contrast, worse results than considering total compatibility were obtained for the case SSM_1 (note it was the case with abnormal modal response) indicating that total strain compatibility was more representative of this case. In future researches it would be interesting to also consider discontinuity in curvature to represent those cases with poor fitting even when opening the possibility of partial strain interaction. Nevertheless, these cases are not representative of the observed response, which concluded that total strain compatibility may be considered in 6 out of 7 comparison cases. Only one case of no connection technology specimen (S00_2) showed better fitting when partial strain interaction was considered.

Finally, a unique theoretical calculation considering total compatibility and material properties (only varying concrete compressive strength) was applied to predict maximum load bearing capacity of tested cases considering experimentally determined value of the concrete strength and the value obtained to fit the internal and external bending moment from experimental data post-processing as previously presented. Results are summarised in Table 4.

Table 4. Experimental data post-processing results.

Specimen	F_{exp} (kN)	Experimental fitting	Considering experimental f_c		Considering fitted f_c	
		f_c (MPa)	F (kN)	Error (%)	F (kN)	Error (%)
S00_1	11.7	0.0	24.8	112	10.2	-13
S00_2	4.9	5.1	25.3	416	16.5	237
S0M_1	9.1	---	25.1	176	25.6	181
S0M_2	20.8	10.4	25.6	23	21.4	3
SSM_1	4.1	4.3	24.1	488	15.4	276
SSM_2	7.5	13.0	25.2	236	22.8	204
SSI_1	21.3	15.0	25.1	18	23.6	11
SSI_2	14.3	2.8	25.3	77	12.5	-13

Results show that the load-bearing capacity predicted by the analytical model considering the superficial concrete strength from impact hammer tests overestimate experimental results. In contrast, when using the compressive strength of the concrete which was adjusted to internally fit the experimental tests results (external bending moment vs. internal one) considering total compatibility, it is observed that calculations meet experimental results for S00_1, S0M_2, SSI_1 and SSI_2 specimens. Hence, it can be concluded that complete strain compatibility ruled these cases. The closer results of SSI specimens point out that SSI configuration is the preferable one because it is the only connection case whose load bearing capacity was predicted with an error below 15% for the two specimens.

To finish, it is concluded that total compatibility design is preferred and SSI connection can assure it. Future designs should be carried out on this basis and those can be supported by total compatibility strain based analytical calculation procedure.

5

Conclusions and future research

5.1. Introduction

The present research was aimed at exploring the structural strength of hybrid slabs made of fiber-reinforced polymer (FRP) attached to concrete slabs, demonstrating the impact of the flexibility of the connection system on bending actions. The hybrid slabs studied will act as load-bearing members in superstructures of the building floors, platforms and footbridge.

Therefore, there is a comparative lack of research in the area of hybrid FRP-concrete slabs that needs to be covered. In addition, it can be seen that the connection systems between FRP and concrete always rely on epoxy-bonded solutions for previously cast concrete, or on mechanical punctual connectors for cast-in-place concrete. The current work was motivated by the continued absence of codes to create composite layers and then FRP-fabricated concrete sections. Therefore, the experimental program and the theoretical approach developed and used in the present thesis aim to address the issues described above, which are critical in reducing the introduction of advanced composite materials in particular types of public works and constructions currently built with traditional materials.

Overall, the objectives initially set for the development of doctoral research have been achieved and the main findings and contributions to the state of the art related to each of the main parts of the work.

Ultimately, as the report identified places where further work is also required, the thesis ends with a variety of potential lines of study.

5.2. Experimental conclusions

5.2.1 Bending

The first goal set was to describe the structural reaction of hybrid slabs with bonded CFRP slabs experimentally. In this regard, eight CFRP-concrete slabs with an omega shape have been designed and their registered behavior has been assessed from multiple perspectives and in a comparative manner.

Three-point destructive characterization assessments have been done on the specimens. The data acquired was complete and accurate enough to be used in the validation of the analytical formulations.

After performing 8 bending tests on CFRP sheet – concrete hybrid slabs with four different connection alternatives: (i) gravel particles, (ii) gravel particles + mesh, (iii) gravel particles + sand particles + mesh and (iv) gravel particles + sand particles + inclined mesh, the following conclusions were obtained:

• Gravel particles bonded to the inner surface of the CFRP sheet bring superficial connection to the concrete. And this form of relation is obviously fragile.

• Using a flexible structural glass fiber mesh as a connection between CFRP surface and concrete enables load bearing capability to be improved, provides residual strength following contact loss and improves the steadiness of the slab vibration reaction.

• The presence of sand particles bound to the internal CFRP sheet surface leads to the formation of a weakness surface that induces earlier partial contact loss, decreases load-bearing capability but increases the relative energy absorbed by the device following failure.

• The inclined orientation of the mesh leads to a more uniform application of the shear stresses, since the fibers are directed in a direction similar to the shear action to be resisted. This configuration makes all CFRP sheets – concrete contact surfaces collaborate in order to increase the load-bearing capacity but the failure becomes more fragile.

• All CFRP sheets – concrete hybrid slabs collapsed as the neutral axis passed through the CFRP region allowing the top portion of the CFRP, and the fiberglass contact mesh to be distorted as current.

• Distinguishing accumulated energy before and after failure gives a qualitative estimation of the energy dissipation potential of the slabs after damage.

• Only the third bending mode was identified in all modal analysis tests, so it was used for comparison among them. Regarding particular results, it is observed that SSM-1 specimen showed an abnormally low vibration frequency (269 Hz) in comparison with the rest of specimens.

Finally, findings seem to suggest that the optimal solution with the variables analyzed would have included gravel particles and an inclined mesh of glass fiber. Checking the specific mixture is also a must for future research.

5.2.2 Shear

In this section, there was an experimental analysis of CFRP-concrete hybrid elements that were subjected to in-plane interface shear tests. Analyzed and discussed the mechanical response of various CFRP-concrete contact strategies (no contact, gravel, gravel + fabric and gravel + sand + inclined fabric); We may make the following concluding remarks:

• As anticipated, specimens without connectors (000) displayed the lowest shear resistance, this fact can give added security when calculating hybrid elements that neglect this contribution.

• Gravel components bonded to the inside surface of the CFRP sheet also created an extensive superficial contact to the concrete, resulting in an improvement in shear resistance while retaining a brittle failure state. Gravel particles also lead to improved stability of the initial shear.

• The use of a flexible structural glass fiber mesh as a connection between the CFRP layer and the concrete improves the shear load efficiency and substantially enhances the post-peak shear power, shifting the mode of failure to progressive.

• It appears that bonding sand particles to the inner surface of the CFRP sheet is counterproductive due to the formation of a weak surface which also reduces the shear stiffness of specimens. This statement however requires further research.

• The inclination of the fabric has resulted in a more even distribution of the shear forces, since all tows are connected to concrete and CFRP sheets, stressing the full connection area in a more uniform manner and allowing the shear strength to be maintained practically at the peak load. It means this relation produced a plastic-like reaction, even though only delicate materials were combined.

Finally, the reported results suggest that the optimal solution may be combining gravel aggregates with inclined fabric without fine (sand) aggregates.

5.3. Analytical conclusion

The second purpose of the inquiry was to suggest an analytical procedure for the calculation of CFRP-concrete hybrid slabs under short-term testing, including calculations and observations for ultimate limit conditions. The following main observations are reported regarding to the analytical procedure:

• The results show that the load-bearing capacity predicted by the analytical model considering the superficial concrete strength of the impact hammer tests is overestimated by the experimental results.

• On the other hand, when using the compressive strength of the concrete that was adjusted internally for the experimental test results (external bending time vs. internal one) considering total compatibility, it is observed that the calculations meet the experimental results for the specimens S00 1, S0M 2, SSI 1 and SSI 2. It can also be inferred that such situations have been sorted out by full strain consistency.

• The closer findings of the SSI specimens suggest that the arrangement of the SSI is advantageous as it is the only contact case whose load bearing efficiency was estimated with an error of less than 15% for the two specimens.

Finally, it is concluded that an absolute compatibility assumption is desired and it can be guaranteed by SSI link. Future designs should be carried out on this basis and can be supported by a total compatibility strain based on an analytical calculation procedure.

5.5. Future lines of investigation

The carried-out investigation also outlined potential future study lines which will be explored in this section:

- All the specimens were failed because of lost connection between CFRP and concrete, so investigate to find new techniques or methods of connection between these two such as mechanical, chemical and etc. is needed.

- After failures, specimens still worked together but partially and it's because of some friction, the used material to increase the friction in this study was sand. In spite of this issue; finding more effective materials to enhance the frictional resistance is also recommended.

- There is no official code or standard for connection system between FRP and concrete, so a manual or code for design and connecting is required.

- The used FRP in this study was carbon in three layers, see the results with other FRP like basalt, aramid and glass with different thickness and layer and area is also interesting.

- In future researches it would be interesting to also consider discontinuity in curvature to represent those cases with poor fitting even when opening the possibility of partial strain interaction.

Finally, finite element models coupled with parametric studies should be built to research how various variables, such as plasticity of concrete injury, dilation angle and viscosity, and so on, influence the relationship between force and slip and the interaction rigidity defining the interface actions.

References

ACI 440.2R-08. 2008. *Guide for the Design and Construction of Externally Bonded FRP Systems for Strengthening Existing Structures*.

Alampalli, Sreenivas. 2006. "Field Performance of an FRP Slab Bridge." *Composite Structures*. doi: 10.1016/j.compstruct.2005.01.017.

American Institute of Steel Construction. 2010. "ANSI/AISC 360-10. Specification for Structural Steel Buildings." *American Institute of Steel Construction*.

Anon. 1996. "Analysis and Design." *Fiber Composites in Infrastructure. Proceedings Conference Tucson, 1996*. doi: 10.1680/bce.58088.343.

Arya, Chanakya. 2009. "Eurocode 5: Design of Timber Structures." in *Design of Structural Elements*.

Bank, Lawrence C. 1987. "Shear Coefficients for Thin-Walled Composite Beams." *Composite Structures*. doi: 10.1016/0263-8223(87)90015-8.

Bank, Lawrence C. 2013. "Progressive Failure and Ductility of FRP Composites for Construction: Review." *Journal of Composites for Construction*. doi: 10.1061/(asce)cc.1943-5614.0000355.

Bedon, Chiara, and Christian Louter. 2016. "Finite-Element Numerical Simulation of the Bending Performance of Post-Tensioned Structural Glass Beams with Adhesively Bonded CFRP Tendons." *American Journal of Engineering and Applied Sciences*. doi: 10.3844/ajeassp.2016.680.691.

Bernat-Masó, Ernest, and Lluís Gil. 2019. "Assessing the Performance of CFRP Strengthening on Masonry Walls Using Experimental Modal Analysis." *Engineering Structures* 193:184–93. doi: 10.1016/j.engstruct.2019.05.036.

Bernat-Maso, Ernest, Elitsa Teneva, Christian Escrig, and Lluís Gil. 2017. "Ultrasound Transmission Method to Assess Raw Earthen Materials." *Construction and Building Materials* 156:555–64. doi: 10.1016/j.conbuildmat.2017.09.012.

Biscaia, Hugo C., Carlos Chastre, and Manuel A. G. Silva. 2013. "Linear and Nonlinear Analysis of Bond-Slip Models for Interfaces between FRP Composites and Concrete." *Composites Part B: Engineering*. doi: 10.1016/j.compositesb.2012.08.011.

BSI. 1985. "Structural Use of Steelwork in Building." *Part*.

de Buhan, Patrick, Jérémy Bleyer, and Ghazi Hassen. 2017. "Mechanical Modeling of Reinforced Materials as Multiphase Systems." in *Elastic, Plastic and Yield Design of Reinforced Structures*.

Canning, L., L. Hollaway, and A. M. Thorne. 1999. "An Investigation of the Composite Action of an FRP/Concrete Prismatic Beam." *Construction and Building Materials* 13(8):417–26. doi: 10.1016/S0950-0618(99)00050-1.

Chakrabortty, Anup, Amar Khennane, Obada Kayali, and Evgeny Morozov. 2011. "Performance of Outside Filament-Wound Hybrid FRP-Concrete Beams." *Composites Part B: Engineering*. doi: 10.1016/j.compositesb.2011.01.003.

Chinese National Standard Management Group. 2012. "GB50017-201X. Code for Design of Steel Structures."

Correia, João R., Fernando A. Branco, and João G. Ferreira. 2007. "Flexural Behaviour of GFRP-Concrete Hybrid Beams with Interconnection Slip." *Composite Structures*. doi: 10.1016/j.compstruct.2005.06.003.

Correia, Joao R., Fernando Branco, José Gonilha, Nuno Silva, and Dinar Camotim. 2010. "Glass Fibre

Reinforced Polymer Pultruded Flexural Members: Assessment of Existing Design Methods." *Structural Engineering International: Journal of the International Association for Bridge and Structural Engineering (IABSE).* doi: 10.2749/101686610793557771.

Correia, João Ramôa, Fernando A. Branco, and João Ferreira. 2009. "GFRP-Concrete Hybrid Cross-Sections for Floors of Buildings." *Engineering Structures.* doi: 10.1016/j.engstruct.2008.04.021.

Crisinel, Michel. 1990. "Partial-Interaction Analysis of Composite Beams with Profiled Sheeting and Non-Welded Shear Connectors." *Journal of Constructional Steel Research.* doi: 10.1016/0143-974X(90)90043-G.

Dan, D., V. Stoian, T. Nagy Gyorgy, A. Fabian, C. Daescu, C. Florut, and I. Demeter. 2010. "The Behaviour of Steel and Steel Concrete Composite Joints." in *Structures and Architecture - Proceedings of the 1st International Conference on Structures and Architecture, ICSA 2010.*

Deskovic, Nikola, Thanasis C. Triantafillou, and Urs Meier. 1995. "Innovative Design of FRP Combined with Concrete: Short-Term Behavior." *Journal of Structural Engineering.* doi: 10.1061/(asce)0733-9445(1995)121:7(1069).

Drzal, L. T., and M. Madhukar. 1993. "Fibre-Matrix Adhesion and Its Relationship to Composite Mechanical Properties." *Journal of Materials Science.* doi: 10.1007/BF01151234.

El-Sayed, Taha A., and Yasser A. Algash. 2021. "Flexural Behavior of Ultra-High Performance Geopolymer RC Beams Reinforced with GFRP Bars." *Case Studies in Construction Materials* 15(March):e00604. doi: 10.1016/j.cscm.2021.e00604.

Faella, Ciro, Enzo Martinelli, and Emidio Nigro. 2002. "Steel and Concrete Composite Beams with Flexible Shear Connection: 'Exact' Analytical Expression of the Stiffness Matrix and Applications." *Computers and Structures.* doi: 10.1016/S0045-7949(02)00038-X.

Fam, Amir, and Hart Honickman. 2010. "Built-up Hybrid Composite Box Girders Fabricated and Tested in Flexure." *Engineering Structures.* doi: 10.1016/j.engstruct.2009.12.029.

Fam, Amir, and Trevor Skutezky. 2006. "Composite T-Beams Using Reduced-Scale Rectangular FRP Tubes and Concrete Slabs." *Journal of Composites for Construction.* doi: 10.1061/(asce)1090-0268(2006)10:2(172).

Fardis, Michael N., and Homayoun H. Khalili. 1982. "FRP-Encased Concrete as a Structural Material." *Magazine of Concrete Research.* doi: 10.1680/macr.1982.34.121.191.

FIB Bulletin 14. 2001. *CEB FIB Bulletin 14, Externally Bonded FRP Reinforcement for RC Structures.*

Fiberline Composites. 2003. "Fiberline Design Manual." *Composites.*

Firmo, João P., João R. Correia, and P. França. 2012. "Fire Behaviour of Reinforced Concrete Beams Strengthened with CFRP Laminates: Protection Systems with Insulation of the Anchorage Zones." *Composites Part B: Engineering.* doi: 10.1016/j.compositesb.2011.09.002.

Frangi, Andrea, and Mario Fontana. 2003. "Elasto-Plastic Model for Timber-Concrete Composite Beams with Ductile Connection." *Structural Engineering International: Journal of the International Association for Bridge and Structural Engineering (IABSE).* doi: 10.2749/101686603777964856.

Gai, Xian, Antony Darby, Tim Ibell, and Mark Evernden. 2011. "Permanent Participating FRP Formwork for Concrete Floor Slabs." in *American Concrete Institute, ACI Special Publication.*

Girhammar, Ulf Arne. 2009. "A Simplified Analysis Method for Composite Beams with Interlayer Slip." *International Journal of Mechanical Sciences.* doi: 10.1016/j.ijmecsci.2009.05.003.

Gonilha, José A., João R. Correia, and Fernando A. Branco. 2014. "Structural Behaviour of a GFRP-Concrete Hybrid Footbridge Prototype: Experimental Tests and Numerical and Analytical Simulations." *Engineering Structures.* doi: 10.1016/j.engstruct.2013.12.018.

Grant, John A., John W. Fisher, and Roger G. Slutter. 1977. "COMPOSITE BEAMS WITH FORMED

STEEL DECK." *Engineering Journal*.

Gray, E. F., H. C. Browne, W. Burkhardt, T. J. Fowler, A. Lizzio, J. F. I. McDermott, D. E. White, G. O. Widera, C. H. Zweben, S. J. Gozzo, and A. Green. 1984. "Structural Plastics Design Manual." *Manuals and Reports on Engineering Practice, American Society of Civil Engineers* (63).

Grimaldi, Antonio. 2007. "Guide for the Design and Construction of Structures Made of FRP Pultruded Elements." *Cnr-Dt 205/2007*.

Guo, Yu-Tao, Mu-Xuan Tao, Xin Nie, Sheng-Yuan Qiu, Liang Tang, and Jian-Sheng Fan. 2018. "Experimental and Theoretical Studies on the Shear Resistance of Steel–Concrete–Steel Composite Structures with Bidirectional Steel Webs." *Journal of Structural Engineering* 144(10):04018172. doi: 10.1061/(asce)st.1943-541x.0002182.

Gutiérrez, E., S. Primi, J. M. Mieres, and I. Calvo. 2008. "Structural Testing of a Vehicular Carbon Fiber Bridge: Quasi-Static and Short-Term Behavior." *Journal of Bridge Engineering*. doi: 10.1061/(asce)1084-0702(2008)13:3(271).

Hassan, A. M. T., S. W. Jones, and G. H. Mahmud. 2012. "Experimental Test Methods to Determine the Uniaxial Tensile and Compressive Behaviour of Ultra High Performance Fibre Reinforced Concrete(UHPFRC)." *Construction and Building Materials*. doi: 10.1016/j.conbuildmat.2012.04.030.

Herrmann, Helmut, and Herbert Bucksch. 2014. "Eurocode 4 - Design of Composite Steel and Concrete Structures." in *Dictionary Geotechnical Engineering/Wörterbuch GeoTechnik*.

Hollaway, L. C. 2003. "The Evolution of and the Way Forward for Advanced Polymer Composites in the Civil Infrastructure." in *Construction and Building Materials*.

Hollaway, L. C. 2010. "A Review of the Present and Future Utilisation of FRP Composites in the Civil Infrastructure with Reference to Their Important In-Service Properties." *Construction and Building Materials*.

Honickman, Hart, and Amir Fam. 2009. "Investigating a Structural Form System for Concrete Girders Using Commercially Available GFRP Sheet-Pile Sections." *Journal of Composites for Construction*. doi: 10.1061/(asce)cc.1943-5614.0000039.

Jnaid, Fares. 2020. "Guidelines for Flexural Design of FRP Reinforced Concrete Beams." *Journal of Composite Materials* 55:002199832097373. doi: 10.1177/0021998320973735.

Jumaat, M. Z., M. M. Rahman, and M. A. Rahman. 2011. "Review on Bonding Techniques of CFRP in Strengthening Concrete Structures." *International Journal of Physical Sciences*.

Karayaka, Metin, and Huseyin Sehitoglu. 1996. "Failure Behavior of Unidirectional AS4/3501-6 Carbon/Epoxy Laminates." *Journal of Composite Materials*. doi: 10.1177/002199839603001005.

Karbhari, Vistasp M., and Lei Zhao. 2000. "Use of Composites for 21st Century Civil Infrastructure." *Computer Methods in Applied Mechanics and Engineering*. doi: 10.1016/S0045-7825(99)90270-0.

Karim, Mohammed R., and Michelle S. Hoo Fatt. 2006. "Rate-Dependent Constitutive Equations for Carbon Fiber-Reinforced Epoxy." *Polymer Composites*. doi: 10.1002/pc.20221.

Khalifa, Ahmed, and Antonio Nanni. 2002. "Rehabilitation of Rectangular Simply Supported RC Beams with Shear Deficiencies Using CFRP Composites." *Construction and Building Materials*. doi: 10.1016/S0950-0618(02)00002-8.

Kim, Yail J., and Amir Fam. 2011. "Numerical Analysis of Pultruded GFRP Box Girders Supporting Adhesively-Bonded Concrete Deck in Flexure." *Engineering Structures*. doi: 10.1016/j.engstruct.2011.07.016.

Lee, E. H. 1964. "Elastic-Plastic Deformation at Finite Strains." *Journal of Applied Mechanics, Transactions ASME*. doi: 10.1115/1.3564580.

Lesko, John J., and Thomas E. Cousins. 2013. "Extren Dwb® Design Guide." 48.

Li, Wen, Wei Chen, Liqun Tang, Zhenyu Jiang, and Peiyan Huang. 2019. "A General Strength Model for Fiber Bundle Composites under Transverse Tension or Interlaminar Shear." *Composites Part A: Applied Science and Manufacturing*. doi: 10.1016/j.compositesa.2019.03.009.

Martinelli, Enzo, Quang Huy Nguyen, and Mohammed Hjiaj. 2012. "Dimensionless Formulation and Comparative Study of Analytical Models for Composite Beams in Partial Interaction." *Journal of Constructional Steel Research*. doi: 10.1016/j.jcsr.2012.02.016.

McCutcheon, William J. 1986. "Stiffness of Framing Members with Partial Composite Action." *Journal of Structural Engineering*. doi: 10.1061/(asce)0733-9445(1986)112:7(1623).

Md Yatim, Mohd Yazmil, and Nandivaram E. Shanmugam. 2016. "Strain Behaviour in Composite Plate Girders with Imperfect Shear Connection." *Jurnal Kejuruteraan* 28(1):37–52. doi: 10.17576/jkukm-2016-28-05.

Mieres, J. M., I. Calvo, A. Miravete, E. Gutiérrez, E. Shahidi, C. López, J. Cuartero, P. Comino, and R. Guzmán De Villoria. 2006. "Descripción de Paso Superior Vehicular de La Autovía Del Cantábrico Realizado Con Materiales Compuestos." *Materiales de Construccion*.

Mohammed, Ali A., Allan C. Manalo, Wahid Ferdous, Yan Zhuge, P. V. Vijay, and John Pettigrew. 2020. "Experimental and Numerical Evaluations on the Behaviour of Structures Repaired Using Prefabricated FRP Composites Jacket." *Engineering Structures*. doi: 10.1016/j.engstruct.2020.110358.

Moradi, E., H. Naderpour, and A. Kheyroddin. 2020. "An Experimental Approach for Shear Strengthening of RC Beams Using a Proposed Technique by Embedded Through-Section FRP Sheets." *Composite Structures* 238(January):111988. doi: 10.1016/j.compstruct.2020.111988.

Moran, P. M., X. H. Liu, and C. F. Shih. 1995. "Kink Band Formation and Band Broadening in Fiber Composites under Compressive Loading." *Acta Metallurgica Et Materialia*. doi: 10.1016/0956-7151(95)00001-C.

Mosallam, Ayman S. 2011. "Design Guide for FRP Composite Connections." *ASCE Manuals and Reports on Engineering Practice*. doi: 10.1061/9780784406120.

Mosallam, Ayman S., and Khalid M. Mosalam. 2003. "Strengthening of Two-Way Concrete Slabs with FRP Composite Laminates." in *Construction and Building Materials*.

Nanni, Antonio, Antonio De Luca, and Hany Jawaheri Zadeh. 2014. *Reinforced Concrete with FRP Bars*.

Nassani, Dia Eddin. 2020. "Experimental and Analytical Study of the Mechanical and Flexural Behavior of Hybrid Fiber Concretes." *Structures* 28(October):1746–55. doi: 10.1016/j.istruc.2020.10.014.

Neagoe, Cătălin Andrei. 2016. "Structural Performance of FRP." Polytechnic university of Catalunya.

Nguyen, Hai, Wael Zatar, and Hiroshi Mutsuyoshi. 2015. "Hybrid FRP-UHPFRC Composite Girders: Part 2 - Analytical Approach." *Composite Structures*. doi: 10.1016/j.compstruct.2014.12.001.

Nie, Jianguo, and C. S. Cai. 2003. "Steel–Concrete Composite Beams Considering Shear Slip Effects." *Journal of Structural Engineering*. doi: 10.1061/(asce)0733-9445(2003)129:4(495).

Nystrom, Halvard E., Steve E. Watkins, Antonio Nanni, and Susan Murray. 2003. "Financial Viability of Fiber-Reinforced Polymer (FRP) Bridges." *Journal of Management in Engineering*. doi: 10.1061/(asce)0742-597x(2003)19:1(2).

Parvin, Azadeh, Selcuk Altay, Cem Yalcin, and Osman Kaya. 2010. "CFRP Rehabilitation of Concrete Frame Joints with Inadequate Shear and Anchorage Details." *Journal of Composites for Construction*. doi: 10.1061/(asce)cc.1943-5614.0000055.

Persaud, Richard, and Digby Symons. 2006. "Design and Testing of a Composite Timber and Concrete

Floor System." *Structural Engineer*.

Pfeiffer. 2002. "Operating Instructions." *Journal of Wildlife Rehabilitation* 25(3):27.

Raza, Ali, Babar Ali, Muhammad Asad Nawaz, and Ibrar Ahmed. 2020. "Structural Performance of FRP-RC Compression Members Wrapped with FRP Composites." *Structures* 27(July):1693–1709. doi: 10.1016/j.istruc.2020.07.071.

Saiidi, M., F. Gordaninejad, and N. Wehbe. 1994. "Behavior of Graphite/Epoxy Concrete Composite Beams." *Journal of Structural Engineering*. doi: 10.1061/(asce)0733-9445(1994)120:10(2958).

Sakr, Mohammed A., Saher R. El-Khoriby, Aymen A. Seleemah, Mustafa M. Aboelnour, and Bothaina Osama. 2021. "Experimental and Numerical Investigation on Cyclic Behavior of Masonry Infilled RC Frames Retrofitted with Partially Bonded CFRP Strips." *Structures* 33(June):2238–52. doi: 10.1016/j.istruc.2021.05.087.

Santhakumar, R., E. Chandrasekaran, and R. Dhanaraj. 2004. "Analysis of Retrofitted Reinforced Concrete Shear Beams Using Carbon Fiber Composites." *Electronic Journal of Structural Engineering*.

Santos Neto, Almir Barros da S., and Henriette Lebre La Rovere. 2010. "Composite Concrete/GFRP Slabs for Footbridge Deck Systems." *Composite Structures* 92(10):2554–64. doi: 10.1016/j.compstruct.2010.02.005.

Schnabl, Simon, Miran Saje, Goran Turk, and Igor Planinc. 2007. "Analytical Solution of Two-Layer Beam Taking into Account Interlayer Slip and Shear Deformation." *Journal of Structural Engineering*. doi: 10.1061/(asce)0733-9445(2007)133:6(886).

Sen, Rajan, Larry Liby, and Gray Mullins. 2001. "Strengthening Steel Bridge Sections Using CFRP Laminates." *Composites Part B:Engineering*. doi: 10.1016/S1359-8368(01)00006-3.

Shi, Feng, Thong M. Pham, Hong Hao, and Yifei Hao. 2020. "Post-Cracking Behaviour of Basalt and Macro Polypropylene Hybrid Fibre Reinforced Concrete with Different Compressive Strengths." *Construction and Building Materials* 262:120108. doi: 10.1016/j.conbuildmat.2020.120108.

Siegel, David J., and David J. Siegel. 2018. "College of Engineering." in *The Call for Diversity*.

Simulia. 2019. "Abaqus User's Manual Version 2019." *Dassault Systèmes Simulia Corp.: Providence, RI, USA*.

Siwowski, Tomasz, Mateusz Rajchel, and Maciej Kulpa. 2019. "Design and Field Evaluation of a Hybrid FRP Composite – Lightweight Concrete Road Bridge." *Composite Structures* 230(August):111504. doi: 10.1016/j.compstruct.2019.111504.

Soltanalipour, Milad, Miquel Ferrer, Frederic Marimon, Josef Holomek, Miroslav Bajer, Jindřich Melcher, and Marcela Karmazínová. 2020. "Shear Transfer Behavior in Composite Slabs under 4-Point Standard and Uniform-Load Tests." *Journal of Constructional Steel Research*. doi: 10.1016/j.jcsr.2019.105774.

Soudki, K., and T. Alkhrdaji. 2005. "Guide for the Design and Construction of Externally Bonded FRP Systems for Strengthening Concrete Structures (ACI 440.2R-02)." in *Proceedings of the Structures Congress and Exposition*.

Speranzini, E., and S. Agnetti. 2015. "Flexural Performance of Hybrid Beams Made of Glass and Pultruded GFRP." *Construction and Building Materials*. doi: 10.1016/j.conbuildmat.2015.06.008.

Standards Australia. 2003. "Composite Structures Part 1: Simply Supported Beams." *As 2327.1-2003*.

Teng, J. G., T. Yu, Y. L. Wong, and S. L. Dong. 2007. "Hybrid FRP-Concrete-Steel Tubular Columns: Concept and Behavior." *Construction and Building Materials*. doi: 10.1016/j.conbuildmat.2006.06.017.

Turkowski, Piotr, Marek Łukomski, Paweł Sulik, and Paweł Roszkowski. 2017. "Fire Resistance of CFRP-Strengthened Reinforced Concrete Beams under Various Load Levels." in *Procedia*

Engineering.

Vasquez, Alvaro, and Vistasp M. Karbhari. 2003. "Fiber-Reinforced Polymer Composite Strengthening of Concrete Slabs with Cutouts." *ACI Structural Journal*. doi: 10.14359/12808.

Wang, Y. C. 1998. "Deflection of Steel-Concrete Composite Beams with Partial Shear Interaction." *Journal of Structural Engineering*. doi: 10.1061/(asce)0733-9445(1998)124:10(1159).

Wu, Zhishen, Wenxiao Li, and Naoki Sakuma. 2006. "Innovative Externally Bonded FRP/Concrete Hybrid Flexural Members." *Composite Structures* 72(3):289–300. doi: 10.1016/j.compstruct.2004.12.002.

Wu, Zhishen, Xin Wang, Xing Zhao, and Mohammad Noori. 2014. "State-of-the-Art Review of FRP Composites for Major Construction with High Performance and Longevity." *International Journal of Sustainable Materials and Structural Systems* 1(3):201. doi: 10.1504/ijsmss.2014.062757.

Xu, Rongqiao, and Yufei Wu. 2007. "Static, Dynamic, and Buckling Analysis of Partial Interaction Composite Members Using Timoshenko's Beam Theory." *International Journal of Mechanical Sciences*. doi: 10.1016/j.ijmecsci.2007.02.006.

Yamaguchi, Eiki, Structural Analysis, J. Y. Richard Liew, N. E. Shanmugam, C. H. Yu, Structural Steel Design, E. M. Lui, Amy Grider, Julio A. Ramirez, Young Mook Yun, Shouji Toma, Lian Duan, Wai-Fah Chen, T. Balendra, W. F. Chen, Birger Schmidt, Christian Ingerslev, Brian Brenner, and J. N. Wang. 2005. "4 Structural Concrete Design 10 Bridge Structures 12 Multistory Frame Structures 15B Tunnel Structures." *Structural Analysis*.

Yao, J., J. G. Teng, and J. F. Chen. 2005. "Experimental Study on FRP-to-Concrete Bonded Joints." *Composites Part B: Engineering*. doi: 10.1016/j.compositesb.2004.06.001.

Zhang, Dawei, and Ying Huang. 2021. "The Bonding Performances of Carbon Nanotube (CNT)-Reinforced Epoxy Adhesively Bonded Joints on Steel Substrates." *Progress in Organic Coatings* 159(June):106407. doi: 10.1016/j.porgcoat.2021.106407.

List of publications

The following peer-reviewed publications have resulted from the main investigation carried by the author in the present doctoral thesis:

A. Mahboob, L. Gil, E. Bernat-Maso, and A. R. Eskenati. Flexible Fiber Fabric for FRP–Concrete Connection of Thin Hybrid Slabs. Polymers (Basel).2021, 13,
doi: 10.3390/polym13172862.
Published (JCR, Q1, Impact Factor: 4.3)

A. Mahboob, L. Gil, E. Bernat-Maso, and A. R. Eskenati. Experimental and numerical study of shear interface response of hybrid thin CFRP–concrete slabs. Materials (Basel).2021, 14,
doi: 10.3390/ma14185184.
Published (JCR, Q2, Impact Factor: 3.6)

A

Experimental results

A.1. Introduction

The present appendix compiles all the experimental reports that describe the testing procedures and results of the three-point bending tests and shear tests performed on samples of the CFRP-concrete composite slabs used in the experimental investigation. The mechanical properties were determined following the recommendation of specific ASTM International standard.

All the experiments were performed by the author at the Laboratory for the Technological Innovation of Structures and Materials (LITEM) from Polytechnic university of Catalunya–BarcelonaTech, under room temperature and normal relative humidity conditions.

The experimental research has been carried out following two main lines: Bending characterization of hybrid elements and Shear characterization of different connection types. Both tests showed failure modes associated with the connection between FRP and concrete and it's clear by looking to the specimens after failure. Different types of connection were tested in the laboratory. Two specimens of each type were produced for repeatability. Figure A. 1 shows different types of connection in bending and shear specimens.

SPECIMENS	
SHEAR	NONE
	STONE
	STONE+MESH
	STONE+SAND+MESH
	STONE+SAND+MESH 45
Bending	STONE
	STONE+MESH
	STONE+SAND+MESH
	STONE+SAND+MESH 45

Figure A. 1. Specimens in shear and bending.

A.2. Dimensions

The dimensions of the bending and shear samples are shown respectively in Figure A. 2:
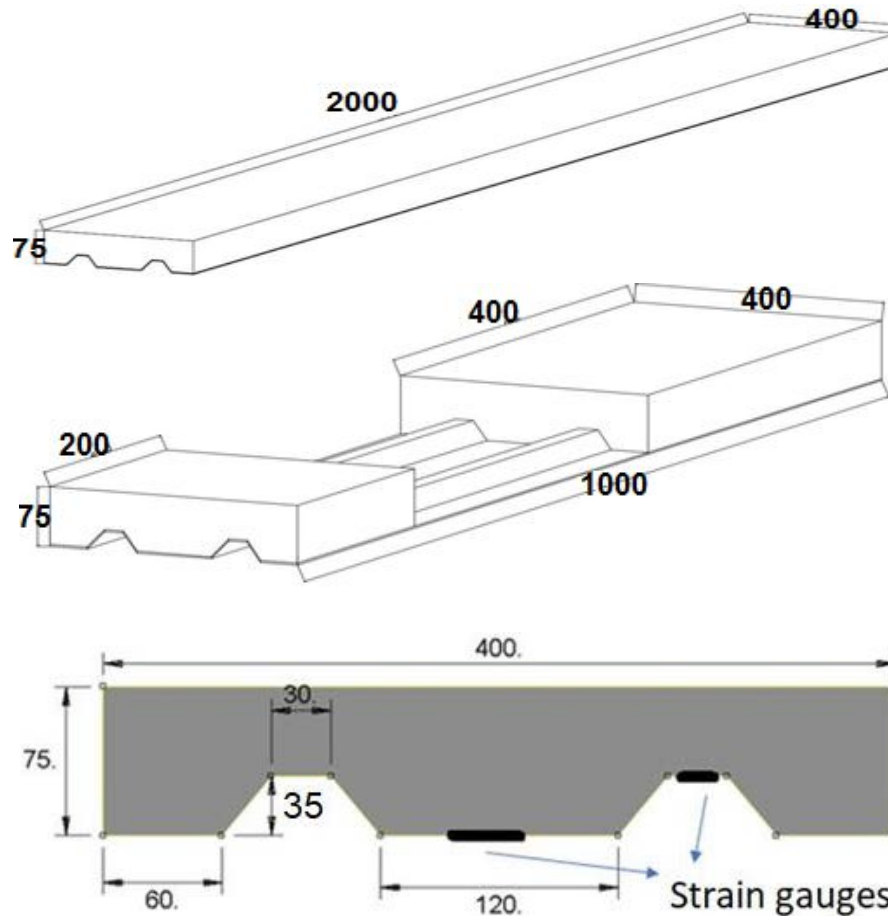
Figure A. 2. Dimensions of samples.

A.3. Tests' setup configuration

A.3.1. Bending

For bending tests, Three-point bending test configuration was used. Supports were materialized by steel cylinders supported on steel rigid structures (Figure A. 3), whereas load was applied with a semi-cylindrical tool to allow rotation under it (Figure A. 4).
Test was conducted by displacement control at fixed rate of 5 mm/min and force was measured with a 50 kN range with 0.2% linearity load cell mounted on the actuator. QuantumX 840A was used as DAQ system working at 50 Hz for acquering data of the following sensors:

- Vertical displacement of actuator; LVDT with 150 mm range and 0.02% linearity.

- Horizontal displacement sensors used to measure the relative displacement between concrete and CFRP at the specimens' extreme edges; LVDT with 20 mm range and 0.02% linearity.

- External vertical displacement sensors; Potentiometer of 100 mm of range and 0.2% linearity to measure the deflection at central section.
- Strain gauges; 350 Ω, four wire connection and temperature compensated for CFRP installed at bottom CFRP and outer part of the top surface of CFRP in the central position, to record the rotation strains.
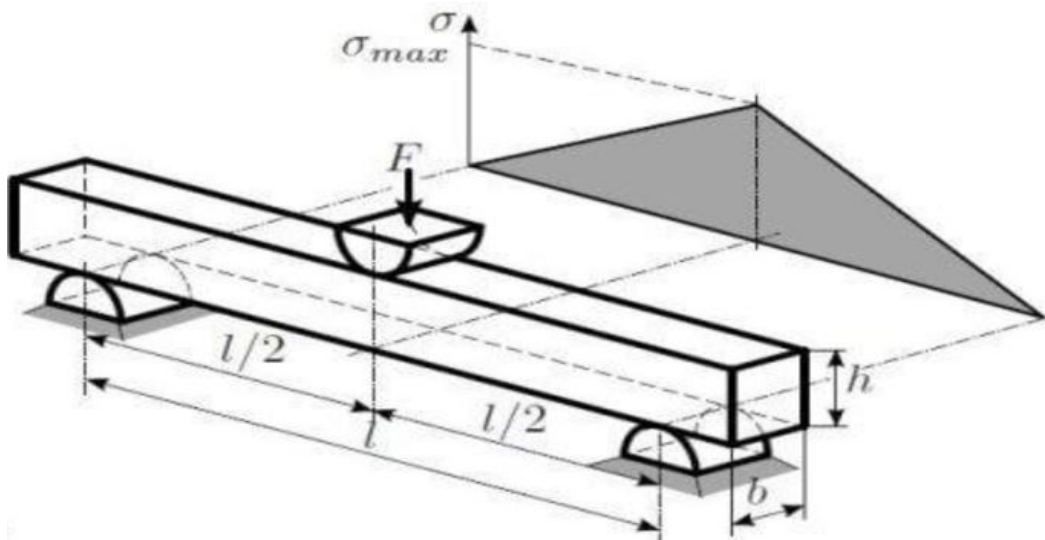
Figure A. 3. Three-point bending test method.

Figure A. 4 Bending setup configuration.

A.3.2. Shear

For shear tests, direct shear test configuration was used (Figure A. 5). Jack with load cell of 10 kN range and 0.2% linearity was placed between two concrete blocks. The longer one was used as reaction point and the shorter one defined the connection to be tested. External displacement sensors were used to measure the relative displacement between CFRP plate and shortest concrete block. These were LVDT with 20 mm range and 0.02% linearity (Figure A. 6).
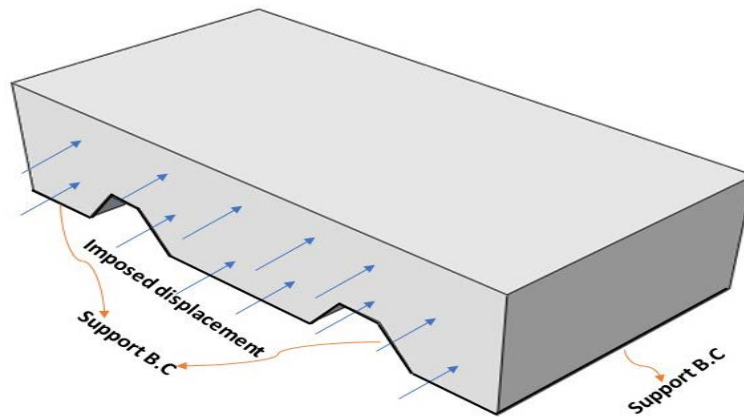
Figure A. 5. Direct shear test method.

Figure A. 6. Shear setup configuration.

A.4. Specimens

A total of eighteen hybrid specimens specifically designed for the experimental tests, ten for three-point bending test and eight for direct shear test. All specimens were made with the same type of CFRP sheets with omega shape and the same concrete but different connection systems between them.

For specimens naming, the format of XYZ- # was formed, where X is 0 if gravel was not used or "S" if gravel was included, where Y is 0 if sand was excluded or "S" if sand was included, where Z is 0 if there was no grid, "M" if mesh was embedded in longitudinal-orthogonal direction or "I" if it was installed with 45⁰ inclination of the tows respect the longitudinal axe of the specimen. For the first and second repetitions of the same test, # displays the values 1 or 2, respectively.

Before implementing bending and shear tests, experimental compressive strength of the concrete and tensile strength of FRP were obtained on the basis of the rebound hammer method (Figure A. 7). Rebound hammer test and ASTM D638 standard (Figure A. 8).
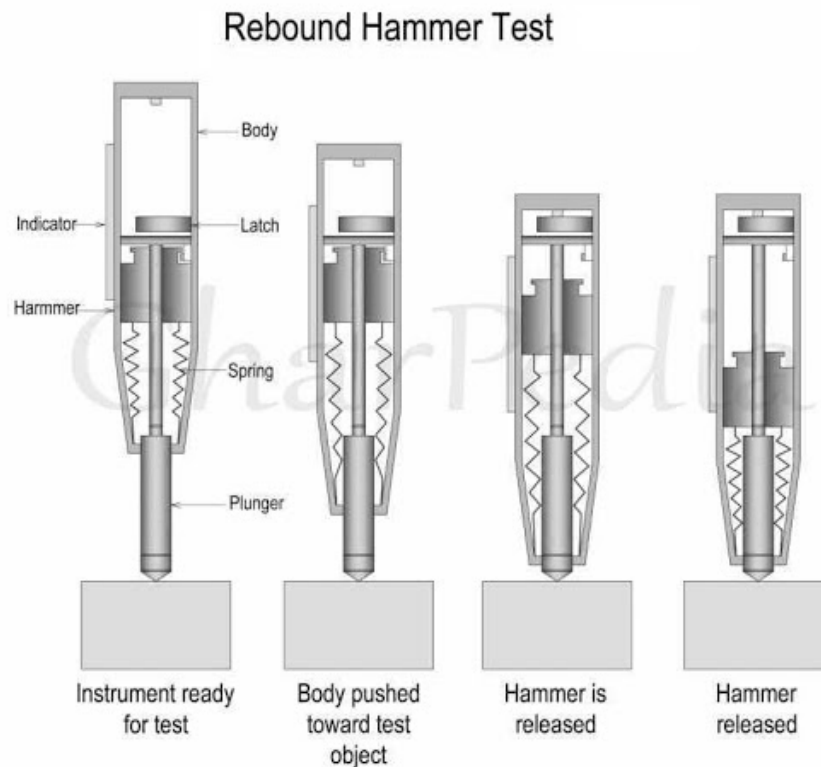
Figure A. 7. Rebound hammer test (Pfeiffer 2002).
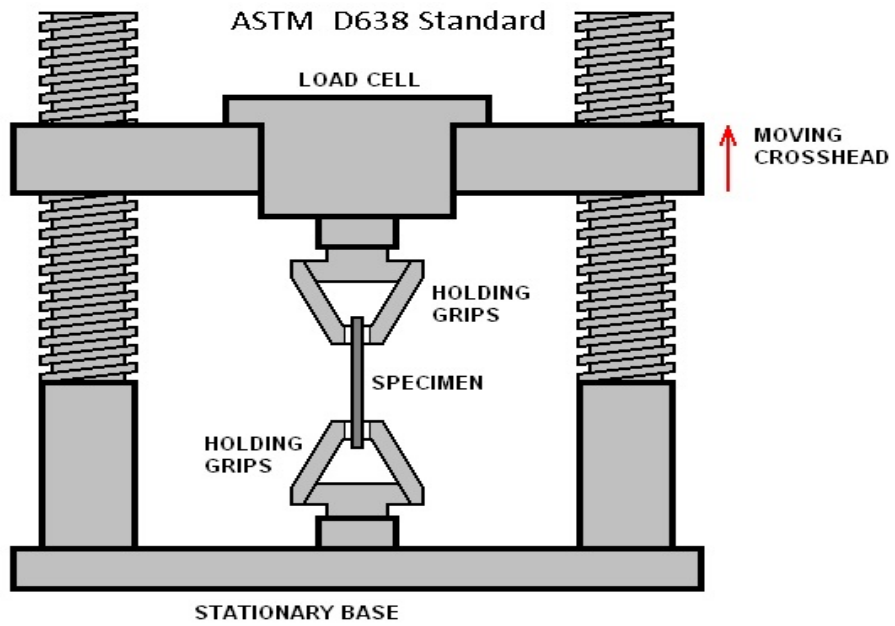
Figure A. 8. ASTM D638 Standard sketch (Grimaldi 2007).

Figure A. 9 and Figure A. 10 show experimental test of concrete's compressive strength and FRPs' tensile strength.

Figure A. 9. Implementing of rebound hammer test for compressive strength.

Figure A. 10. Implementing of ASTM D638 test for tensile strength.

A.5. Experimental results

The practical work contains testing of four sets of reinforced hybrid slabs with and without Mesh for bending and five sets with the same structure for shear. The only difference is having one more model in shear without any reinforcement materials (000) due to understand of each material effect in shear resistance, Gravel and Sand connection elements also has been used. Totally, there were eighteen of hybrid slabs which were cast at the laboratory (eight in bending and ten in shear). Two specimens were tested for each study parameter to ensure the consistency of test results.

The following plots provide information regarding to the structural response of bending and shear tests. The graphics are complemented by the observations that were made in laboratory.

A.6. Bending plots

A.6.1. S00-1
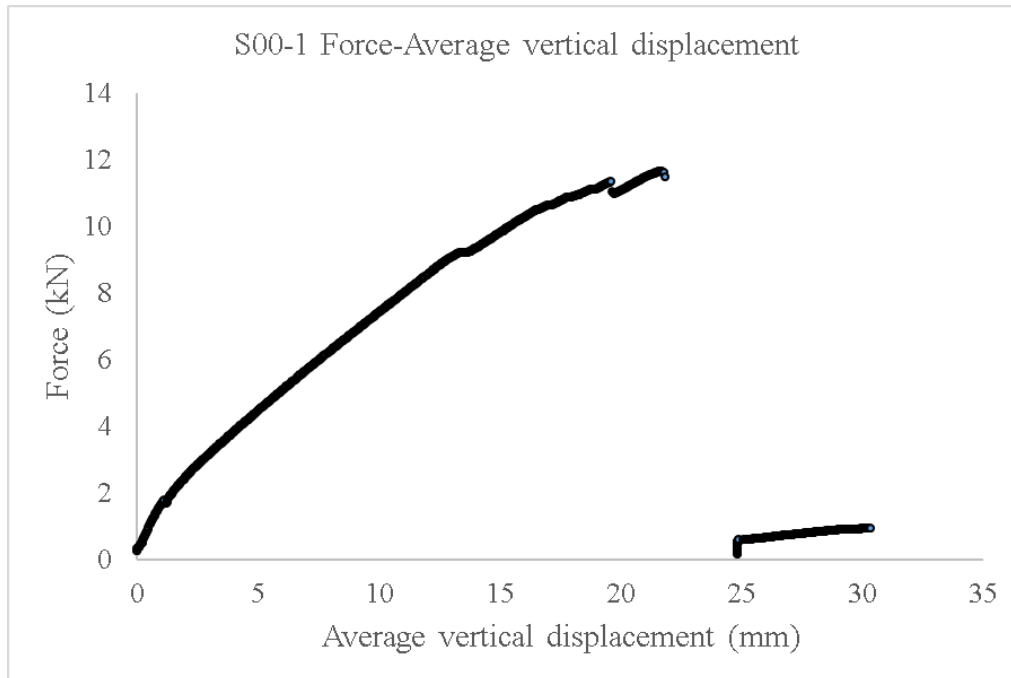
Figure A. 11. S00-1 Force-Average vertical displacement.

Corresponding to the graph, force axis reaches 11.9kN as maximum after 22mm of displacement and after failure, force tends to zero. Maximum displacement is 31mm. Sudden drop in force is observed. Neutral axis 0-reference was the bottom of the section. When neutral axis position was over 35mm all CFRP sheet was subjected to tensile stresses, whereas when this variable was below 35mm it indicated that the top part of the CFRP sheet was compressed. All cases showed a suddenly drop of the neutral axis position from over 35mm to under 35mm, which was associated with the qualitative CFRP-concrete disconnection failure observation. In addition, this drop corresponded with the maximum load applied during test. It has to be remarked that when the neutral axis was below 35mm, the fiberglass mesh was compressed, so no longer connection between CFRP and concrete was expected to be provided by this component.

Figure A. 12. S00-1 Neutral Axis-Average vertical displacement.

According to the plot, neutral axis starts moving from 50mm and reaches its maximum possible value 75mm and then slowly decrease till 39mm then sharply drop to 15mm as final behavior. The CFRP-concrete shear stress was calculated by dividing the total compressive or tensile force normal to the mid-span section by the CFRP-concrete idealized contact surface in half of the length of the slab (length x width = 1m x 0.4m = 0,4m^2). This total compressive/tensile force was calculated from strain distribution and force equilibrium

Dashed line indicates the theoretical balanced case associated with perfect compatibility between concrete and CFRP in the connection.
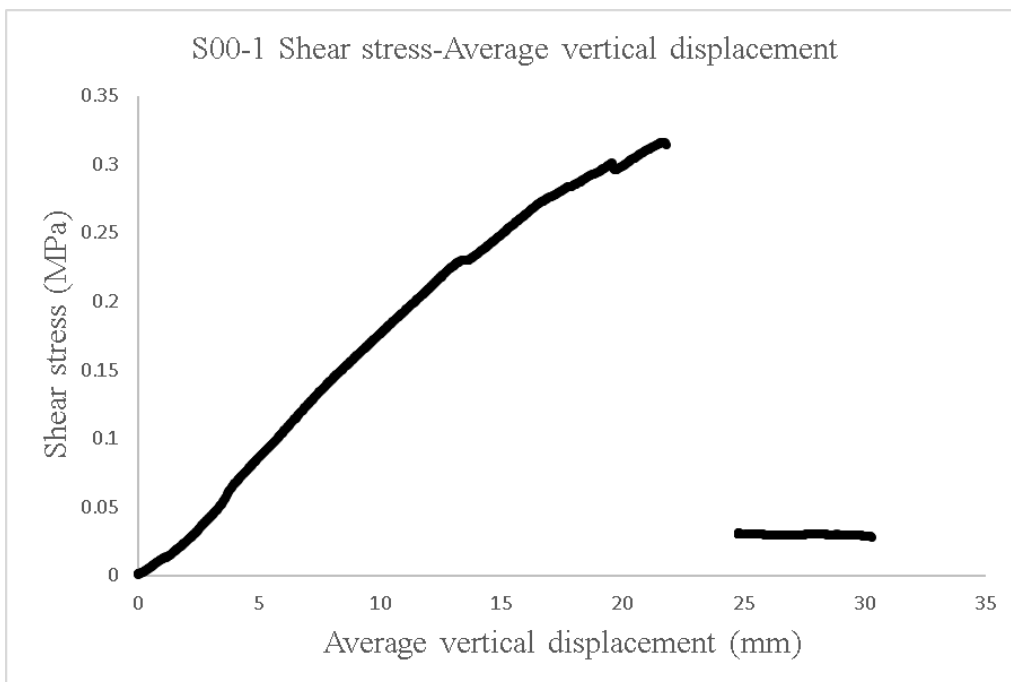
Figure A. 13. S00-1 Shear Stress-Average vertical displacement.

100

Regarding to the graph, constant increases of shear stress seen from zero to 0.32MPa. Broking point is at 22.5mm of vertical displacement at mid-span.
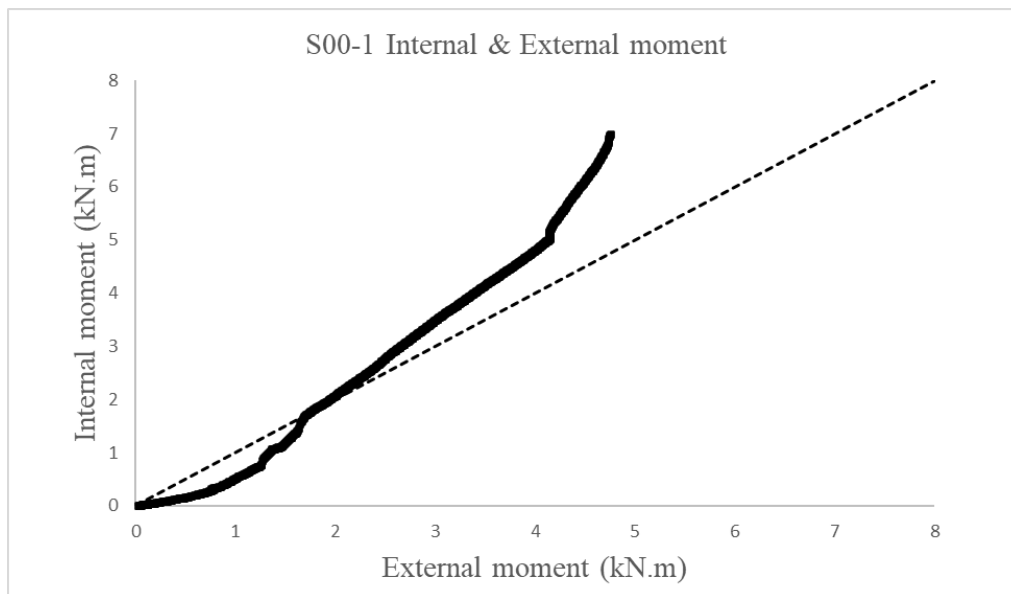
Figure A. 14. S00-1 Internal & External moment.

Corresponding to the graph, equilibrium line is near to the draw line before failure starts and it means quality of components' connection is acceptable but not perfect.

External energy was calculated from force and vertical displacement at the loaded section (mid-span). These plots are divided in two parts: before (solid line) and after (dashed line) reaching the maximum load. The qualitative result that arises from these plots is the proportion between the energy cumulated before the peak load and the energy absorbed by the system after it, which is an indirect measurement of the energy dissipation capability of the damaged structure. Hence, this result is related with the safety this type of slabs may offer.

The following plot shows the cumulative external energy (obtained from applied force and displacement under actuator) divided between the energy supplied before failure point (continuous line) and the energy supplied after failure (dashed line). It provides an idea about ductility of the hybrid system.
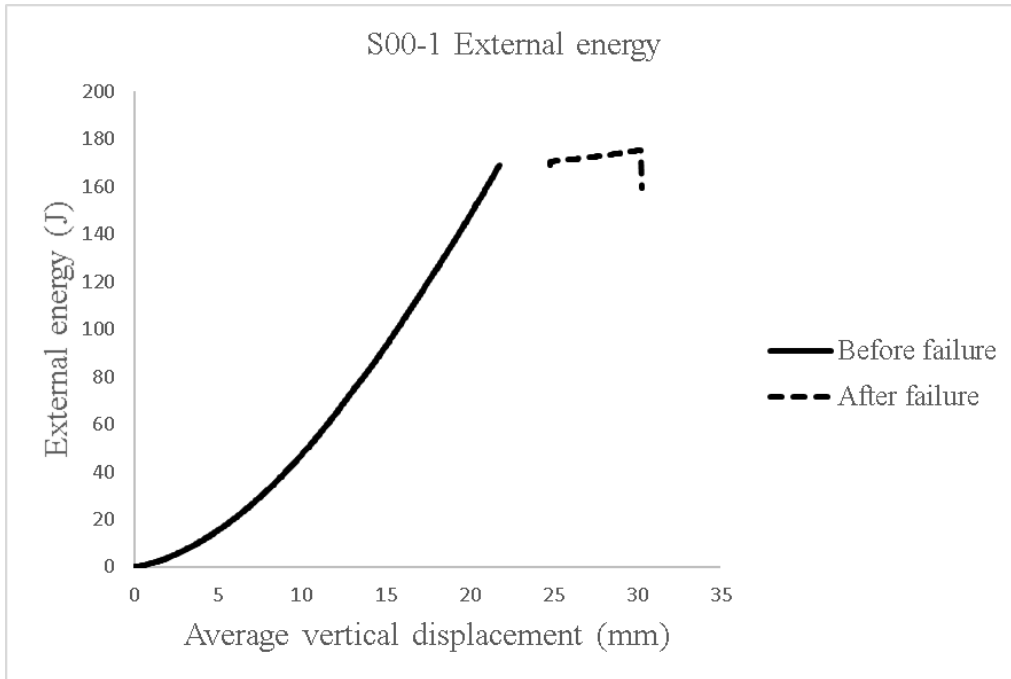
Figure A. 15. S00-1 External energy.

Regarding to the plot, distribution of energy before failure is too much bigger than after failure. The ultimate external energy before failure is 175 J.
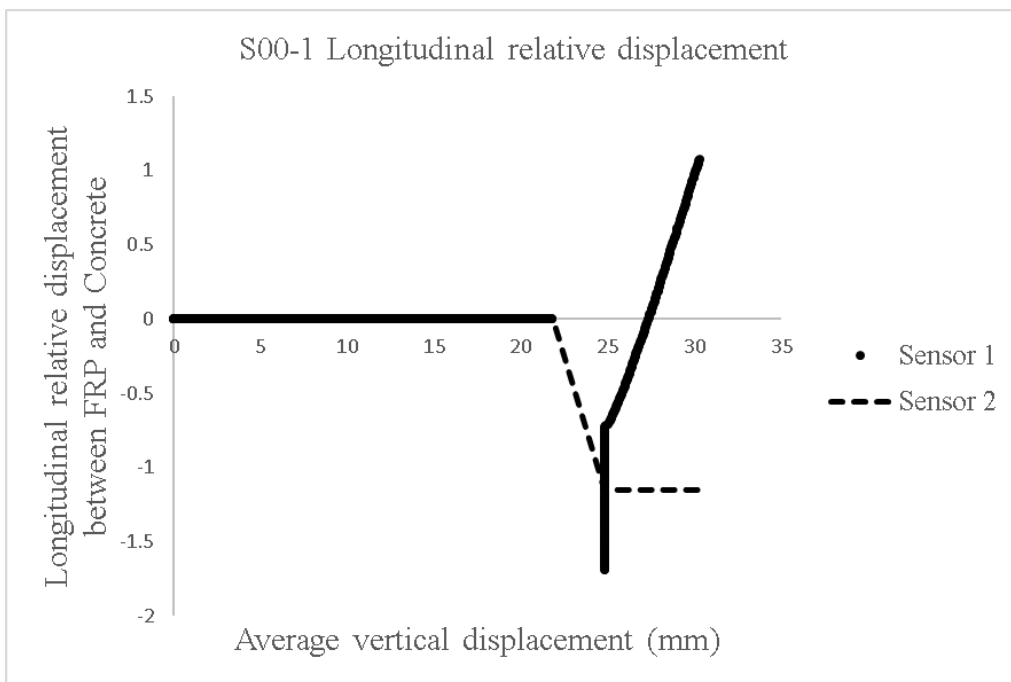
Figure A. 16. S00-1 Longitudinal relative displacement.

Regarding to the plot, the specimen breaks after 22mm and sliding is measured in both specimens' endings but in the same direction.

A.6.2. S00-2
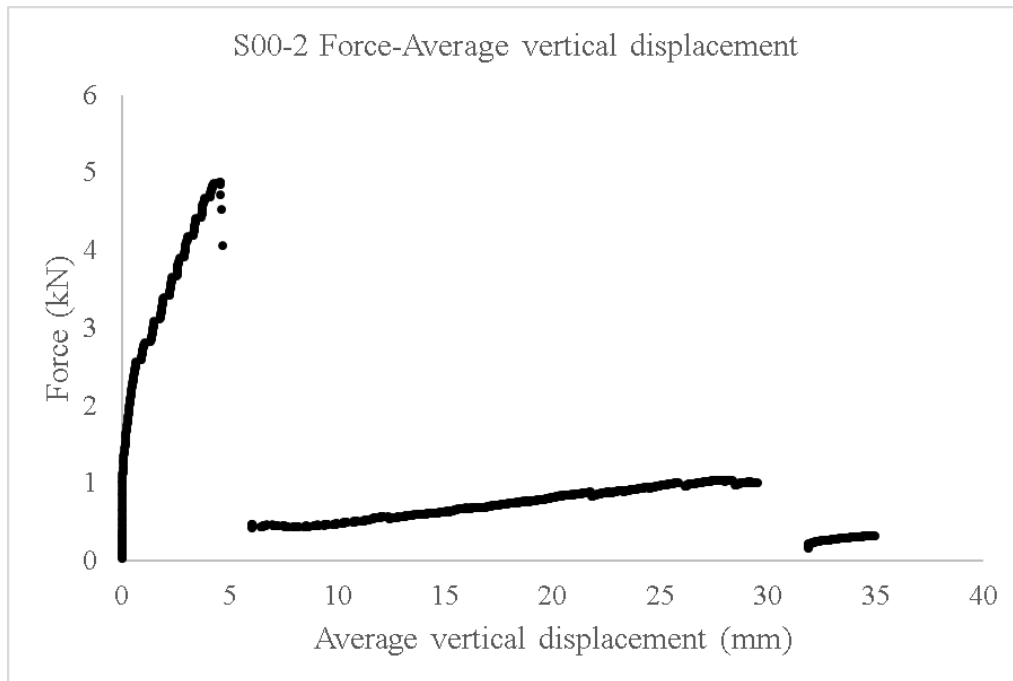
Figure A. 17. S00-2 Force-Average vertical displacement.

In the plot above, maximum force is 4.9kN and failure happens after 6mm only. The graph shows 35mm as ultimate displacement.
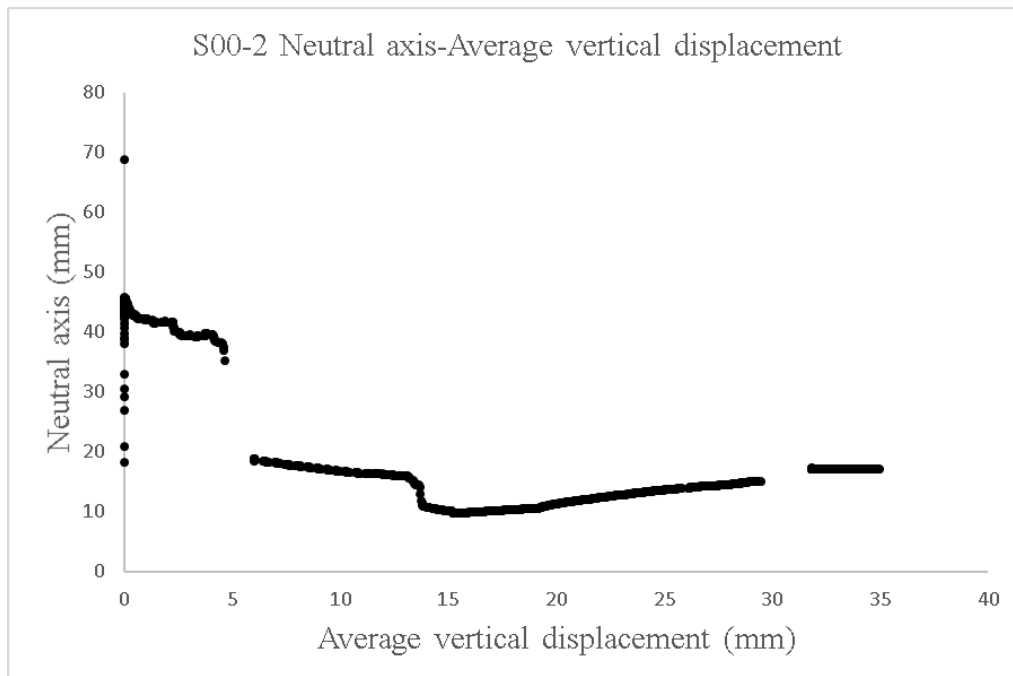
Figure A. 18. S00-2 Neutral Axis-Average vertical displacement.

According to the graph, neutral axis position is above 35mm before failure and fells down below 35 mm (interface between CFRP and concrete) after failure point.
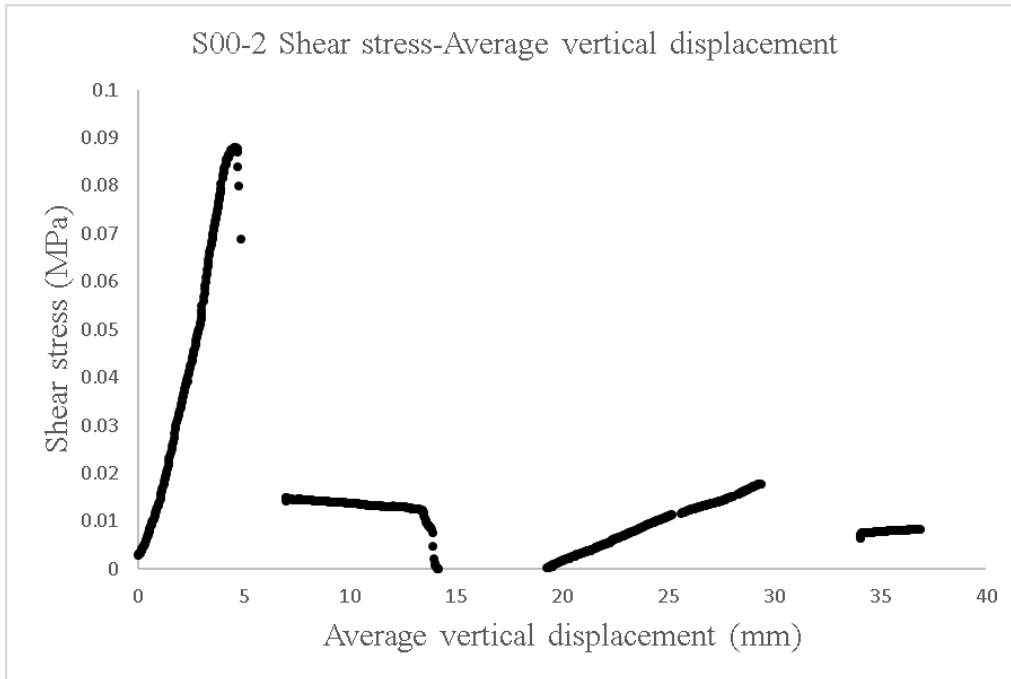
Figure A. 19. S00-2 Shear Stress-Average vertical displacement.

Observing the graph, maximum shear stress is 0.09MPa and specimen fails after 5mm of vertical deflection at midspan.
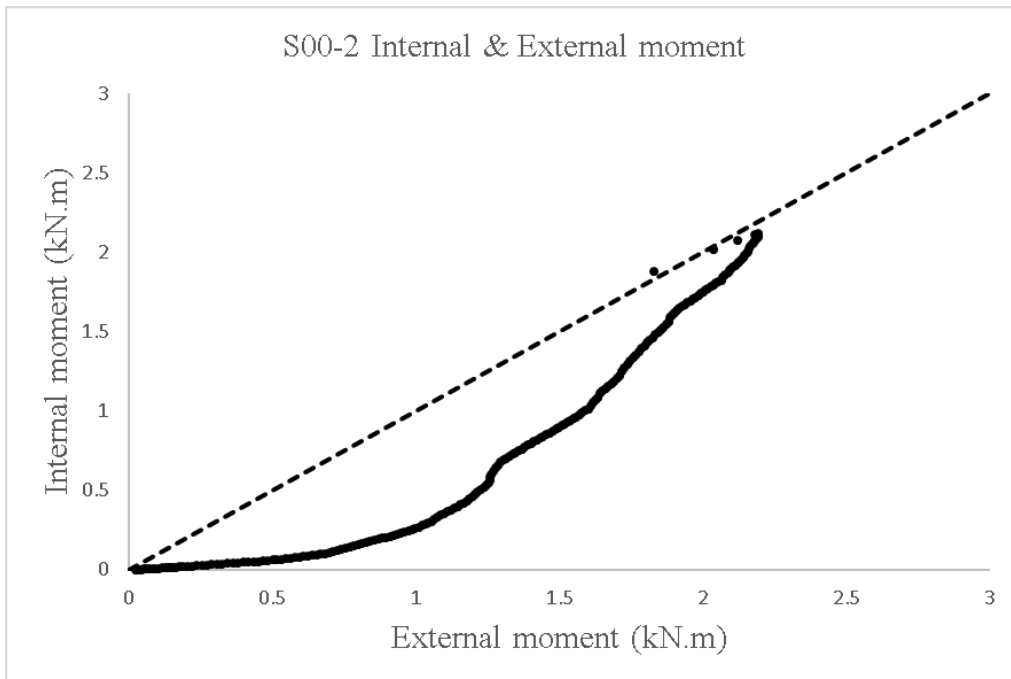
Figure A. 20. S00-2 Internal & External moment.

According to the graph, balance of internal and external moment is so far from draw line from the beginning and it means quality of connection in this case is poor.
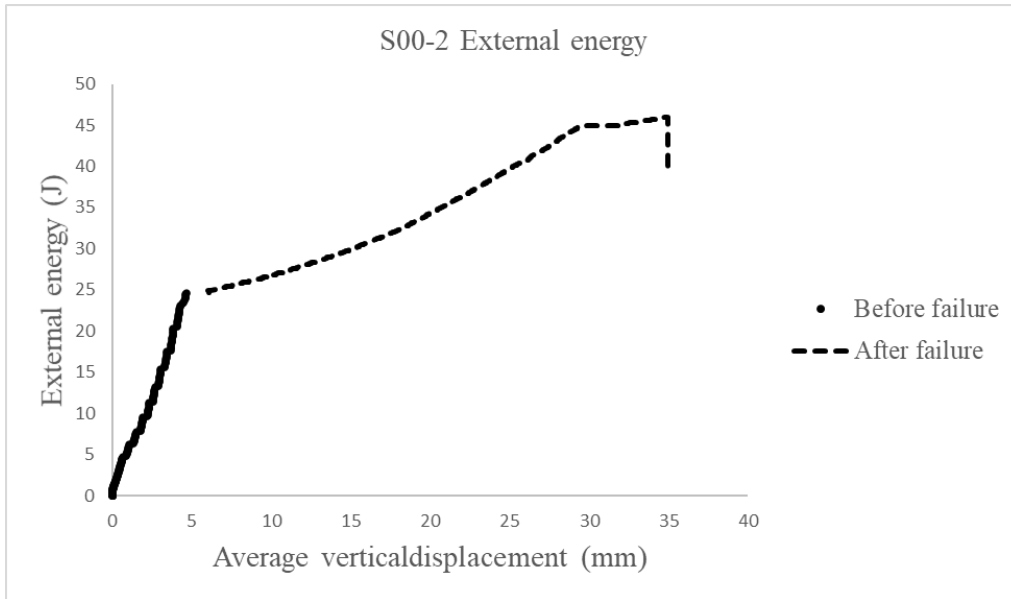
Figure A. 21. S00-2 External energy.

Regarding to the plot, cumulated energy after failure's is similar to cumulated energy before failure.
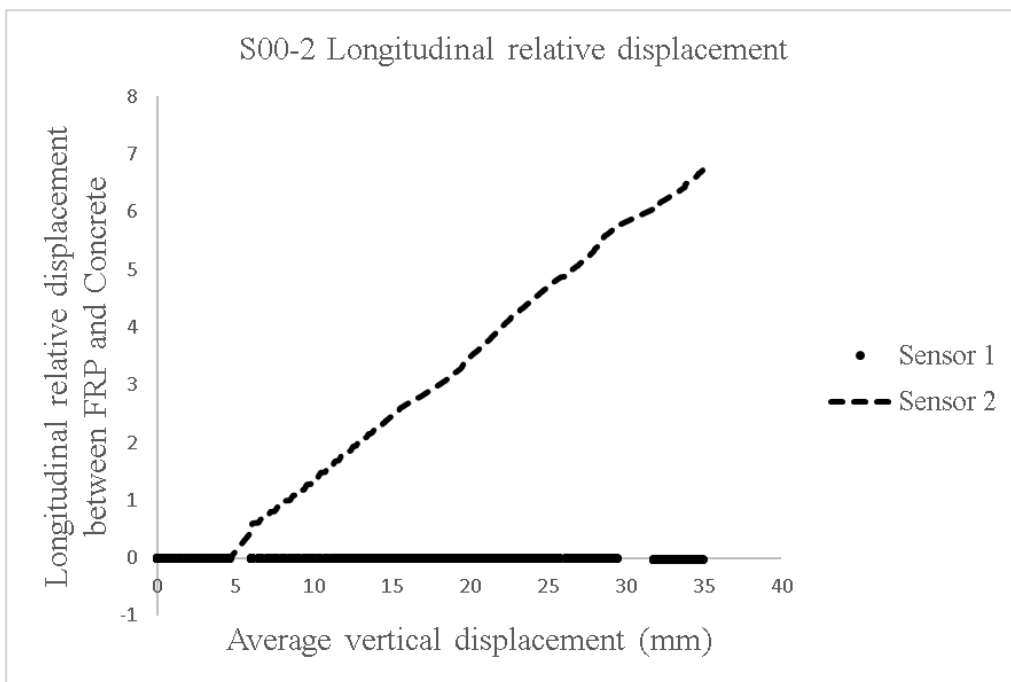
Figure A. 22. S00-2 Longitudinal relative displacement.

According with the plot, the CFRP-concrete interface slid in one of specimens' endings from the start of the failure and reaching a final longitudinal displacement is 6.8mm.

A.6.3. S0M-1
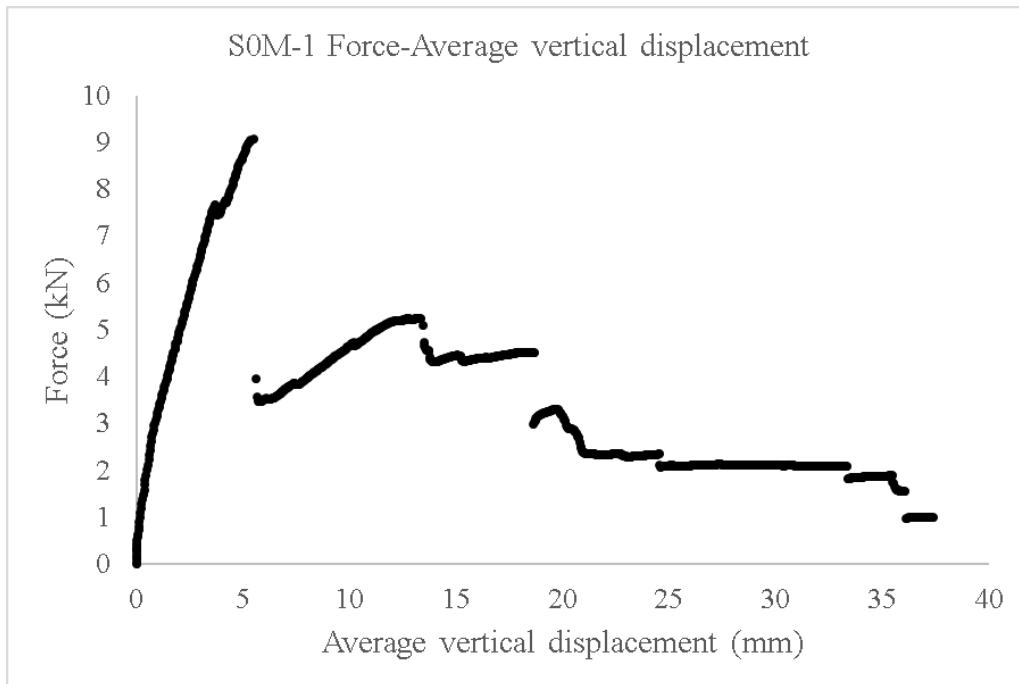
Figure A. 23. S0M-1 Force-Average vertical displacement.

In this plot, specimen tolerated 9.2kN as final resistance and failure happened after 5.2mm of displacement. As shown above, maximum displacement is 37.5mm.
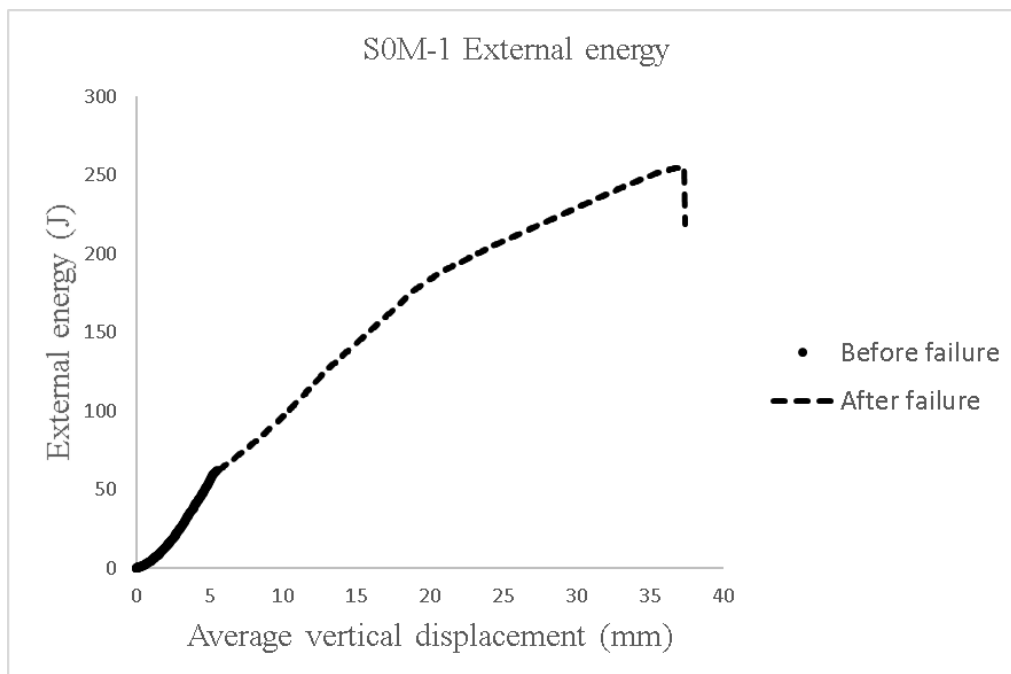
Figure A. 24. S0M-1 External energy

Regarding to this plot, the energy absorbed after failure is greater than before it. Slab can dissipate significant amount of energy after failure.

Note: Other plots of S0M-1 are not available because of technical problem (second strain gauge failure).

A.6.4. S0M-2
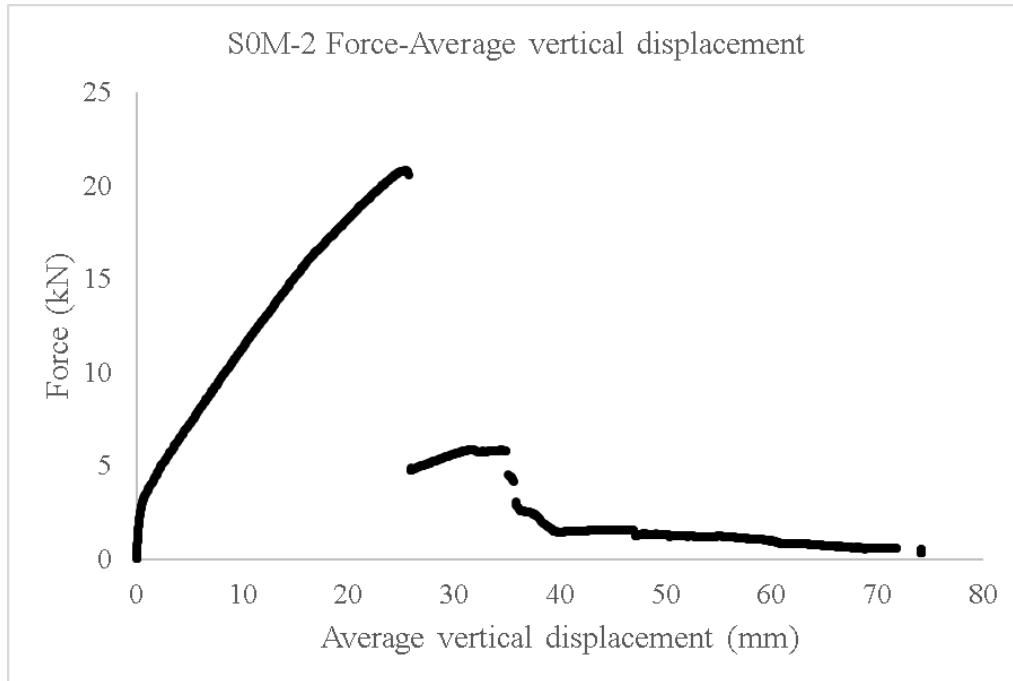
Figure A. 25. S0M-2 Force-Average vertical displacement.

Corresponding to the graph, specimen endures 22kN as maximum strength and starts failure after 25.5mm. peak of average vertical displacement shows 75mm by end of the test.
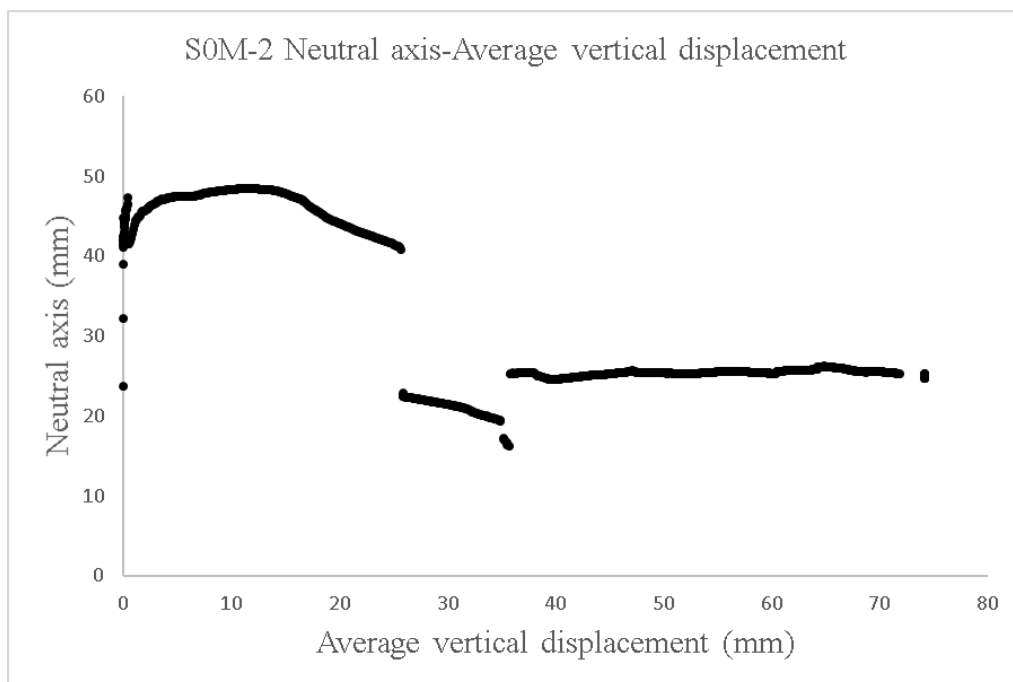
Figure A. 26. S0M-2 Neutral Axis-Average vertical displacement.

Regarding to the graph, neutral axis stayed above 40mm before failure and specimen crashed after 26mm of vertical deflection at mid-span, afterward neutral axis fell into range (<=35mm) where top part of CFRP was compressed.
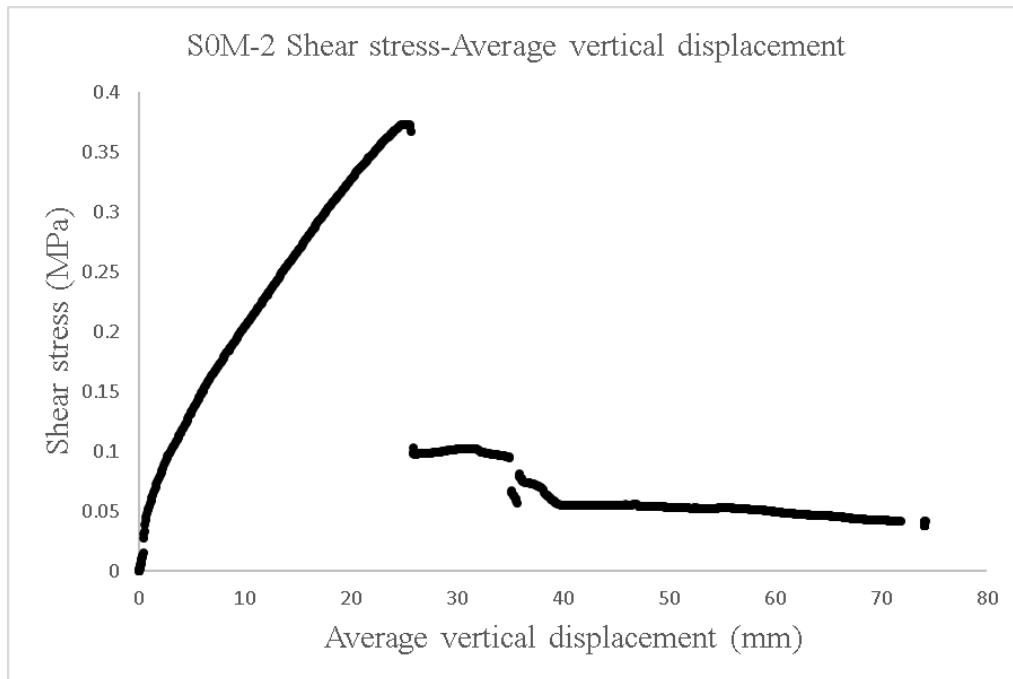
Figure A. 27. S0M-2 Shear Stress-Average vertical displacement.

Depending on the plot, maximum shear stress is 0.37MPa and specimen fails after 27.5mm displacement.
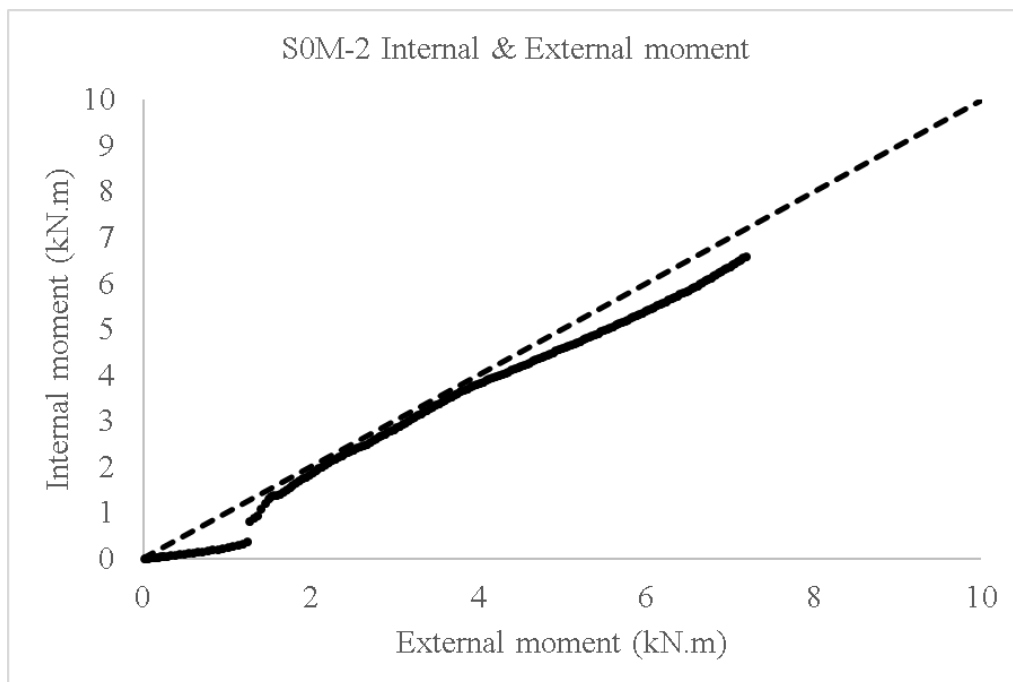
Figure A. 28. S0M-2 Internal & External moment.

Regarding to the result, except first section of the test, the equilibrium line overlaps with the line draw and it shows good bonding condition between materials.
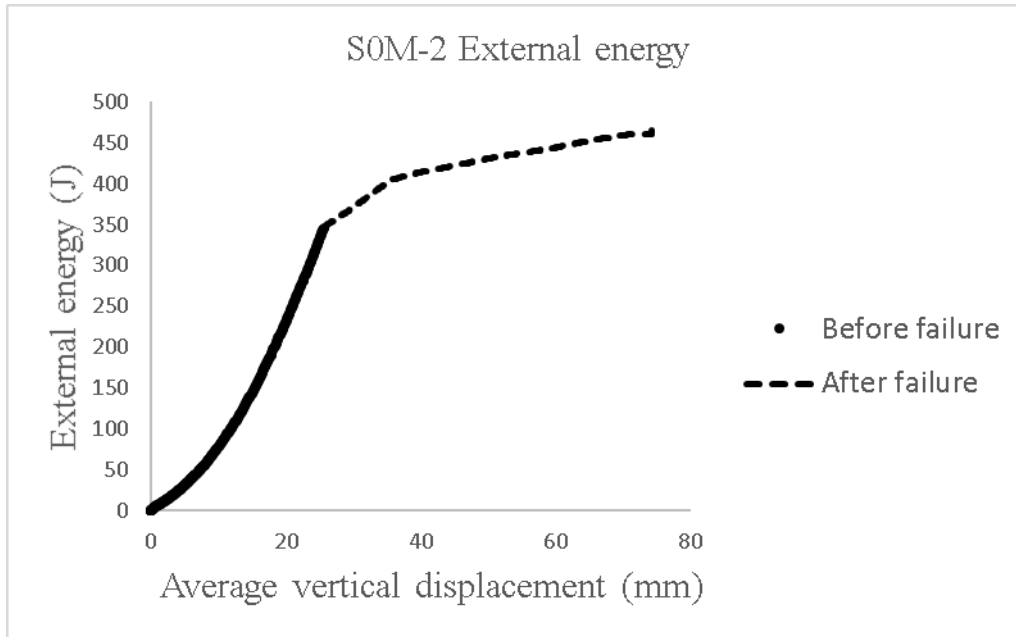
Figure A. 29. S0M-2 External energy.

According to the graph, energy provided to the specimen before failure is far greater than after failure before. Little energy can be assumed after failure of this specimen.
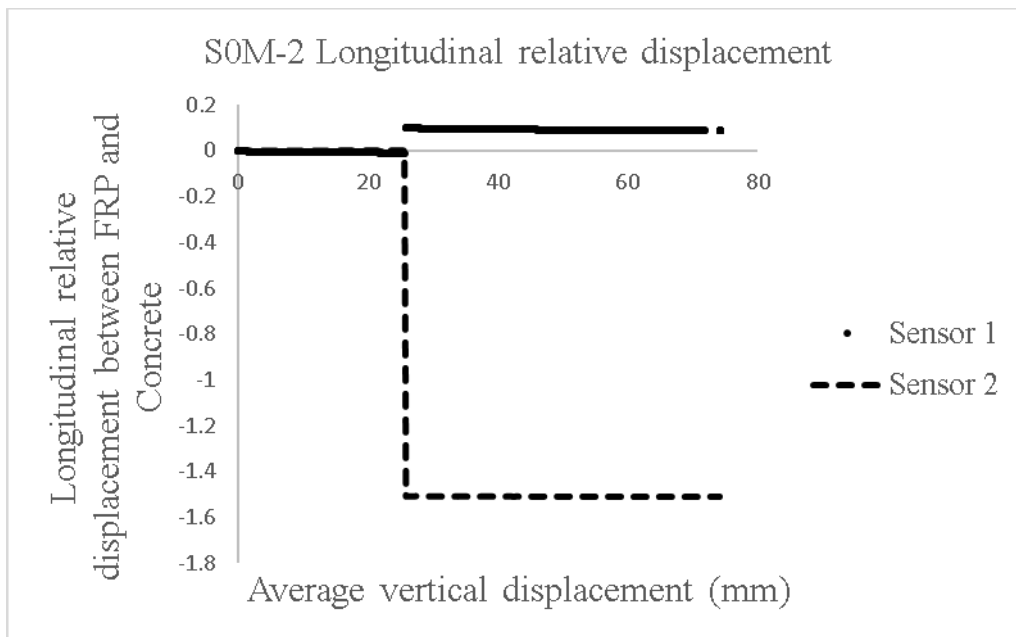
Figure A. 30. S0M-2 Longitudinal relative displacement.

Depending on the plot, no gradually displacement in sliding happened during the test, only some jumps due to sensor position change associated with sudden movements at the failure moment.

A.6.5. SSM-1
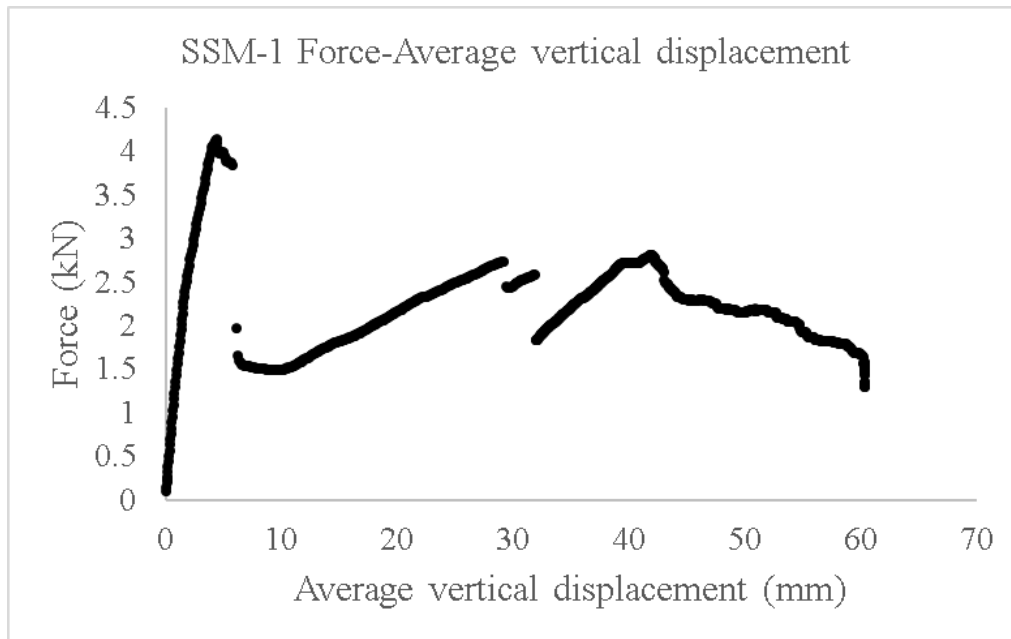
Figure A. 31. SSM-1 Force-Average vertical displacement.

According to the graph, the force increases to 4.2kN which is the maximum point, and then falls to 1.7kN, which no longer works as a composite slab. It then again increases and decreases until the end. The displacement at the breaking point is 1.98mm and at the end of the test is around 60mm.
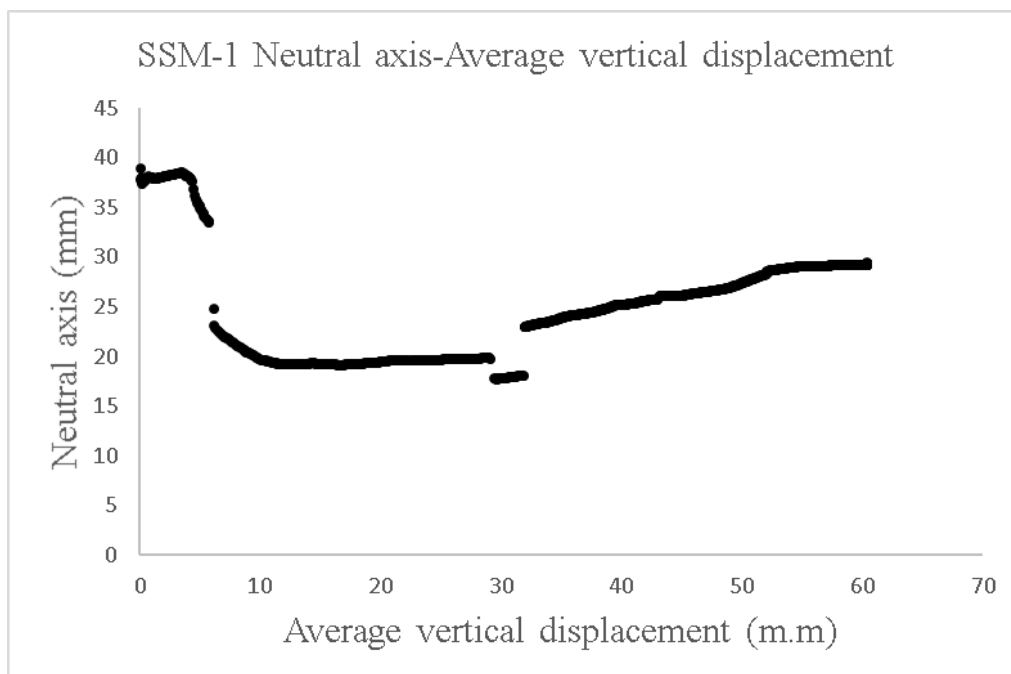
Figure A. 32. SSM-1 Neutral Axis-Average vertical displacement.

From the beginning until the breaking point, the neutral axis has a constant position of approximately 37mm. The break happens after around 6 mm displacement.
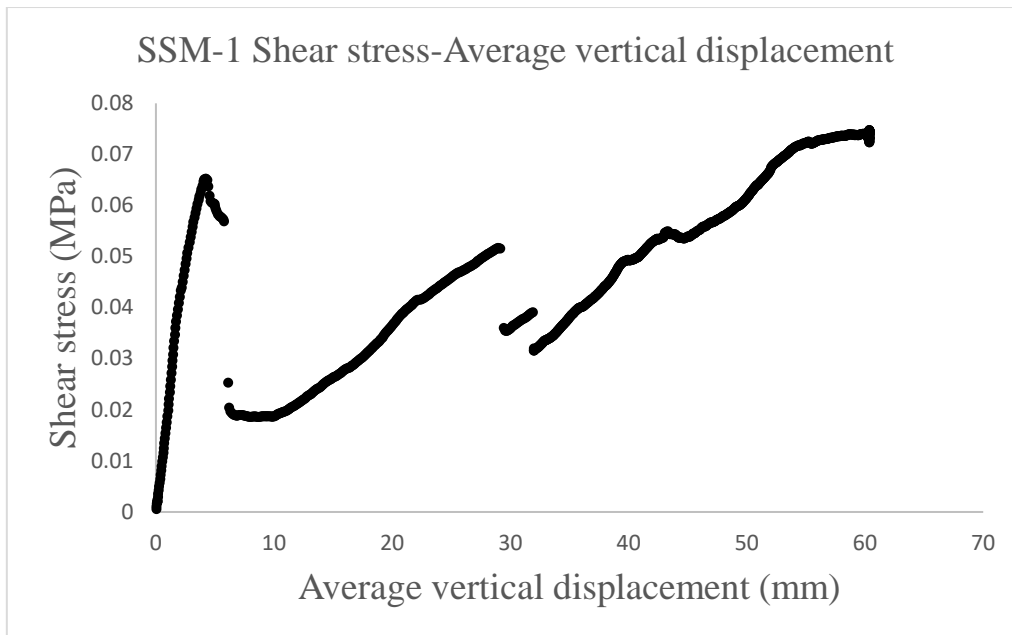
Figure A. 33. SSM-1 Shear Stress-Average vertical displacement.

In this graph, the shear stress reached a relative maximum at 0.06 MPa, when the maximum load was supported and the FRP-concrete connection started to fail. However, in the post-critic region the specimen reached the maximum shear stress of 0.07 MPa by ending point of the test in 60 mm of displacement.
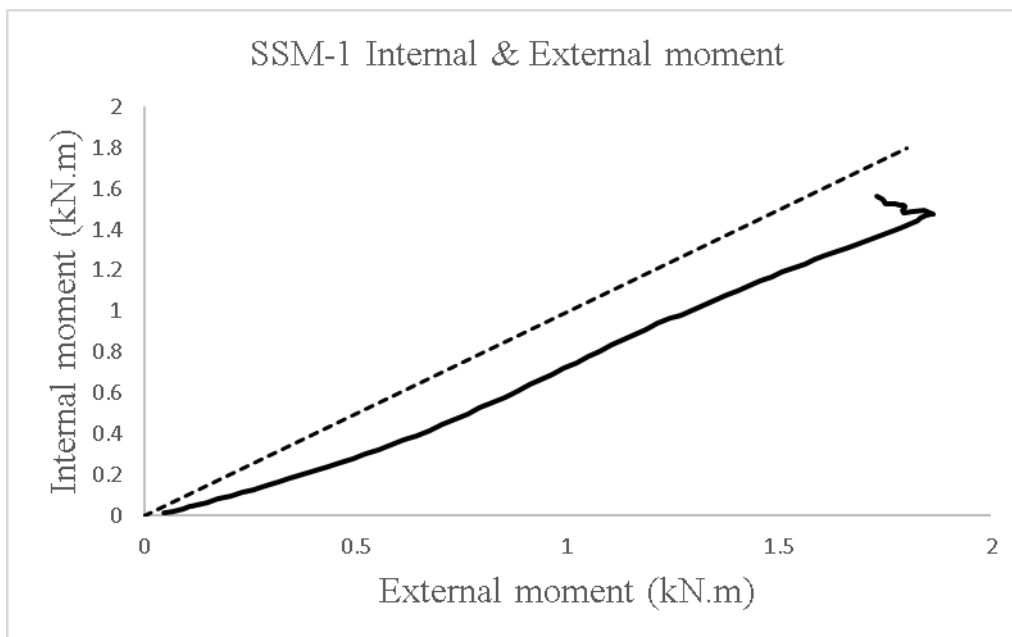
Figure A. 34. SSM-1 Internal & External moment.

As observed in the graph, equilibrium of internal and external moment is so far from the balance and it represents weak bonding between CFRP and concrete in this case.
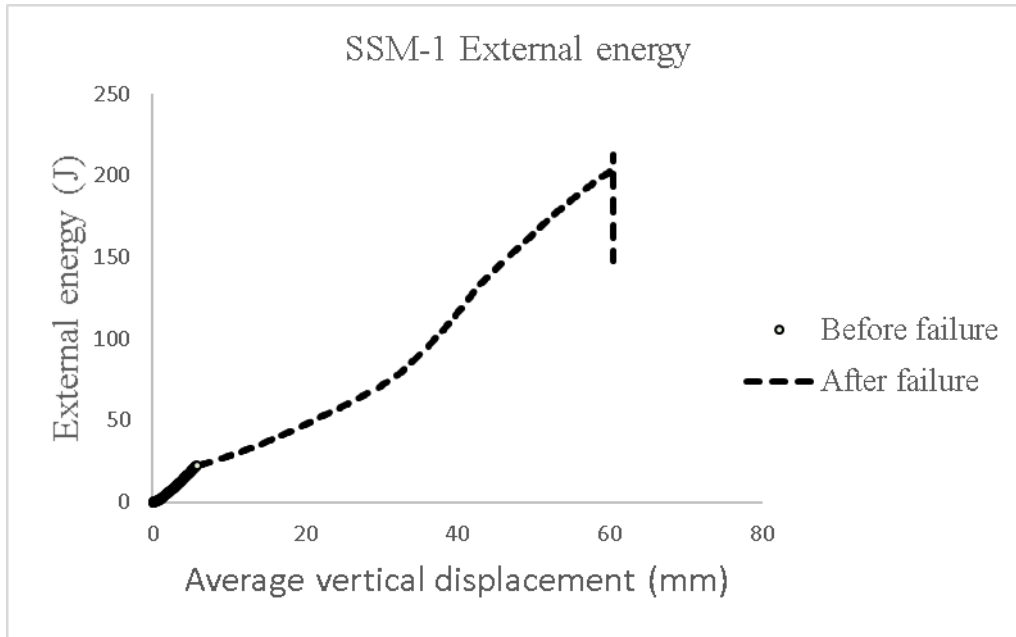
Figure A. 35. SSM-1 External energy.

Regarding to the plot, distribution of energy after failure is more massive respect to before failure conditions. The following plot shows the relative displacement between CFRP and concrete at both extreme specimen's edges. It provides an idea about the CFRP-concrete sliding phenomena.
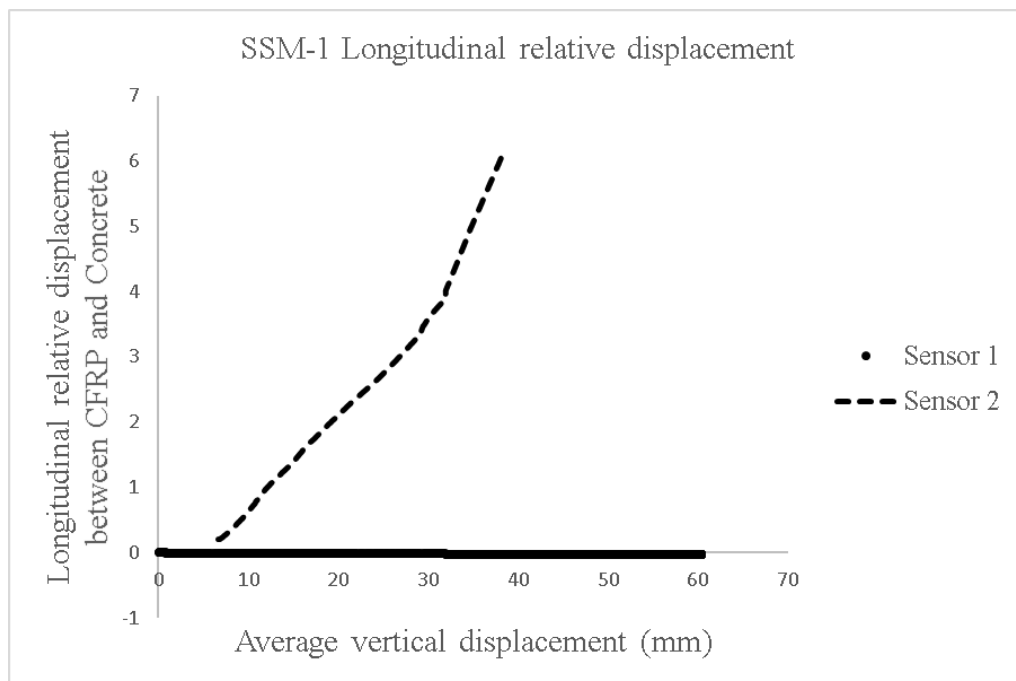
Figure A. 36. SSM-1 Longitudinal relative displacement.

Corresponding on the graph, specimen starts sliding after 8mm of vertical deflection till reaching 4mm sliding between CFRP and concrete. The final sliding goes up to 6.1mm.

A.6.6. SSM-2
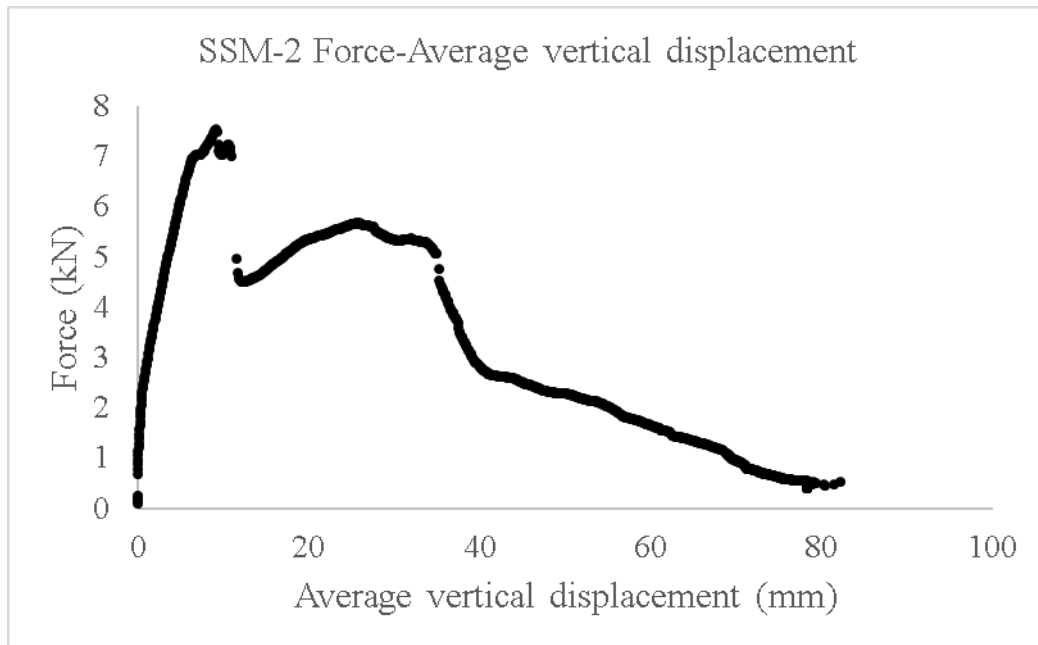
Figure A. 37. SSM-2 Force-Average vertical displacement.

Regarding to the graph, the force increases to 7.7kN as maximum point, then falls to 5.1kN due to failure, afterwards increases a bit to 5.6kN, then tend to zero till end of the test. The displacement of breaking point is 1.98mm and plot represents 80mm of displacement as maximum.
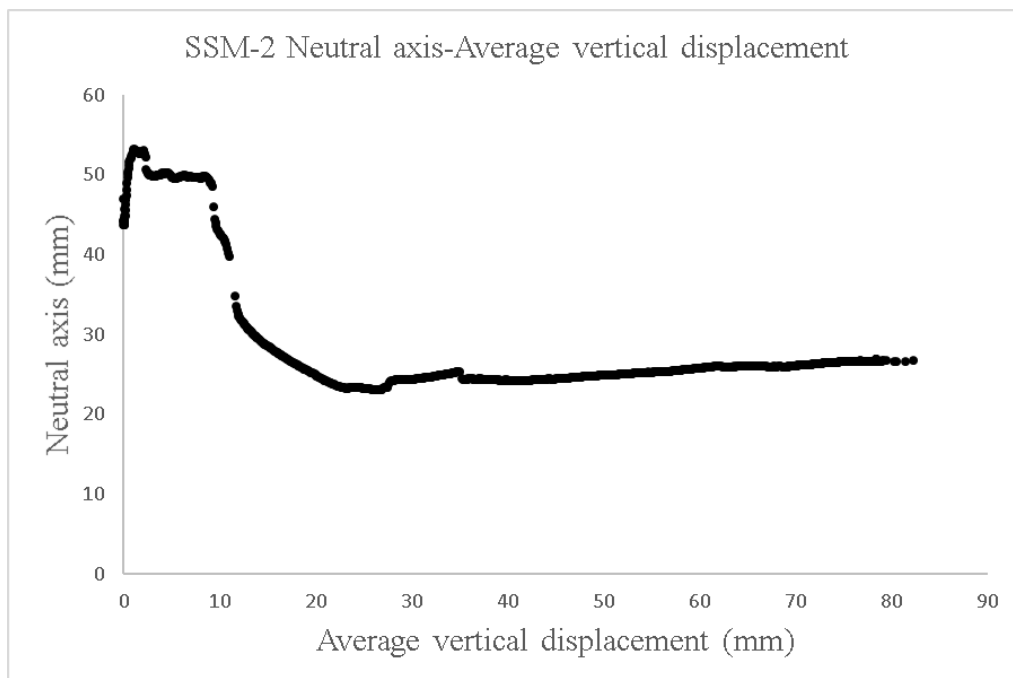
Figure A. 38. SSM-2 Neutral Axis-Average vertical displacement.

Depending on the plot, neutral axis placed at 53mm as maximum and failure happened after 10mm of displacement.
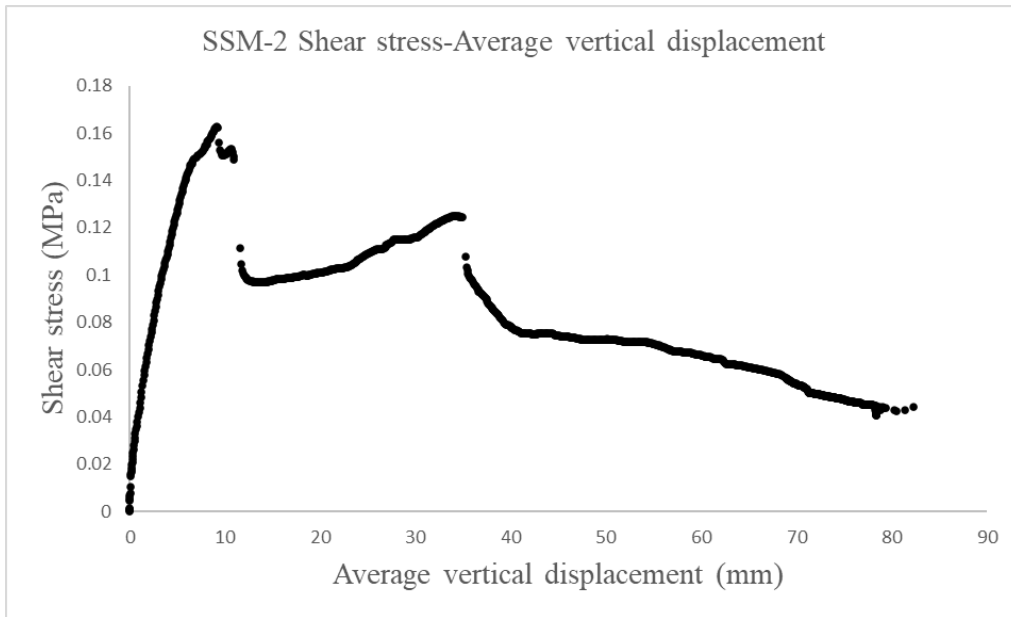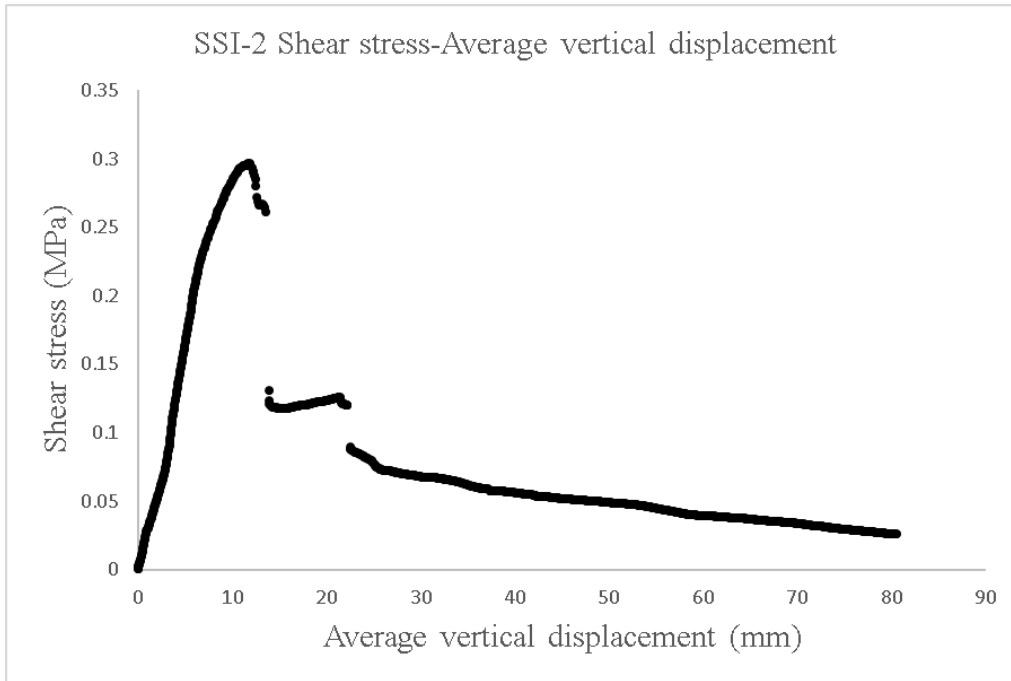
Figure A. 39. SSM-2 Shear Stress-Average vertical displacement.

According to the graph, 0.165MPa is the maximum shear stress and failure happens after 10mm of displacement.
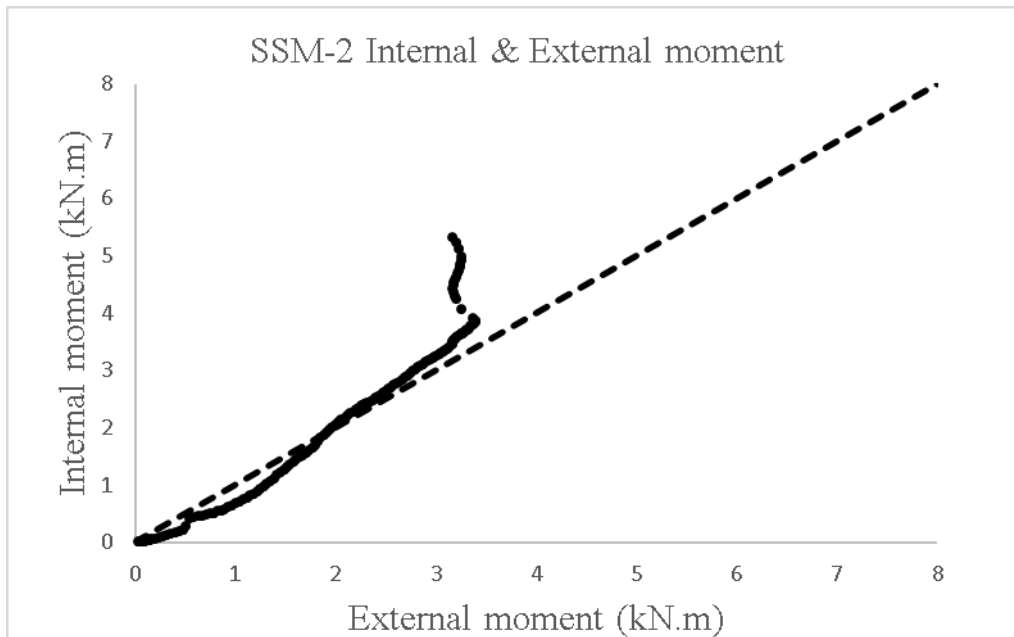
Figure A. 40. SSM-2 Internal & External moment.

Regarding to the plot, equilibrium of Internal and external moment is presented and it shows totally bonding situation between CFRP and concrete.
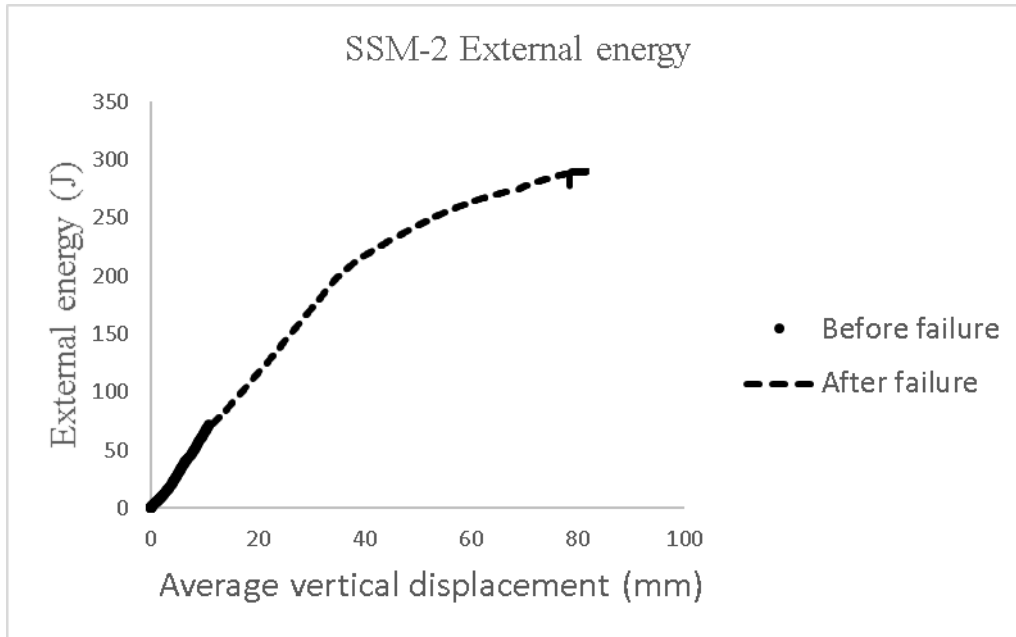
Figure A. 41. SSM-2 External energy.

Depending on the graph, length of after failure's dash line is bigger than two times of before failure's solid line and it means more energy is applied after failure.
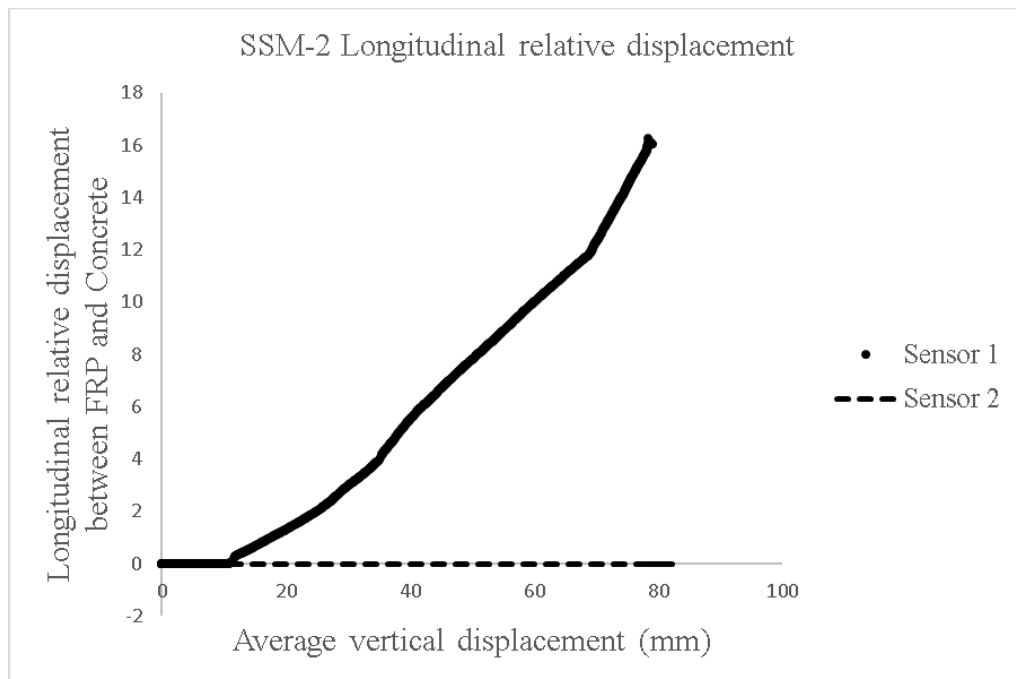
Figure A. 42. SSM-2 Longitudinal relative displacement.

According to the plot, specimen starts sliding for a vertical displacement of 12mm until 16.2mm of final sliding between CFRP and concrete.

A.6.7. SSI-1
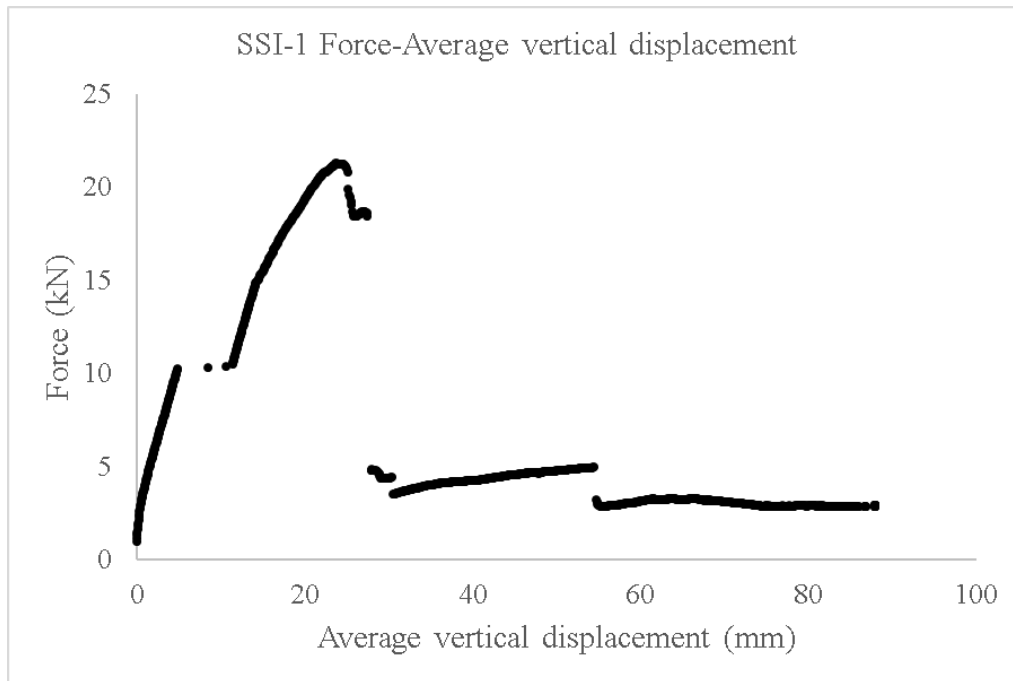
Figure A. 43. SSI-1 Force-Average vertical displacement.

Regarding to the graph, ultimate force is 22kN and breaking point is 28mm. Maximum displacement is 89mm.
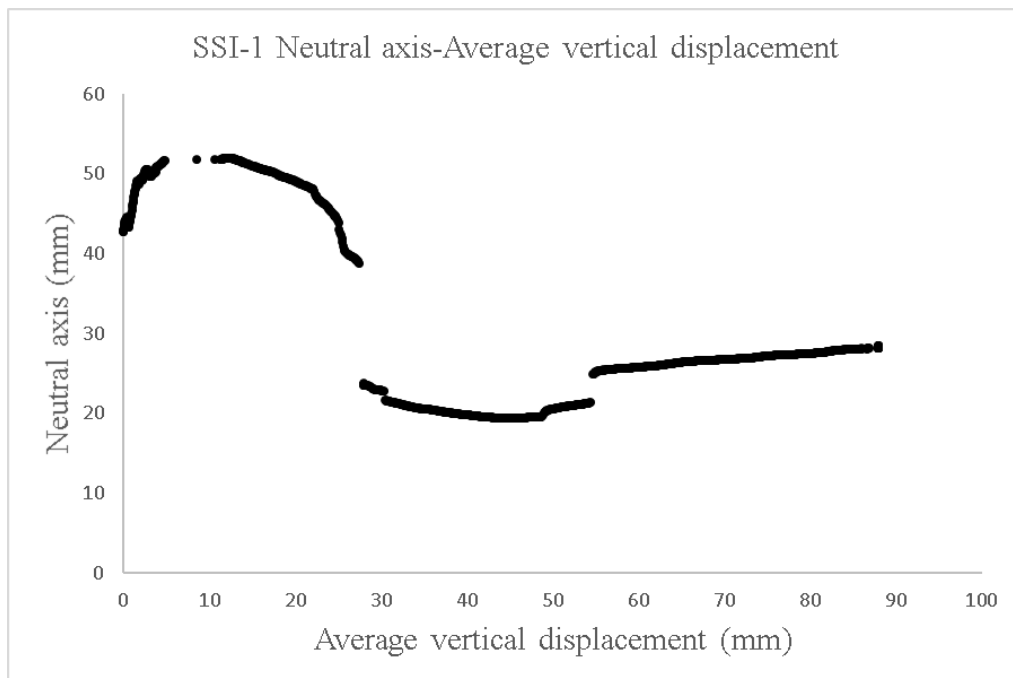
Figure A. 44. SSI-1 Neutral Axis-Average vertical displacement.

According to the plot, neutral axis position placed over 35mm before failure and fell down below 35mm after broken.
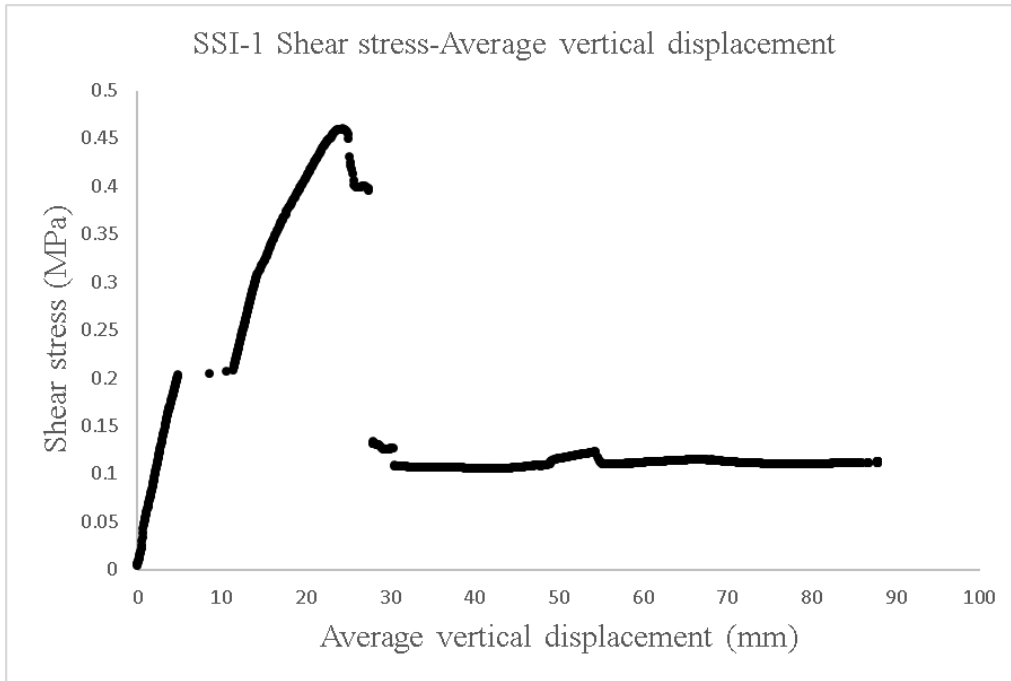
Figure A. 45. SSI-1 Shear Stress-Average vertical displacement.

Observing the plot, ultimate shear stress is 0.47MPa: Shear stress is then reduced until the main failure happened at 0.39MPa.
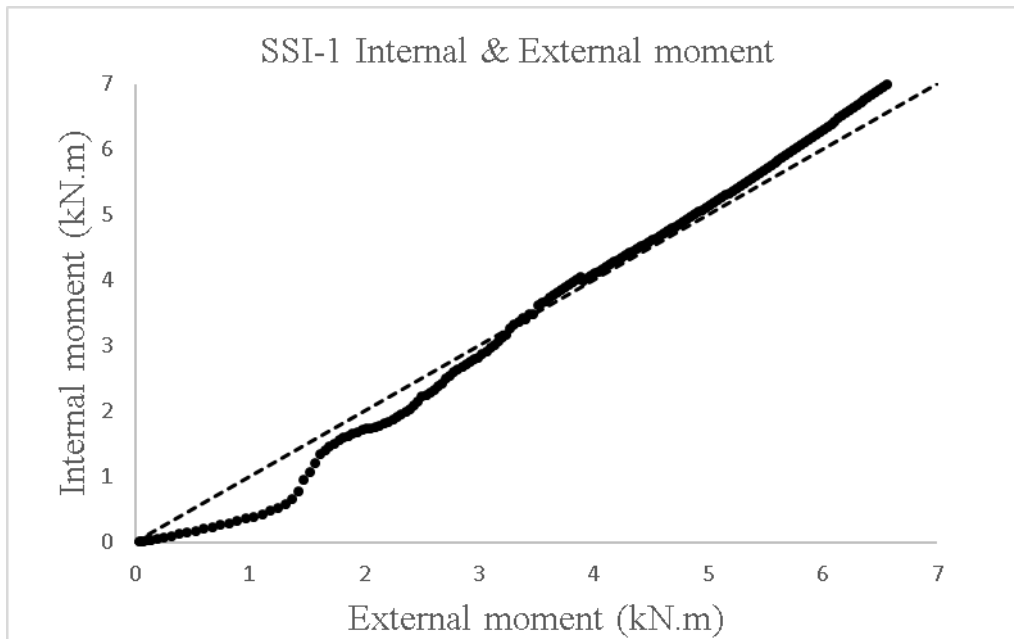
Figure A. 46. SSI-1 Internal & External moment.

According to the graph, equilibrium of internal and external moment is overlapped with draw dash line and it shows good connection level between components.
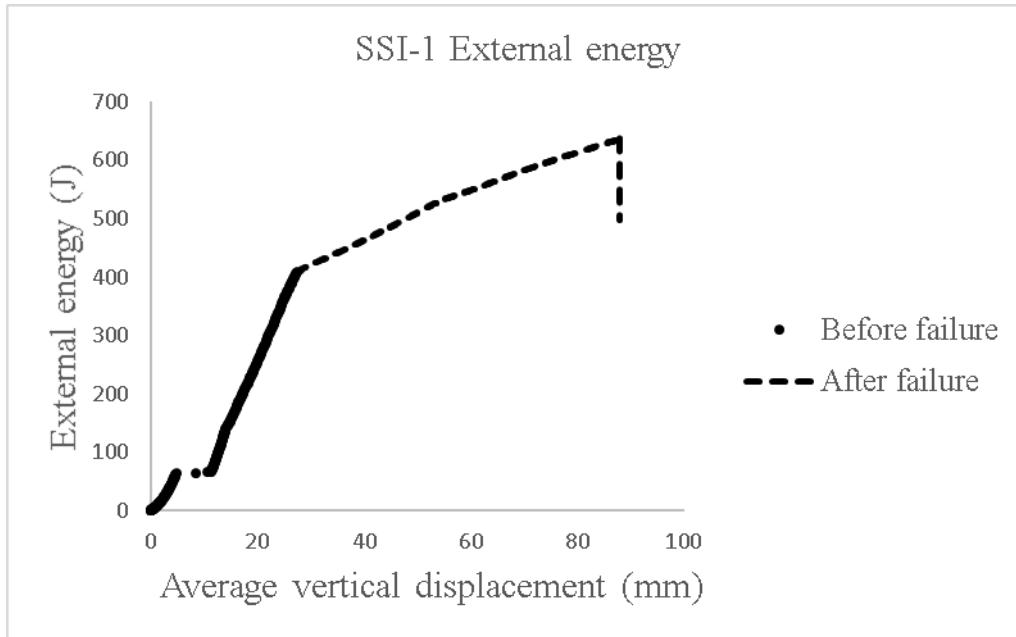
Figure A. 47. SSI-1 External energy.

According with the graph, external energy that specimen absorbed before failure was 415 J and ultimate energy after failure is 620 J. So 2/3 of input energy were assumed before failure and only 1/3 after failure.
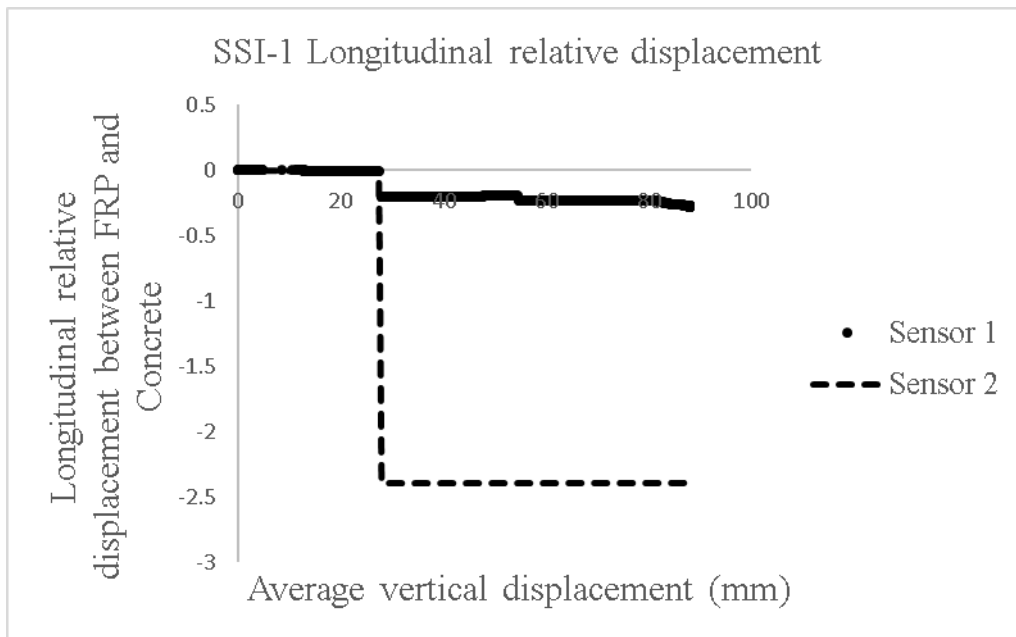
Figure A. 48. SSI-1 Longitudinal relative displacement.

Corresponding to the plot, significant longitudinal sliding displacement does not happen, only some vibrations and jump recorded by the sensors due to sudden movement at failure. Slightly sliding may be noticed in sensor 1 but it is not significant.

A.6.8. SSI-2
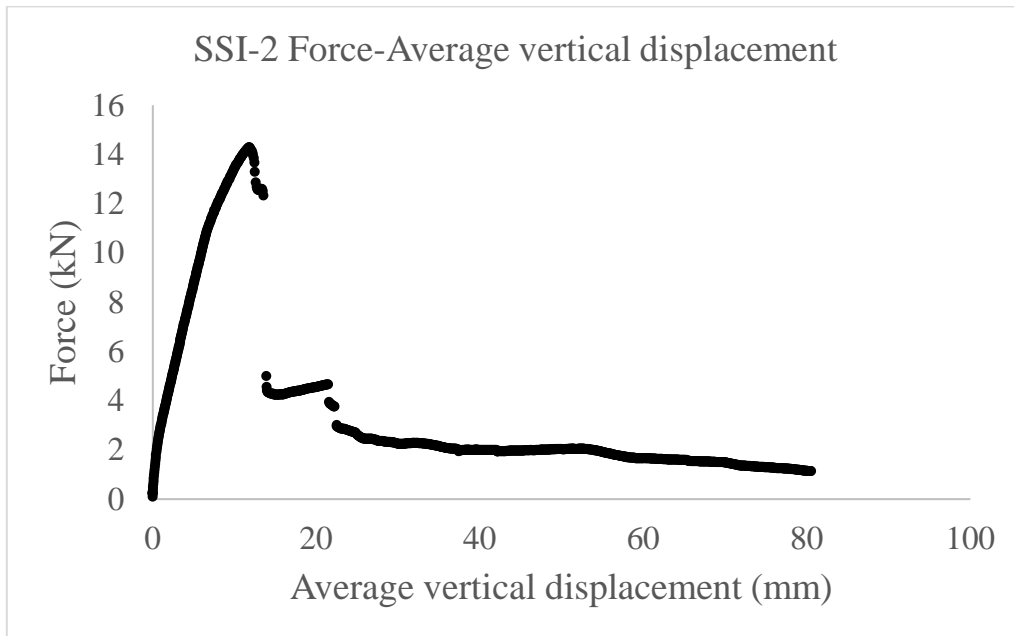
Figure A. 49. SSI-2 Force-Average vertical displacement.

According to the graph, ultimate force is 14.4kN and drop happens after 16mm and maximum displacement reaches 83mm.
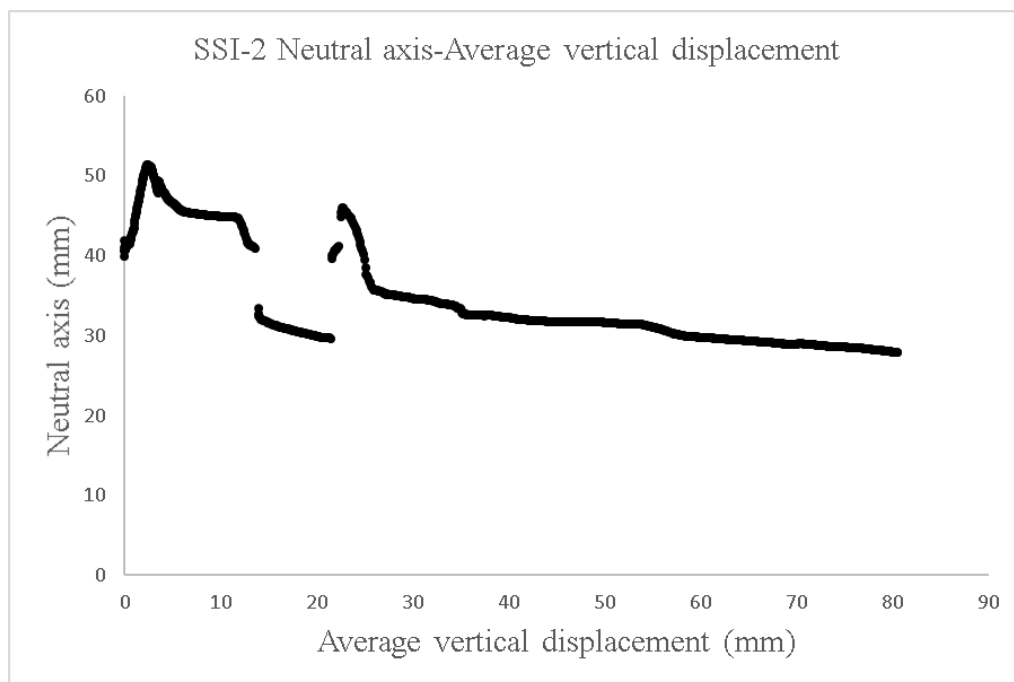
Figure A. 50. SSI-2 Neutral Axis-Average vertical displacement.

Depending on the plot, neutral axis starts from 40mm and reaches 50mm as ultimate point and failure happens after 14mm of mid-span vertical deflection when neutral axis drops down to 33mm. It rises again after few reductions to 45mm and the second drop down below 35mm indicates the failure.

Figure A. 51. SSI-2 Shear Stress-Average vertical displacement.

Regarding to the graph, maximum shear stress is 0.3MPa and failure happens after 14mm of vertical displacement at mid-span.
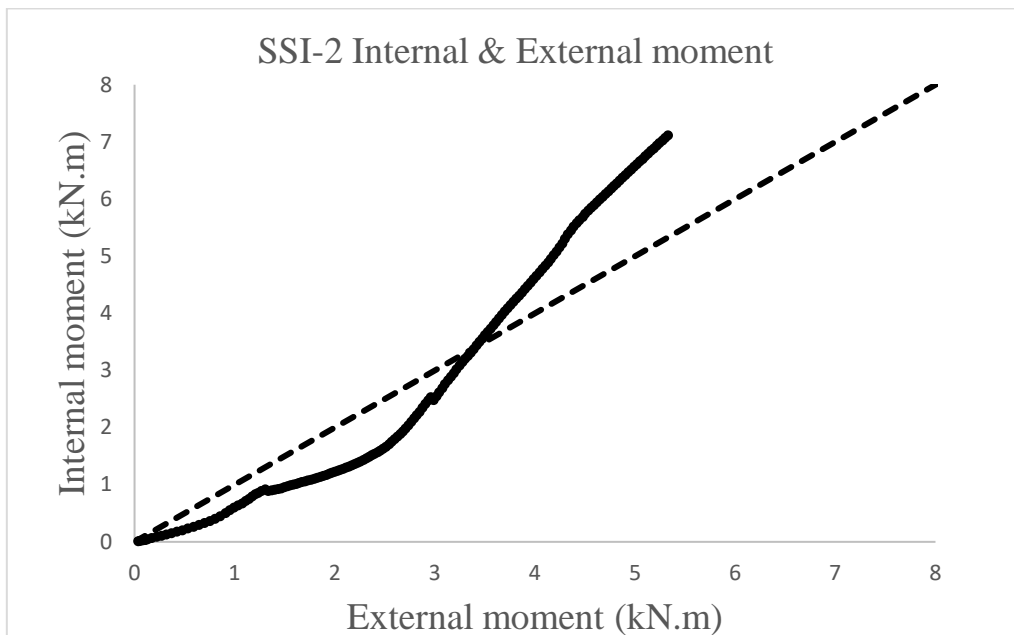
Figure A. 52. SSI-2 Internal & External moment.

According to the graph, equilibrium of moments fluctuates under balance line before failure and jump over the balance line after failure and it means in this case connections between components was not complete.
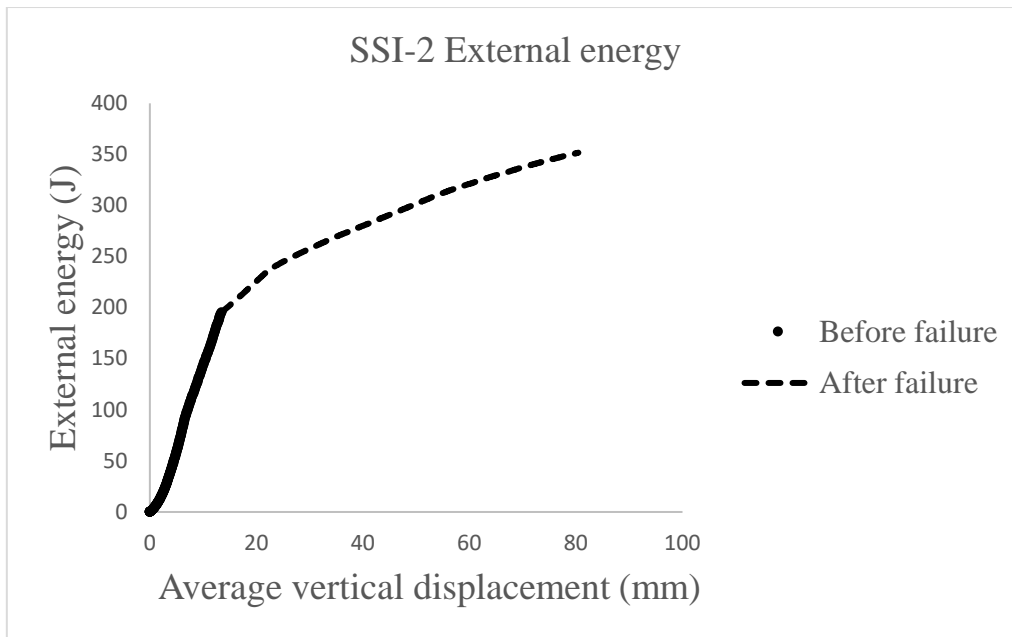
Figure A. 53. SSI-2 External energy.

Regarding to the plot, cumulated energy before and after failure are 200 and 350 J respectively.
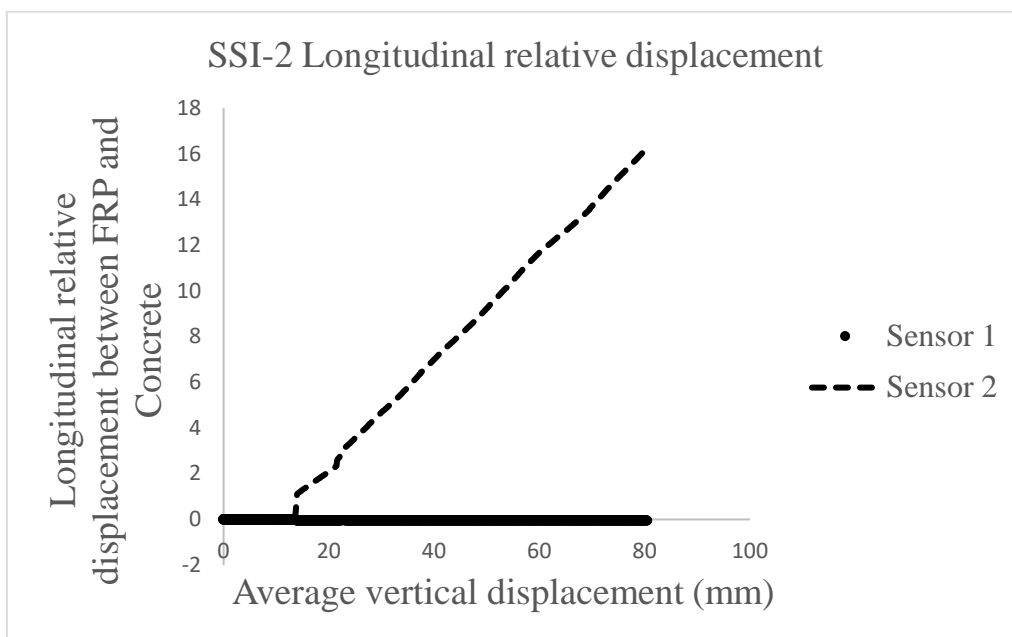
Figure A. 54. SSI-2 Longitudinal relative displacement.

As observed in the graph, CFRP slides from concrete in one ending longitudinally and maximum displacement in length is 16mm.

A.7. Shear plots

A.7.1. 000-1
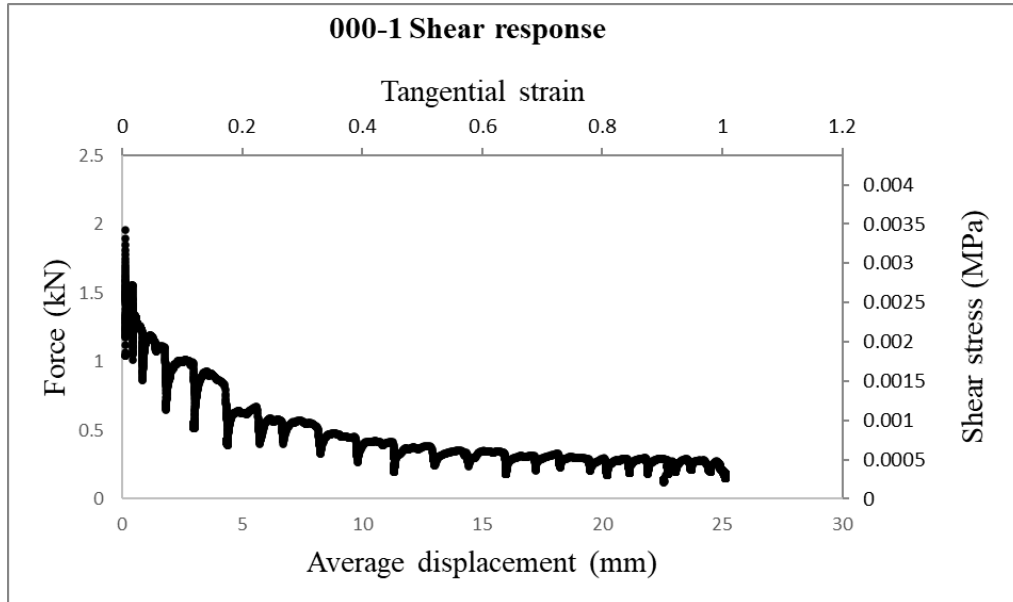
Figure A. 55. 000-1 Shear response.

Depending on the graph, force and shear stress increase until 2kN and 0.33 MPa, afterwards reduction happen till 1.1kN and 0.003 MPa. Average displacement and corresponding tangential strain growth up to 26mm and 1 respectively.

A.7.2. 000-2
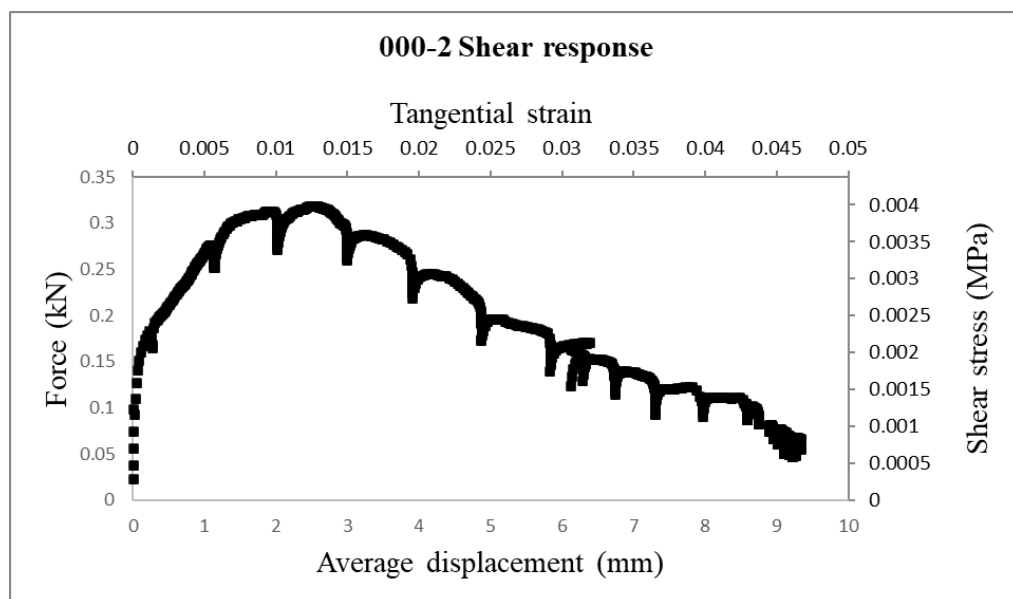
Figure A. 56. 000-2 Shear response.

Regarding to the plot, maximum force and shear stress are 0.32kN and 0.004MPa in order. Final amount of displacement is 9.5mm and ultimate amount of tangential stress is 0.047.

A.7.3. S00-1
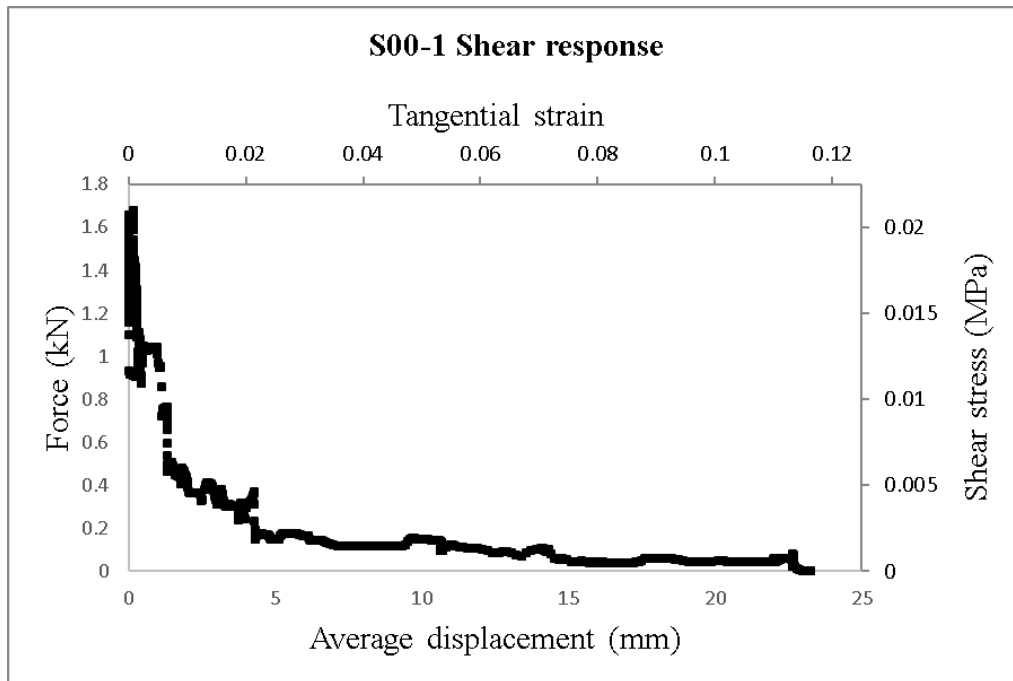
Figure A. 57. S00-1 Shear response.

In this case, failure happened so fast only after 1.6kN force with 0.02 MPa of shear stress. Maximum displacement and tangential strain are 24mm and 0.15 in order.

A.7.4. S00-2
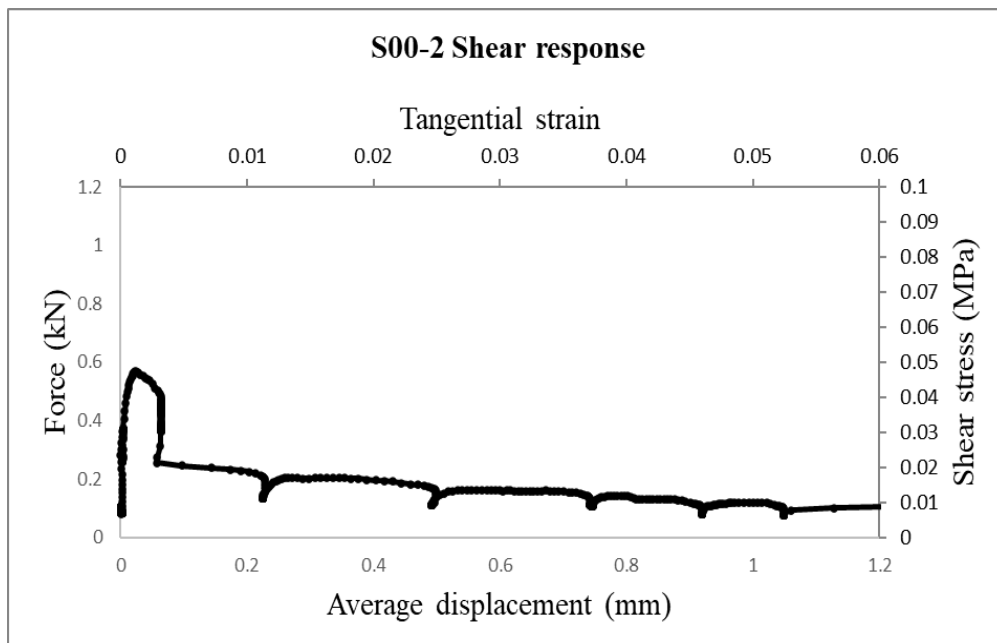
Figure A. 58. S00-2 Shear response.

Regarding to the graph, maximum force and shear stress are 0.59kN and 0.45MPa. final displacement is 12.5mm and 1.08 of tangential strain is represented from plot.
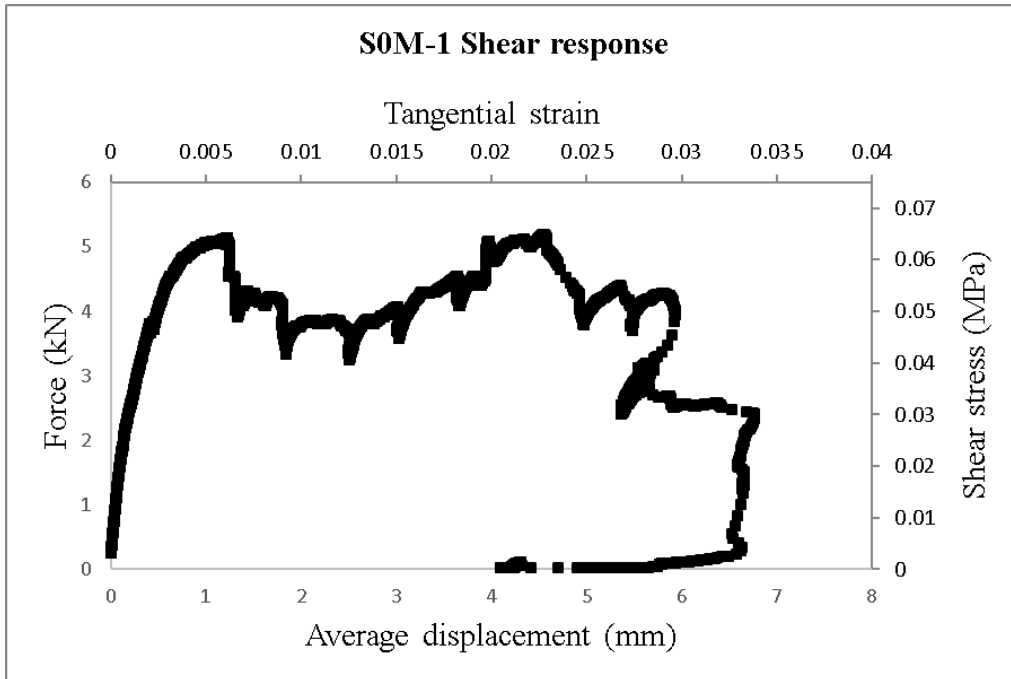
A.7.5. S0M-1

Figure A. 59. S0M-1 Shear response.

Regarding to the graph, force and shear stress increase until 5.2kN and 0.65 MPa then face a reduction until 3.2kN and 0.04 MPa and increase again till 5.3kN and 0.67 MPa. Average displacement and corresponding tangential strain growth up to 6.6mm and 0.33 respectively. The maximum stress of 0.067Mpa was observed on 0.023 of tangential strain.
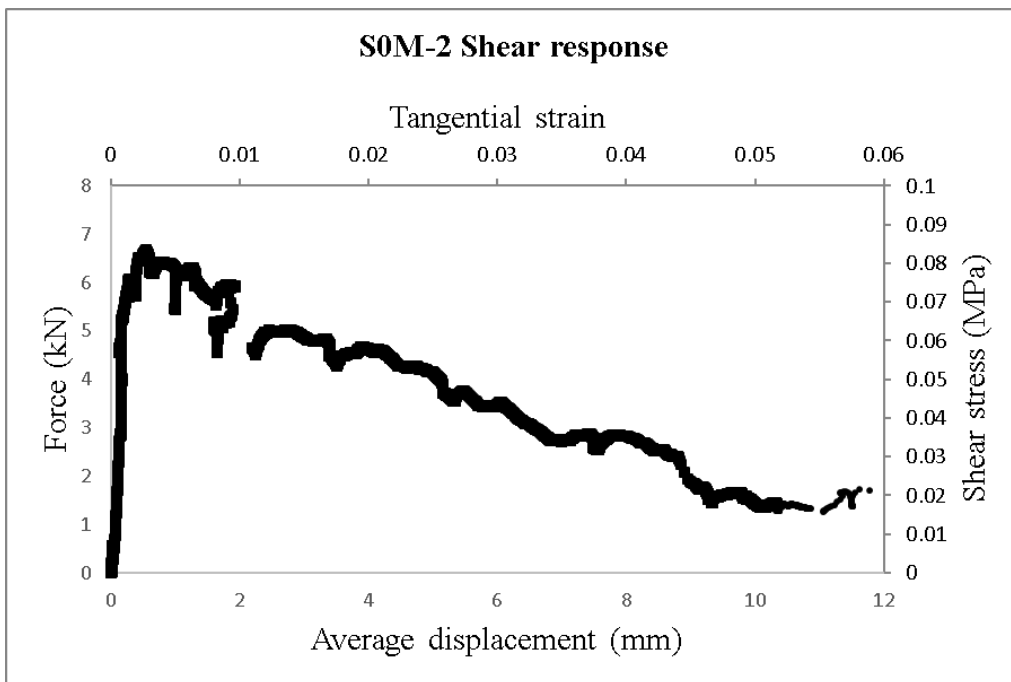
A.7.6. S0M-2

Figure A. 60. S0m-2 Shear response.

Force and shear stress were recorded at 6.7kN and 0.85 MPa as maximum and 1.8kN and 0.021 MPa as minimum. Ultimate displacement and tangential strain are 11.9mm and 0.058 respectively. Shear stress of 0.082Mpa was observed on 0.002 of tangential strain.
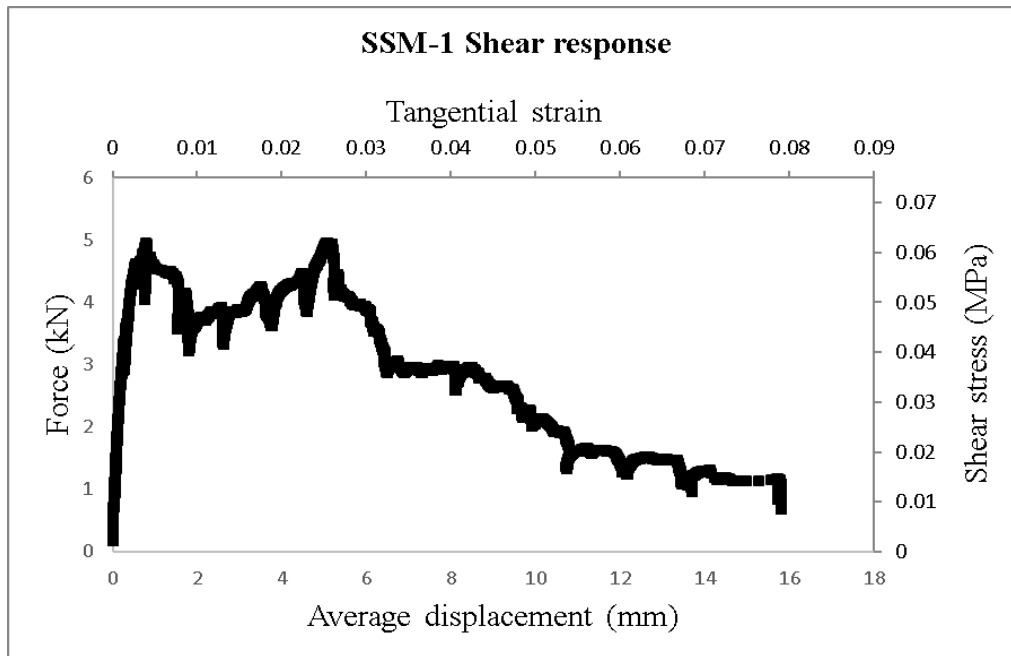
A.7.7. SSM-1

Figure A. 61. SSM-1 Shear response.

According to the graph, force and shear stress increase until 5kN and 0.06 MPa then face a reduction until 3.2kN and 0.04 Mpa, afterwards going up again till the peak and confront a drop step by step until 0.5kN and 0.01 Mpa from beginning spot up to the end; Average displacement and corresponding tangential strain growth up to 16mm and 0.08 respectively. The maximum stress of 0.06Mpa was observed on 0.025 of tangential strain.
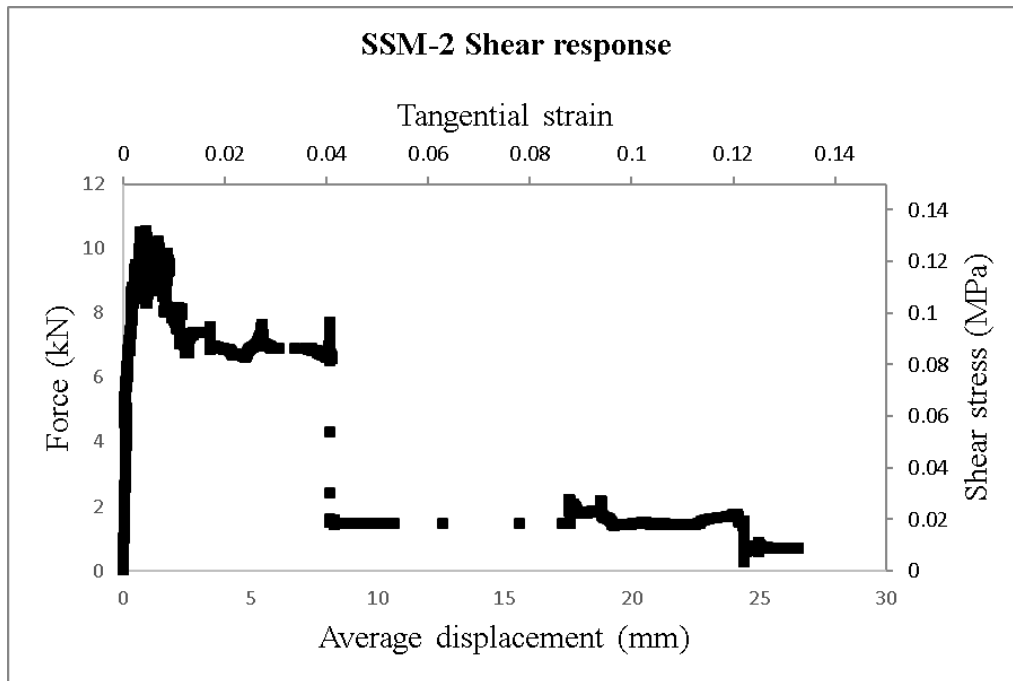
A.7.8. SSM-2

Figure A. 62. SSM-2 Shear response.

Regarding to the graph, force and shear stress increase until 10kN and 0.12 MPa then face a reduction until 6.4kN and 0.09 MPa and afterwards face a sharp reduction to 1.7kN and 0.02 MPa. Average displacement and corresponding tangential strain growth up to 27mm and 0.13 respectively. The maximum stress of 0.13Mpa was observed on 0.004 of tangential strain.
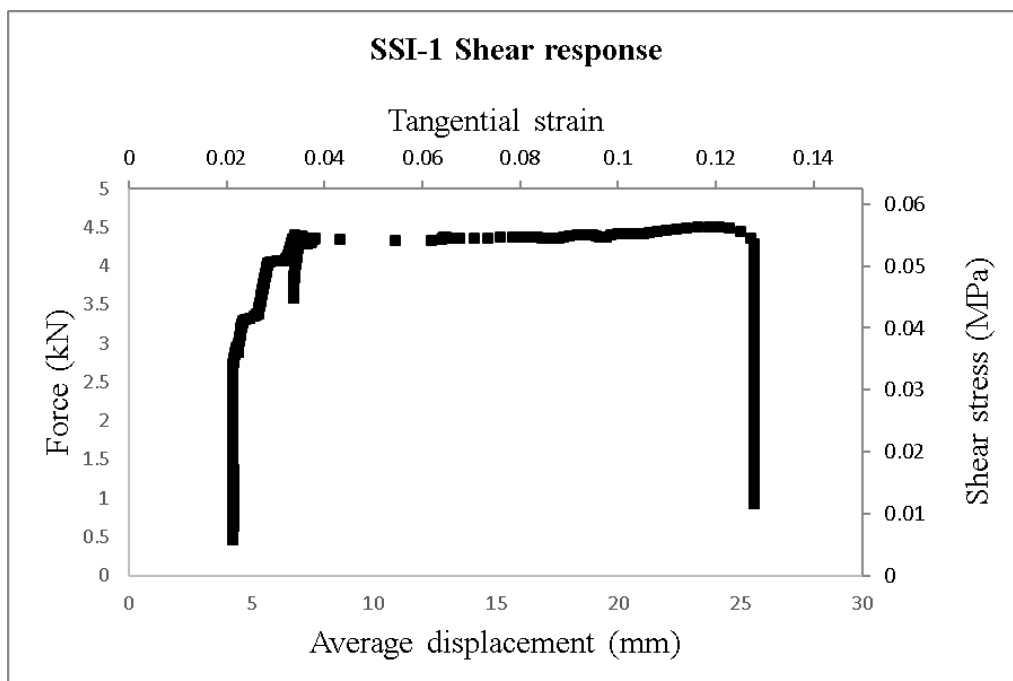
A.7.9. SSI-1

Figure A. 63. SSI-1 Shear response.

Force and shear stress are recorded at 4.5kN and 0.055 MPa. Ultimate displacement and tangential strain are 26mm and 0.13 respectively.
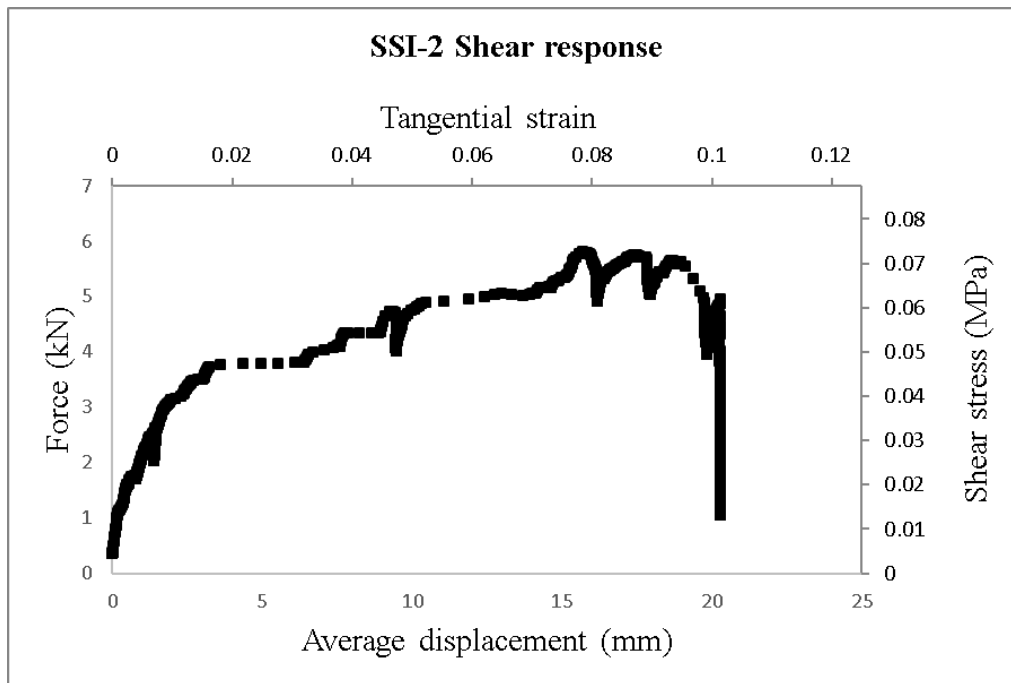
A.7.10. SSI-2

Figure A. 64. SSI-2 Shear response.

Corresponding to the graph, force and shear stress increase slightly until 5.9kN and 0.074 MPa. Maximum displacement is 21mm and tangential strain is 0.1.

B

Modal analysis results

B.1. Introduction

The following annex shows all reacted modes by specimens during the modal analysis tests (Figure B. 1) but the only mutual mode between them is third bending mode (mode B) which is represented in chapter three (experimental campaign) also.
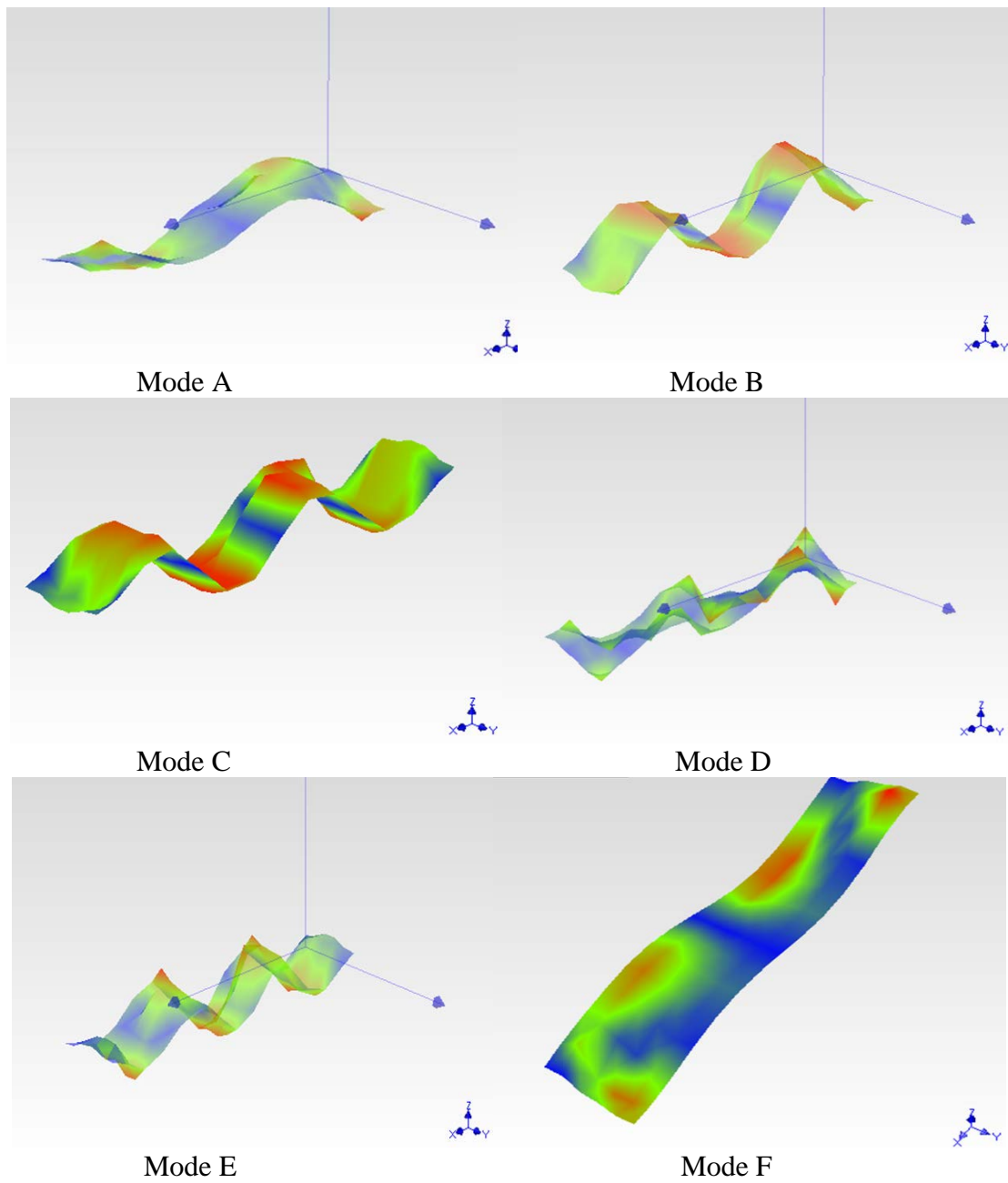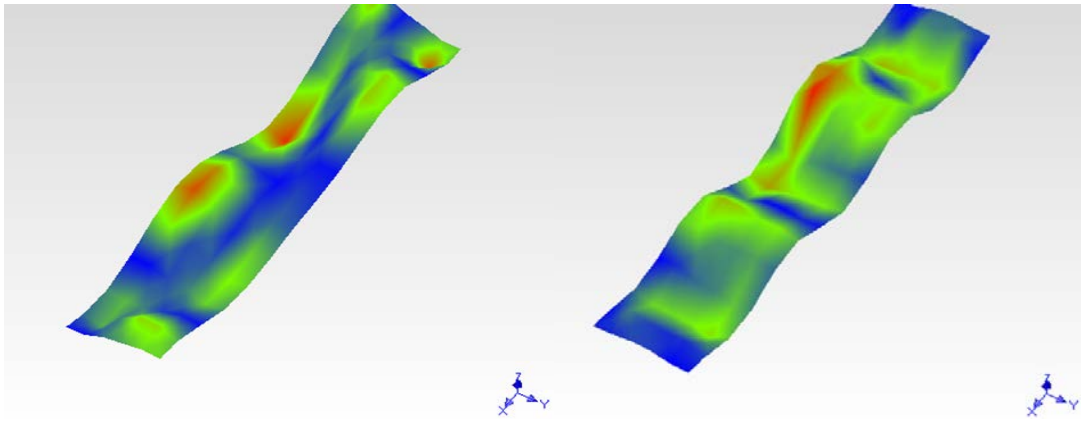
B.2. Test Results

Table B. 1 shows presentation of each specimen in each mode. In; blank area means specimen didn't show that specific mode and Y means specimen have shown that specific mode.

Table B. 1. Presentation of each specimen in each mode.

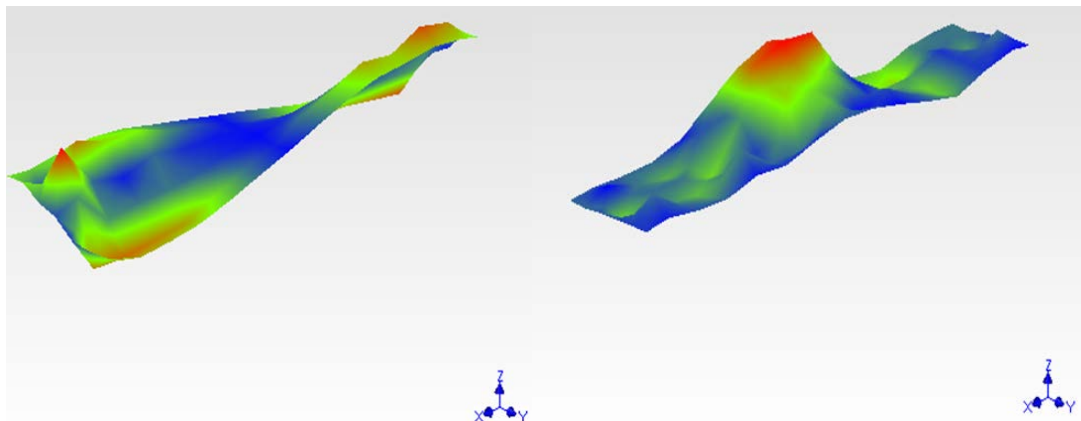|	S00-1	S00-2	S0M-1	S0M-2	SSM-1	SSM-2	SSI-1	SSI-2
A	Y							
B	Y	Y	Y	Y	Y	Y	Y	Y
C	Y	Y						
D	Y		Y					Y
E	Y							
F		Y	Y			Y	Y	
R			Y				Y	Y
S			Y					
I				Y	Y			
ñ					Y			
Q					Y	Y		
T					Y	Y		
U					Y			
O					Y			
P					Y		Y	
J		Y						
Z		Y						
Y				Y				
M				Y				
N				Y				
1					Y			
2						Y	Y	Y
3							Y	
4							Y	
5		Y		Y				
6		Y						
7		Y				Y		

Figure B. 1 shows all the modal analysis:

Mode A

Mode B

Mode C

Mode D

Mode E

Mode F

Mode R

Mode S

Mode l

Mode ñ

Mode Q

Mode T

Mode O

Mode P

Mode J

Mode Z

Mode Y

Mode N

Mode N

Mode 1
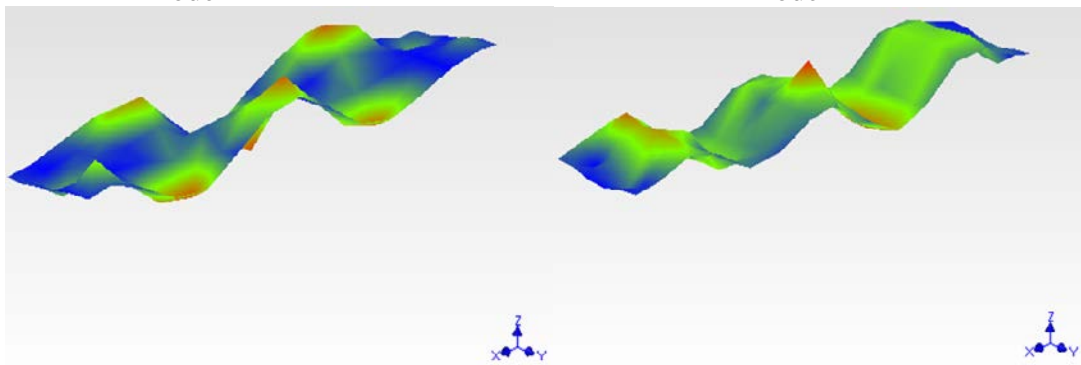

Mode 2

Mode 3

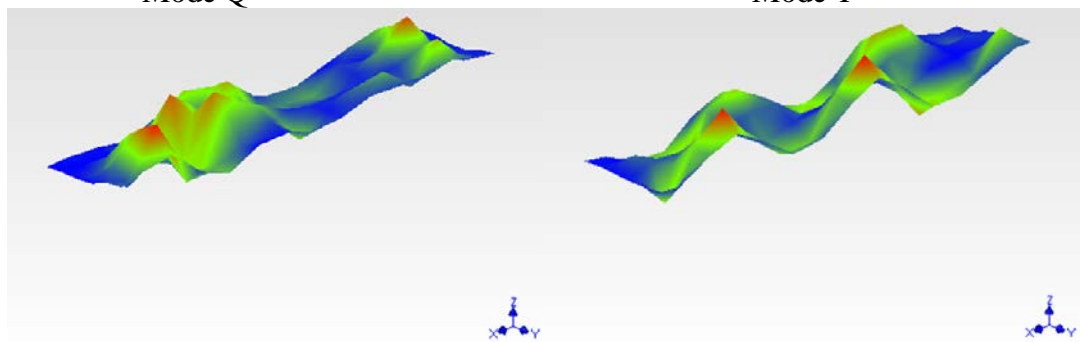Mode 4   Mode 5

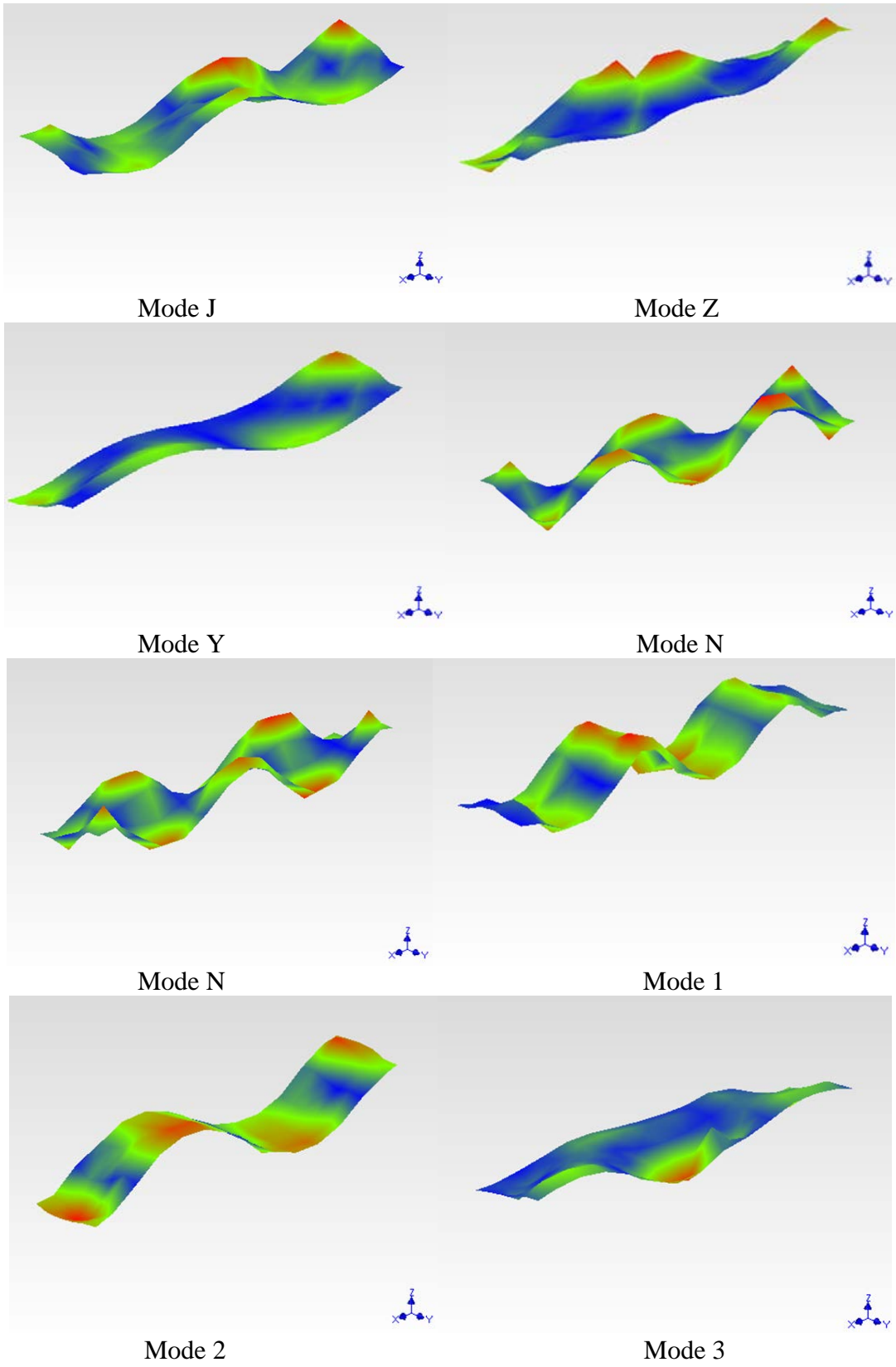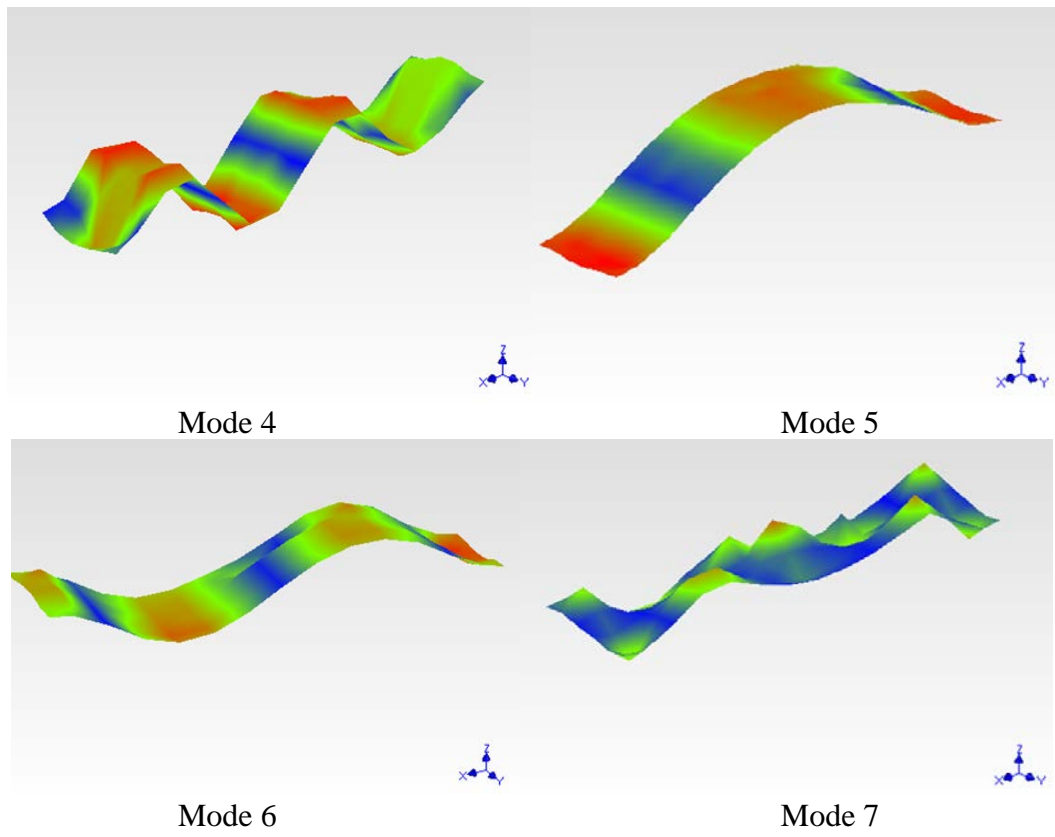Mode 6   Mode 7

Figure B. 1. All reacted modes by specimens during modal analysis tests.

The End